The University of Sydney
School of Geosciences

Ordovician igneous rocks of the central Lachlan Fold Belt: Geochemical signatures of ore-related magmas

Eath Chhun
2004

Submitted in completion of the requirements
for the degree of Master of Science by Research

The University of Sydney
School of Geosciences
Division of Geology and Geophysics
Edgeworth David Building (F05)
Sydney, NSW, 2006
Australia

ABSTRACT

The majority of economic gold deposits in NSW are associated with Ordovician-aged igneous rocks and are examples of the Cu-Au porphyry-skarn-epithermal association commonly developed in convergent margin to orogenic settings. They are among the oldest porphyry Cu-Au deposits in the Pacific Rim region. They are similar to younger deposits in terms of tectonic setting and structure, but the largest are chemically distinct, being associated with shoshonite magmas (Cadia, Ridgeway and Northparkes). The Lachlan Fold Belt (LFB) porphyries are subdivided into four sub-groups based mainly on their age relative to development of the Lachlan Transverse Zone (LTZ) structure. Two subgroups pre-date the LTZ, one group is syn–LTZ and one group post-dates the LTZ. No mineralisation has been found or reported among pre-LTZ porphyries, but it is common in post-LTZ porphyries.

Petrographic analysis and microprobe results establish a wide range of primary and secondary features within the Ordovician rocks examined in this study. Calc alkaline to shoshonitic affinities are supported by the variable abundance of primary K-feldspars. Primary mineral phases such as pyroxenes and igneous magnetite provide an indication of fractioning mineral assemblages responsible for igneous trends in magma chemistry. The hydrothermal mineral assemblages documented in these LFB study areas are characteristic of younger Cu-Au Porphyry style mineralisation. As expected, the most pervasive alteration is associated with highly mineralised shoshonitic Ordovician rocks at Ridgeway and Cadia. The less strongly mineralised calc alkaline Ordovician rocks at Cargo, Copper Hill and Fairholme, are correspondingly less strongly altered overall, although secondary mineral assemblages are locally abundant. Many varieties of oxides and carbonates are observed at the different study localities.

Most of the studied samples conform to igneous chemical trends because they are weakly altered, although post magmatic processes, such as veining, are detectable in certain trends. The K_2O enrichment of the studied samples is consistent with subduction-modified mantle wedge sources. A few effects, such as the high Fe_2O_3 contents of some Ridgeway samples, probably reflect porphyry-style hydrothermal alteration processes. Host rocks at the Cadia and Ridgeway are entirely alkalic on the K_2O versus SiO_2 plot and shoshonitic on the Total Alkalies versus SiO_2 plot. Igneous rocks at the other deposits display a range of compositions between low K tholeiites to shoshonites that in some cases reflects multiple igneous suites.

The LREE and LILE enrichments, and HFSE depletions (Nb, Ta and Ti) of the magmas associated with these deposits are characteristics of a subduction-related tectonic setting. They all fall in the volcanic-arc granite and syn-collisional granite field of the Nb-Y tectonic discrimination diagram. Several magma types are identified by differences in the HFSE and REE trends. Differences in the extent and style of magma fractionation are evident in the trace element data. The Ridgeway samples define a wider range of trace element concentrations than the Cadia samples that may indicate a greater extent of fractionation during emplacement of the Ridgeway magmas. Fairholme samples display a high Nb and Zr trends that are distinct from the main fields on Zr variation diagrams.

Compositional differences between larger Cu-Au deposits, Cadia-Ridgeway and smaller deposits, Copper Hill, Cargo and Fairholme are evident in terms of Nb-Ta depletion and variation. The smaller deposits show constant Nb/Ta or negative Nb/Ta trends that extend to high Nb. The larger deposits display positive Nb/Ta trends that do not extend to high Nb. This distinction reflects a difference of preferential incorporation of Nb in a mineral phase (magnetite). Comparisons between Cadia-Ridgeway and other shoshonite (altered samples of Bajo de la Alumbrera, Argentina), calc alkaline magmas

from New Zealand and rocks from other areas indicate that Nb/Ta is not directly correlated with the shoshonitic classification, K_2O vs. SiO_2, and that the Cadia-Ridgeway Nb and Ta variation is not the result of alteration. The fact that the weakly altered LFB Capertee shoshonites exhibit a narrow range of Nb and low Nb/Ta suggest the shoshonite trend for the LFB as a whole is a steep one on the Nb/Ta versus Nb plot. The results of this study could provide important information for exploration within the LFB. Only the Cadia and Ridgeway deposits display a wide range of Nb/Ta values and lack the near-horizontal trend seen for other localities associated with smaller deposits.

The tectonic evolution of the LFB is a major factor contributing to occurrence of large porphyry Cu-Au deposits. The sequence of important events, however, commences with sub-crustal generation of oxidised magma and finishes with efficient Cu-Au accumulation by hydrothermal processes at favourable structural sites. The increase in Au-Cu deposit size from small (Copper Hill-Cargo) to world class (Cadia-Ridgeway) indicates the importance of magma composition during this process. The most obvious differences between the Cadia-Ridgeway and New Zealand rocks is that the latter are volcanic in origin and associated with an arc-back arc system. Therefore, they did not form in a tectonic regime suitable for the evolution of porphyries and the focussed movement of hydrothermal fluids during dilatant episodes. As a result, they are not linked to mineralisation despite having Nb-Ta and Nb/Ta variations that are typical of the high oxidation states in Au-prospective magmas of the LFB.

TABLE OF CONTENTS

FIGURES AND TABLES

ACKNOWLEDGEMENTS

My first thanks must go to my supervisor, Dr. Derek Wyman, who gave me the opportunity to do research on the geochemical signatures of Ordovician ore related magmas in the Lachlan Fold Belt. They are the most exciting, economically interesting and one of the world's most prospective sources for porphyry Cu-Au. His support and enthusiasm has encouraged me and I thank him for always being available for advice.

Newcrest Mining Ltd, especially John Holliday, Paul Dunham, Geoff Smart and Craig McIntosh are thanked for access and assistance in collecting samples from the Ridgeway mine and Fairholme deposit. My gratitude is given to Max Rangott of Rangott Mineral Exploration Consultancy, Orange NSW, who has provided me with a job and research documents. I am grateful to Kim Stanton Cook, Brett Ferris, Tim Feming and Robert Watkins of Delta Gold N.L for their support when I worked for the company in Cobar, NSW. Angus Collins, Triako Resources Ltd, and Ian Paterson, Geological Survey of NSW, are thanked for encouraging me to do my postgraduate research and providing me with work in Mineral Hill, Broken Hill and in the Department of Mineral Resources.

Thanks to Golden Cross Resources Ltd for provision of geochemical data and core samples of Copper Hill and Cargo, the Department of Mineral Resources for access to the core library, Gateway Mining Ltd for assisting in collecting samples at Nasdaq prospect. I am thankful to Phillip Blevin for the provision of whole rock geochemical data of Copper Hill and Cargo. Thanks also to George Navratil for sample preparation, and John Twyman and Ivan Teliatnikov for IT technical support, Joel Fitzherbert for his tireless help on the microprobe, and the EMU unit of the University of Sydney and NSW for unfunded access to the microprobe laboratory.

Ultimately I am much indebted to my parents, family, son and daughter whose love and support are priceless. They have cared and put up with my tiredness. My research and study would not have been possible without their continuous and unlimited support throughout the years. Their belief that I would come up with a new discovery that would lead to enormous wealth has been inspirational.

CHAPTER 1
THE GEOLOGY OF GOLD MINERALISATION IN NEW SOUTH WALES

1.1 INTRODUCTION

The majority of economic gold deposits in NSW are associated with Ordovician-aged igneous rocks and are examples of the Cu-Au porphyry – Skarn Epithermal association commonly developed in convergent margin to orogenic settings (Cooke et al., 1998; Dawson and Kirkham, 1996).

Although the igneous rocks of the Lachlan Fold Belt (LFB) in NSW and Victoria have featured prominently in the granite literature (Chappell and White, 1992), comparatively little trace element data has been available for the intrusive rocks or related volcanic sequences. Characterizations of LFB igneous suites, such as the supposed uniformly shoshonitic character of Ordovician suites (Wyborn, 1992), have only recently been rigorously assessed.

These new studies employed modern analytical techniques capable of providing data for a wide range of trace elements. The studies have established a diversity of igneous suites among Ordovician rocks of the LFB (Blevin, 2002, Green, 2001, Glen et al., 1998) that highlight a need for a careful re-evaluation of LFB tectonic models and additional study of the relationships between gold mineralization and Ordovician magmatism.

1.2 RESEARCH OBJECTIVES

The objectives of the present research were to investigate the major and trace element geochemical characteristics of LFB Ordovician igneous in NSW with particular reference to known gold mineralization. The research builds on recent published studies (Blevin, 2002; Holliday et al. 2002; Green, 2001), and a database provided by P. Blevin (ANU). New contributions of the research include the analysis and study of igneous units not assessed, or not assessed in detail, by the previous studies.

Specific objectives of the study are:

1. Characterization of the multiple intrusive phases of the Ridgeway deposit and comparison with nearby intrusions of the Cadia pit and other Ordovician intrusions within and near the Lachlan Transverse Zone (see below; Green, 2001; Glen and Walshe, 1999).
2. Characterization of unweathered intrusive rocks at the Copper Hill and Cargo gold deposits and the Fairholme gold prospect.
3. An assessment of the four study areas in terms of possible variations in magma generation and evolution that may be linked to a) the overall tectonic development of the LFB, or b) proximity to major structural features that may control the distribution of economic gold deposition (Glen et al., 1997).
4. A comparison of the Niobium-Tantalum systematics of the Ordovician magmas with recently published data for other intrusive and extrusive igneous rocks. These elements are typically concentrated in oxide mineral phases that are sensitive to the evolving oxidation state of magmas. Accordingly, their trends within suites of related igneous rocks may be distinctive for gold related intrusions that are often highly oxidized.

1.3 GOLD IN NSW

The official discovery of payable gold in Australia was made at Ophir, at the junction of Summer Hill and Lewis Ponds Creeks, 22 km northeast of Orange in the Central West of NSW. It generated the first gold rush in Australia and in turn accelerated the population growth of the country and the development of infrastructure.

The NSW gold sector has continued its growth of recent years with production increasing 5.5 percent in 1999-2000 to reach 20.17 t (DMR, 2002a). Projected increases to 32 t in 2002-03, result mainly from increased production at the Cadia-Ridgeway deposits located near Orange.

These deposits and many others in the LFB are hosted in or intimately associated with Ordovician igneous rocks. Accordingly, there is a clear need to understand the evolution of these igneous system and their possible role in the genesis of mineralization. The following section provides an overview of the geological aspects of NSW that are relevant to gold mineralization.

1.4 THE LACHLAN FOLD BELT IN NSW

New South Wales can be divided into eight major geological provinces (Packham, 1969, 2000) (Fig. 1.1), that include fold belts related to subduction and accretion tectonics plus basins formed either during subduction tectonic episodes or in distinct crustal thinning or sagging episodes.

The Lachlan Fold Belt extends northwards from eastern Tasmania through Victoria and NSW, disappearing under the Great Australian Basin in the north. Scheibner and Basden (1998) suggested that the LFB formed by complex accretinary processes from the mid-Cambrian to the Carboniferous, which were related to the closure of the Wagga Marginal Basin. Glen et al. (1998, 2003) showed that the Ordovician quartz turbidites and arc-related volcanic rocks of the eastern LFB were accreted during the early Silurian, and the four separate belts of pre-Silurian assemblages result from the splitting of a single Macquarie arc.

Three accretionary subduction complexes spanning ages from the mid-Cambrian to the mid-Devonian age are recognised: the Stawell and Bendigo (western Victoria), Tabberabbera (eastern Victoria) and Narooma (along the eastern coastline of SE Australia; Fergusson, 2003). In addition, the Early Ordovician Howqua subduction complex, along the eastern margin of the Melbourne Zone, is interpreted as a short-lived west-dipping subduction (Fergusson, 2003). Turbiditic sediments filled the Wagga Marginal Basin from earliest Ordovician. The basin sequence was inverted into the Wagga-Omeo Metamorphic Belt during the Late Ordovician-Early Silurian Benambran Orogeny. The belt is bounded by the Gilmore Suture in the east, and in the west by the Wonnangatta Line in Victoria and a zone of Early Devonian rifting in NSW (Suppel and Scheibner, 1990). Foster et al. (1999) and Gray and Foster (1997) documented deformation events in the Carboniferous eastern LFB that produced tight north-south trending folds in the Siluro-Devonian sequences and east and west-dipping thrusts within the Ordovician turbdites and volcanic rocks.

Glen et al. (1997, 1998b, 2003) provided comprehensive detail of the Ordovician igneous rocks in term of geochemistry, petrography, age and locations. They are mainly high-K calc alkaline in composition. Shoshonitic types also occur and are more prevalent along the Lachlan Transverse Zone (see 1.6 and 5.3) than to the north and south of this structural zone. The Early Ordovician igneous intrusions, 484-455 Ma, have high K calc-alkaline geochemistry and range from monzogabbro to monzonite. They are present in the Junee-Narromine Volcanic Belt. The Middle Ordovician igneous rocks, 450-445 Ma,

generally are of medium-K, calc alkaline affinity. They are present in all belts and consist mainly of felsic types but locally extend to mafic compositions. Late Ordovician, 439 Ma, igneous rocks are shoshonites that range from monzodiorite to monzonite and occur in all belts except the Kiandra Volcanic Belt. The LFB composes of lower and upper Palaeozoic rocks. Cambro-Ordovician Wagonga basalt, chert and limestone occur at Batemans Bay and Narooma. The Jindalee volcanics, chert, quartzite, schist and serpentinite are localized in Gundagai, Cootamundra and Thuddungra and are the same age as the Wagonga Group.

Outcrops of Ordovician rocks are extensive and consist of volcanic facies and a quartz-rich greywacke-black shale facies. The later is composed of quartz-rich greywackes, grey slates and black graptolite-bearing shale and chert. It is the oldest Ordovician unit and is exposed from south of the Bathurst Batholith through the central and southern highlands and into eastern Victoria. It extends west into the Riverina and northwards through Wagga Wagga to Bourke.

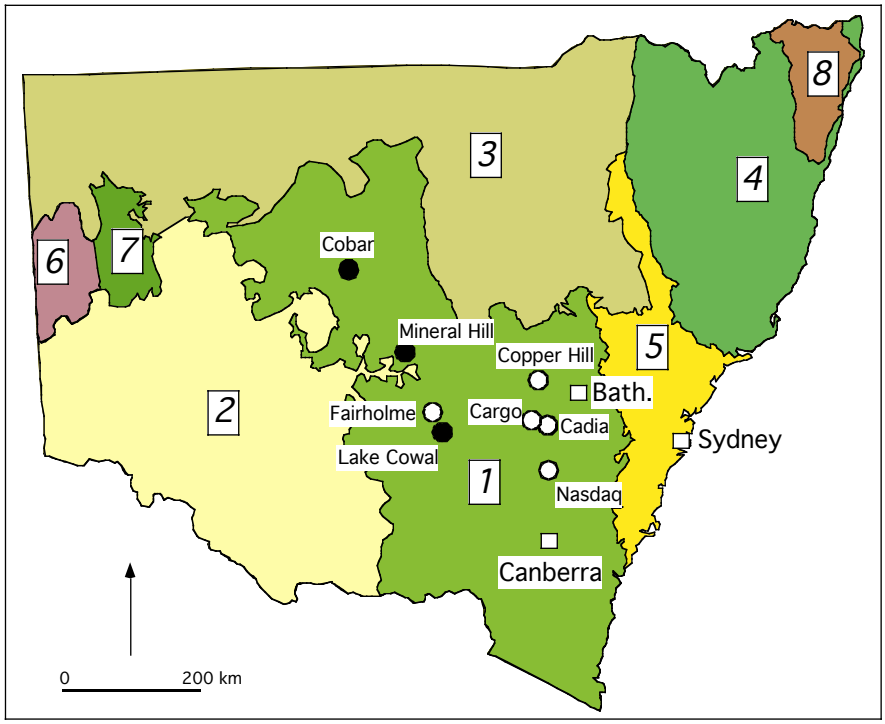

Figure 1.1. Major geological provinces of NSW and selected Lachlan Fold Belt gold deposits. 1 = Lachlan Fold Belt; 2 = Murry Basin; 3 = Great Australian Basin; 4 = New England Fold Belt; 5 = Sydney-Gunnedah-Bowen Basin; 6 = Curnamona Craton; 7 = Kanmantoo Fold belt; 8 = Clarence – Moreton Basin. Bath. = Bathurst. Open circles are deposits examined in this study. Map modified from DMR (2002a) and Branagan & Packham (2000).

The less widespread volcanic facies comprise basaltic, andesitic volcanic units along with limestones. The limestones delineate a palaeogeographic platform in the Molong-Cargo-Cliefden area known as the Molong Rise or Molong High.

Silurian rocks have been identified in a number of localities in the LFB. They are deep to shallow marine sediments, volcanic subtypes, granitic intrusions, and metamorphic rocks. The Devonian and Carboniferous units occur mainly in Darling and Barka basins, Trundle, Parkes, and Molong, east of the Sofala, east of Wonnangatta Suture and around Lake Bathurst. They include felsic volcanic rocks, granitic intrusions along with shallow marine and fresh water sediments.

1.5 GOLD MINERALIZATIONS IN THE LFB OF NSW

The Lachlan Fold Belt contains the majority of currently producing NSW gold mines and is also the largest gold producer among the provinces of the state (Fig. 1.1), (Mineral Resources NSW, 2001). Corbett (1998) recognized a variety of gold deposit types in the LFB that includes shallow-level epithermal ("hotspring"), deeper hydrothermal (quartz ± carbonate veins), and porphyry (intrusion-related) deposits. Skarn mineralisation forms where magmatic-derived fluids react with carbonate host rocks to produce assemblages of secondary calc-silicate minerals (skarns) that are overprinted by later mineralization. Many of the world's large porphyry Cu-Au deposits are associated with nearby skarns (Grasberg, Ok Tedi, Bingham Canyon). LFB skarn deposits include Browns Creek and Yetholme; Cadia is also associated with nearby skarns.

The initial gold rush in the LFB focused on hydrothermal vein gold deposits and related placer deposits with greatest activity being focused on central Victoria in the Bendigo-Ballarat district. More recently, however, production has been derived increasingly from lower grade high tonnage intrusion-related deposits. The Cadia Hill-Ridgeway porphyry Cu-Au operation now challenges The Super Pit at Kalgoorlie (WA) as Australia's largest gold operation producing 50,000 tonnes Cu and 17 tonnes Au per year (DMR, 2002a).

By comparison, the Hillgrove gold mine, the only gold mine in the New England Fold Belt, produces antimony and gold (as a minor commodity) producing 30,000 ounces Au per year (DMR, 2002a).

In the Central West of NSW Cu-Au deposits are spatially associated with Ordovician volcanic rocks and related intrusive rocks. Most of the volcanic rocks have

been classified as shoshonitic or calc alkaline in character based on relatively high potassium contents at a given SiO_2 abundance (Le Maitre et al., 1989).

The Ordovician volcanic rocks lie in four belts, three in the Central West of NSW (Fig. 1.1). From west to east, these are the Junee-Narromine volcanic belt, the Molong volcanic belt, the Rockley–Gulgong volcanic belt and the Kiandra volcanic belt in the south of the state (Fig. 1.2). In the Central West, the Ordovician igneous rocks are associated with three prominent structural "transverse zones" that are likely to play a role in the localisation of gold deposits, as described below.

Several distinct styles and ages of LFB gold mineralisation are illustrated in the following summaries.

COBAR GOLD FIELD

The Cobar gold field is located on the margin of the Early Devonian Cobar Basin in the northwestern part of Lachlan Fold Belt (Fig. 1.1). It includes Girilambone sedimentary rocks of Cambro-Ordovician age; Wild Wave granodiorite of Silurian age; unnamed silicic volcanics of Early Devonian; Kopyje, Nurri, Amphitheatre, Winduck and Mulga Downs sedimentary rocks of Early to Mid-Late Devonian age (Stegman and Pocock, 1996).

The deposits can be divided into two groups: those in fine grained sedimentary rocks of turbidite facies and those in felsic volcanic rocks and in interbedded sedimentary rocks (Suppel, 1984).

Stegman and Pocok (1996) identified the mineral deposit nature of the Cobar gold field. It includes polymetallic varying from Au-Cu-Pb-Zn at the Peak and New Occidental, Au-Cu at New Cobar and Chesney, and Cu-minor Au at the Great Cobar, Queen Bee and Gladstone. The gold mineralisation occurs as discrete lense within the broader envelopes of base metal mineralisation. Gold mineralisation is restricted to two zones; the Great Chesney fault and the Peak shear system. They are localized along the western margin of the Chesney-Narri anticline at the contact between sandstones of the Chesney Formation and slates and siltstones of the Great Cobar slate.

The Rookery Fault System (RFS) marks the eastern edge of the Cobar gold field. It is a west-dipping fault. It swings in strike from NNW in the south to N at the latitude of Cobar. The Cobar Basin is cut by three main series of internal faults: a set of oblique-slip N to NNW faults, a set of WNW thrusts and a set of NE tear faults (Glen et al, 1996).

Gold production has been active in Cobar since 1880. It has produced 2.5 million ounces of gold and 140,000 tonnes of copper. The Peak, New Cobar mines, and New Occidental are the main gold producers in the Cobar gold field, with the New Occidental being the largest (Stegman, 2001)

NEW OCCIDENTAL GOLD DEPOSIT

The New Occidental gold deposit lies on the contact between the Great Cobar slate and the Chesney formation in the Cobar gold field (Fig.1.1). The Great Cobar slate consists of siltstone and mudstone. The Chesney formation comprises siltstone and sandstone.

The New Occidental gold deposit is localized along the Great Chesney fault. It occurs at or near the southern end of this fault. The orebody is superimposed on the Chesney formation-Great Cobar slate contact and parallels the trace of the Great Chesney fault. The orebody plunges steeply to the north (80°-85°) and dips steeply to the east (85°) parallel to the regional cleavage.

The New Occidental gold deposit comprises at least six lodes developed along a network of curvi-linear north-northwest trending main shears and northwest trending cross-shears. The best gold mineralisation occurs at the intersections of these two shear orientations. It consists mainly of gold with some pyrrhotite and chalcopyrite and occurs principally in quartz and quartz-sulphide veins, and as dissemination (Stegman, 2001): The reserve and resource of the deposit are 1.79 Mt @ 8.00 g/t Au and 0.83 Mt @ 6.00 g/t Au respectively (DMR, 2002a).

MINERAL HILL

MINERAL HILL DEPOSIT

The Mineral Hill deposit (Fig. 1.1) is an example of gold mineralisation in the central LFB in NSW. The oldest rocks in the area are the Cambro-Ordovician Girilambone beds, a sequence of metasediments and mafic volcanics. These are overlain unconformably by the Mineral Hill volcanics-ignimbrites and submarine pyroclastics with intercalated sediments of Siluro-Devonian age. Sandstone and conglomerates of the Devonian Talingaboolba formation in turn overlie these unconformably.

Mineral Hill lies in a NNW corridor of major structures defining the eastern margin of the Cobar trough. Several intrusives and volcanic centres lie in flexures along this belt. It is interpreted as a pull-apart basin and may have been re-activated by dilational sinistral movement at the time of ore formation.

Mineralization is predominantly hosted by the Mineral Hill felsic volcanics that erupted in a sub-aerial to shallow marine setting. Styles of mineralization include porphyry Cu-Zn-Pb-Ag-Au, stratabound Zn-Pb, supergene Cu-Au and epithermal (Collins 1998). The reserve and resource of the deposit are 205 600 t @ 0.74 % Cu, 8.02 g/t Au and 915 600 t @ 0.40 % Cu, 4.10 g/ Au respectively (DMR, 2002a).

PARKES AREA

NORTHPARKES PORPHYRY CU-AU DEPOSIT

The Parkes area contains many deposits including the Peaks Hill and Northparkes (Fig. 1.2). The latter includes four economic porphyry Cu-Au deposits, the Endeavour 22, 26, 27 and 48 ore bodies, that occur within the Ordovician Goonumbla Volcanic Complex of central west NSW (Lickfold et al., 2004). The Northparkes deposit is related to porphyry intrusive rocks hosted by Late Ordovician to Early Silurian volcanics and sediments and Late Devonian sediments. The deposit is located within the Bogan Gate Synclinorial Zone where the Late Ordovician to Early Silurian sequence form a north trending belt which is flanked to the east and west by Late Devonian sediments (Heithersay et al. 1990).

Hydrothermal alteration at the Endeavour deposits, Northparkes, is typically restricted to within 750 m of the quartz monzonite porphyry complexes. The alteration assemblages are largely discontinuous, nonsymmetrical, and do not all occur in all deposits (Lickfold et al., 2004). Disseminated and fracture or vein controlled mineralisation occurs both in the intrusives and the surrounding volcanics. The strongest mineralisation is associated with quartz stockwork veining within the central potassic alteration zones and diminishes outward, accompanied by reduced vein and or fracture density (Heithersay et al. 1990). The proven reserves are 74 Mt @ 1.10 % Cu, 0.4 g/t Au and 103.5 Mt indicated resources @ 1.1% Cu, 0.4 g/t Au (DMR, 2002a).

ORANGE AREA

Two closely associated major gold deposits, the Cadia and Ridgeway deposits, are known southwest of Orange.

CADIA PORPHYRY CU-AU DEPOSIT

The oldest outcropping unit in the Cadia area (Fig. 1.2, 1.5, 2.1) is the Late Ordovician Malongulli formation, which is composed of interbedded quartzose sediments and andesite lavas. They are disconformably overlain by the Late Ordovician Angullong formation. It consists of porphyritic andesite lavas and pyroclastics, sediments and minor limestone.

The Panuara formation of Silurian age unconformably overlies the Angullong formation. It consists mainly of siltstone, with ash tuff, limestone and conglomerate at the base. Tertiary olivine basalt and sanidine trachytes with interbedded clay peat cap the plateau area to the north of Cadia (Bowman, 1995).

The Cadia Hill monzonite intruded Forest Reefs volcanics (volcaniclastics, lavas, subvolcanic intrusions, and minor limestone) and Weemalla formation (siltstone, mudstone, minor volcaniclastics). Emplacement of the Cadia Hill monzonite was probably localized by the development of a major NW to SE trending dilational structure zone (Holliday et al, 1999).

Sulphide mineralisation styles at Cadia include sheeted quartz vein, stockwork quartz vein, disseminated and skarn, all of which are genetically related to an intrusion of predominantly monzonitic composition (Newcrest Mining staffs, 1998; Holliday et al, 1999). The Cadia gold mine produces gold and copper with 200 Mt proven reserves @ 0.73g/t Au and 0.17 % Cu (DMR, 2002a).

RIDGEWAY PORPHYRY CU-AU DEPOSIT

The hosts to the Ridgeway deposit (Fig. 2.1 and 2.2) consist of Late Ordovician monzonite porphyry, monzodiorite and pyroxene porphyry. They intruded relatively flat-lying conformable Forest Reefs volcanics and Weemalla formation to the west of the main Cadia intrusion (Holliday et al., 2002).

Structures cutting the mineralisation had significant pre-mineral movement with the conformable Forest Reefs volcanics-Weemalla formation contact offset by a NW-SE alignment. The northern edge of the deposit is cut by the North fault, a vertical, NW-SE

aligned structure along which a pre-mineral pyroxene porphyry dyke was intruded (Holliday et al, 1999).

The most intense stockwork veining and alteration, and the highest Au and Cu grades, occur immediately adjacent to the monzonite porphyry. The highest-grade portion of the ore-body occurs above the monzonite with reduced grades along the monzonite margins. The intensity of veining and alteration declines both outwards and inwards from the monzonite porphyry margin. This results in a relatively low-grade central portion in the porphyry. Sulphide mineralisation occurs within veins, but also as disseminated grains (Holliday et al., 1999).

The Ridgeway deposit contains 32 Mt probable Au-Cu reserves with @ 2.7g/ Au and 0.76 % Cu. The measured resources is 26 Mt with @ 3.2 g/t Au and 0.92 % Cu. The deposit indicated resources is 13 Mt with @ 2.3 g/t Au and 0.74 % Cu (DMR, 2002a).

BLAYNEY

The Browns Creek gold-copper skarn deposit west of Blayney is an example of post-Ordovician skarn mineralisation. It occurs within a sequence of Ordovician basalt/andesite flows, associated pyroclastics, interbedded limestone and calcareous tuff at the contact with the Late Silurian Carcoar Granodiorite.

The thick Cowriga limestone occurs within the volcanic sequence and forms a triangular inlier in the hinge zone of an open anticline, which plunges gently NNE. The limbs of this anticline dip 45 degrees N to NE, and are cuts by several north trending faults. The limestone lies conformably within the andesite sequence and is truncated to the south by faults and the granodiorite (Creelman et al, 1990).

Faulting and microfracturing of the contact skarn controlled mineralisation. Wollastonite skarn is the preferred host for copper sulphide and gold mineralisation (Surman, 1991). The deposit contains 3.75 Mt indicated resource @ 4.4 g/t Au, 0.28 % Cu (DMR, 2002a).

LAKE COWAL PORPHYRY CU-AU DEPOSIT

The Lake Cowal area in the central western part of the LFB (Fig. 1.2) is covered by a 1-3m thick veneer of Quaternary sediments and a Tertiary laterite profile averaging 10m in thickness. Ordovician volcanic sediments and lava flows are the main host rocks for mineralisation. The volcanic rocks have been subdivided into three units: The Great Flood, The Golden Lava and the Cowal conglomerate. The great flood unit consists of

massive to non-welded pyroclastic debris. The golden lava unit is composed of porphyritic trachyandesite. The Cowal conglomerate consists of massive to graded beds of polymictic volcanic debris interbedded with laminated siltstone and mudstone sphalerite (North Limited Mine Staff, 1995).

Diorite-gabbro stocks, mafic and intermediate dykes, intrude the units. The sequence is offset by two major faults sets; one that strikes 340 degrees and is steeply to vertically dipping; the other strikes 290-300 degrees with a steep northerly dip.

All rocks in the deposit have been altered to assemblages of chlorite, sericite, quartz, epidote, haematite, carbonate, pyrite and K-feldspar. Gold mineralisation occurs primarily in dilational quartz-carbonate-sulphide and carbonate-quartz-sulphide veins. They often contain small amounts of visible gold and better gold grades are commonly associated with sphalerite (North Limited Mine Staff, 1995): The deposit's main commodity is gold. It has 66.4 Mt indicated resources at 1.5 g/t Au (0.8 g/t Au cut off) (DMR, 2002a).

1.6 TECTONIC SETTING

The Ordovician volcanic rocks in Central West NSW are subduction related and are arc-related. Neodymium and Pb isotopic data show no influence of continental crustal material in the source region, the most likely setting is an intra-oceanic island arc developed on an ocean floor crust that may have been Cambrian volcanic rocks that form the basement below the Silurian-Devonian troughs (Glen et al., 1997).

The formation of the arc is ascribed to contemporaneous west-dipping subduction of the palaeo-Pacific plate. The separated volcanic belts (Junee-Narromine belt, Molong belt, Rockley-Gulgong and Kiandra) are structural relics of one large volcanic entity that was dismembered by extension and strike slip faulting (Glen et al., 2003).

Three main zones of Ordovician volcanic rocks have been identified in the LFB: the Junee-Narromine Volcanic belt in the west, a central Molong Volcanic Belt and an eastern Gulong Volcanic Belt. These belts are intersected by prominent northwest trending structural corridors termed the Nyngan Tranverse Zone, (NTZ; Hilyard et al. 1996), the Hunter River Tranverse Zone (HRTZ; Glen and Beckett, 1997) and the Lachlan Tranverse Zone (LTZ; Glen and Wyborn, 1997). The intersections of the Ordovician volcanic belts with the transverse structural zones appears to have provided a locus for the restricted emplacement of high-K to shoshonitic magmas associated with

porphyry gold-copper mineralisation at many of the major deposits in the LFB. For example, the Cadia, Ridgeway, Browns Creek and Northparkes Cu-Au deposits are localised in the LTZ (Glen et al. 1997).

The LTZ is a WNW-trending feature that crosses N-S, arc parallel, LFB Ordovician volcanic belts at high angle (Fig 1.2) (Glen et al., 1997). It is a major crustal tear oblique to the convergent margin between the Australian and proto-Pacific plates (Glen et al. 1998b). The location of its boundaries varied since its inception in the Middle Ordovician (Glen et al. 1999). Whereas Lower Ordovician volcanic rocks are widespread in the LFB, the restricted association of Middle Ordovician volcanic rocks with the LTZ suggest it became active during west dipping subduction at this time (Glen et al. 1998, 1999 and 2003).

Hills (1956) first suggested that the NWN alignment of the Lachlan River was controlled by a tectonic lineament. Scheibner and Stevens (1974) suggested the presence of a Lachlan River Lineament based on the common trends of the elongated shape of the Bathurst Batholith and Tertiary volcanics around Mt. Canobolas as well the orientation of smaller lineaments. The Lachlan Transverse Zone is wider than, but incorporates the Lachlan River Lineament. Glen and Watkins (1994) defined a structural zone of plunge changes east of Orange between Mt. Canobolas and Bathurst Batholith called the Lachlan River Fault Zone that corresponds to the northern part of the Lachlan Transverse Zone. The southern part of the Lachlan Transverse Zone may extend south to the largely buried Moorilda Monzonite, and large intrusive in the Blayney Basalt (Wyborn and Henderson, 1993) and to the northern edge of the east-west trending Forest Reefs Complex and Weemala Formation. The western part of the Lachlan Transverse Zone is defined structurally by west-northwest-trending faults. Farther east, in Eastern Belt, the Lachlan Transverse Zone is defined as a corridor containing west-northwest-trending folds and faults (Glen and Walshe, 1999).

Seismic studies provide evidence that supports the existence of the LTZ. First, they identify the presence of north-and south-dipping reflections that lie oblique to the east and west-dipping reflections north of the Lachlan Transverse Zone (Glen et al. 2002). These north-and south-dipping reflections correlate with the east west to west-northwest-trending structures inferred to exist within the Lachlan Transverse Zone.

The second line of evidence is supported by the refraction data that show major changes in crustal velocity oblique to the north-south line, centered approximately under the proposed location of the Lachlan Transverse Zone. A prominent south-dipping

velocity boundary occurs in the basement between the Molong Volcanic Belt and the turbidite basin (Finlayson et al. 2002). The boundary corresponds closely to a major (35 km long) fault that has previously been interpreted as the southern limit of the Lachlan Transverse Zone (Glen and Walshe, 1999).

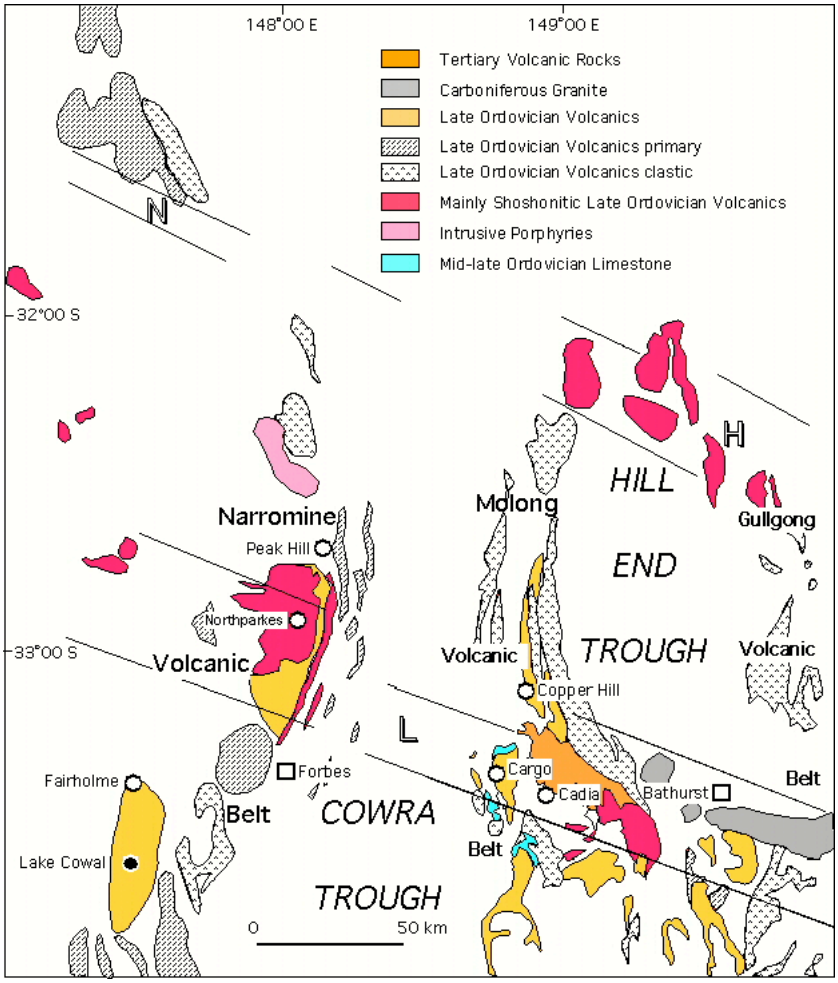

Figure 1.2. Distribution of Ordovician igneous rocks in relation to main transverse structures and gold deposits in the central Lachlan Fold Belt in NSW (after, Glen et al., 1997). N = Nyngan Transverse Zone; H = Hunter River Transverse Zone; L = Lachlan Transverse Zone.

1.7 COMMON FEATURES OF CU-AU PORPHYRY DEPOSITS

Studies of Cu-Au deposits associated with porphyry-style intrusions world-wide have described certain common features such as deposit size, shape and grade; mineralisation types dominated by networks of thin veins; characteristic alteration mineral assemblages linked to sequential or progressive alteration processes; and recurring structural or

tectonic settings (Lowell and Guilbert, 1970). These studies have resulted in common generalised models being applied to porphyry deposits. Although deposits of the LFB do not share all of the features of typical porphyry, it is useful to summarise the general model to establish a point of reference.

American Porphyry Cu-Au deposit models have been heavily influenced by studies such as those on the San-Manuel – Kalamazoo deposit (Arizona) described by Lowell and Guilbert (1970). It consists of a cylindrical porphyry body that are surrounded by successive alteration envelopes and a network of thin veins that contain the ore (Fig. 1.3). The terminology applied to the alteration assemblages is now widely used for similar occurrences associated with numerous hydrothermal deposits.

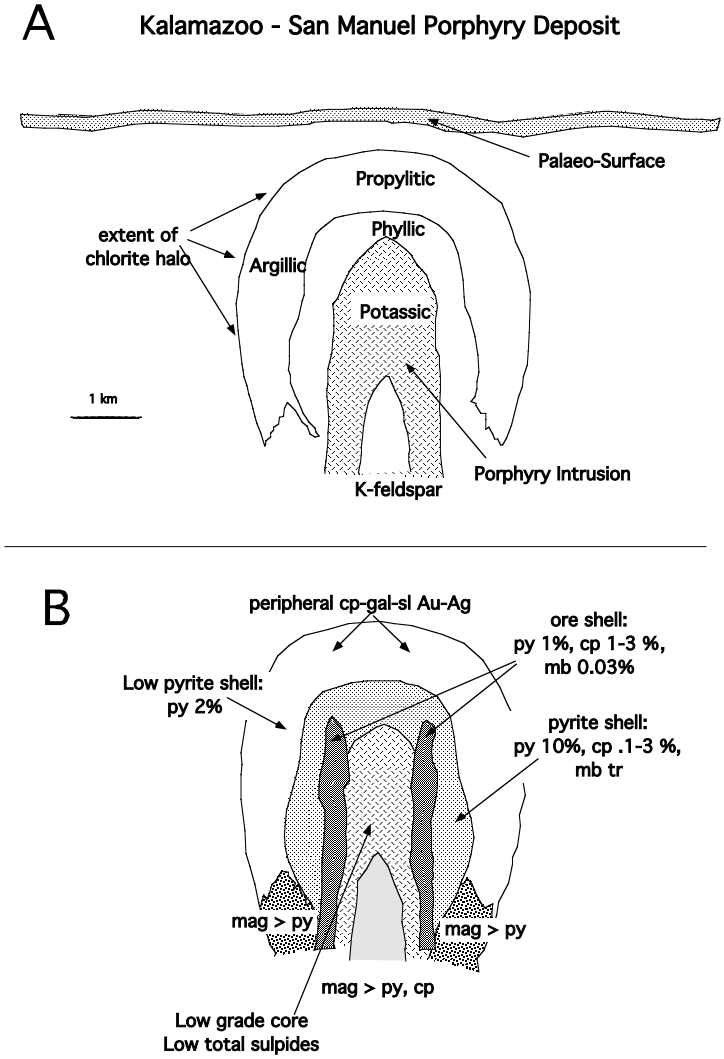

Figure 1.3. Simplified model of the Kalamazoo – San Manuel porphyry deposit illustrating the typical form of examples in the southwest United States. Simplified from Guilbert and Park (1986). A. Distribution of alteration mineral assemblages (Potassic is equivalent to K-silicate in Table 1.1.). B. The distribution of porphyry-related mineralisation.

The assemblages typically develop progressively over time. Table 1.1 summarizes these assemblages in their typical order. The earliest alteration types are generally focussed at greater depths than later assemblages, although this is not always true and may be difficult to confirm because of overprinting by successive assemblages.

Table 1.1 Typical Porphyry Deposit Alteration Mineral Assemblages

Alteration Type	**Associated Mineral Assemblage**
K-silicate	biotite, magnetite, orthoclase, quartz, anhydrite, chalcopyrite, actinolite;
Propylitic	chlorite, epidote, calcite, pyrite, albite
Intermediate Argillic	sericite, chlorite, kaolinite or illite, pyrite, calcite
Phyllic (sericitic)	sericite, quartz, pyrite
Advanced Argillic	alunite, kaolinite, pyrophyllite, quartz, dickite, gibbsite, pyrite, enargite, covellite
Calc-silicate	garnet, pyroxene, epidote, wollastonite -restricted to deposits associated with carbonate host rocks

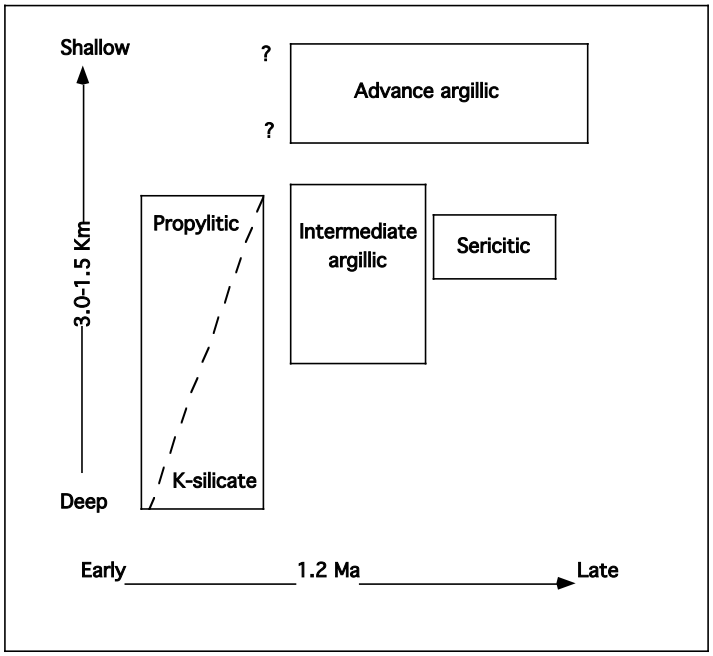

Figure 1.4 Schematic time-depth relations of principal alteration types in gold-rich porphyry copper systems and other types of porphyry deposits (after Sillitoe, 1993b).

Most of the western Pacific porphyry Cu-Au deposits are Tertiary to Quaternary in age. In contrast Cadia Cu-Au deposit is a relatively rare example of a major Ordovician porphyry deposit (Cooke et al., 1998). Although there is still some debate about the tectonic setting of the LFB during the Ordovician, most young porphyry deposits display a strong association with convergent margins and subduction zones at both continental margins and in island arcs (Sillitoe, 1993). For example, many < 10 million year old deposits are documented around the Pacific Rim (Sillitoe, 1989) where their young age allows for detailed study of the structural setting at the time of minersalisation.

Tectonic and structural studies of Irian Jaya – Papua New Guinea have been combined with mine-scale studies of major porphyry deposits such as the 2.6 – 4.4 Ma Grasberg deposit and the 1.1 – 2.6 Ma Ok Tedi deposit to resolve the key structural requirements of these major mineralisation events (e.g. Hill et al., 2002). As discussed further in Chapter 5, these young deposits are sited along major trans-crustal fracture zones that bear some resemblance to the transverse zones documented in the LFB (see 1.7). Similar structures have localized ore related magmatism near the Domeyko-West fault in northern Chile which hosts the Chuquicamata, El Abra, La Escondida deposits and the Kalimantan Suture in Indonesia, which hosts the Kelian deposit, Mt Muro (Corbett, 1998). There are many similarities but also some distinctions between LFB magmatic Cu-Au deposits and the typical magmatic Cu-Au systems described worldwide.

As noted above, epithermal, porphyry, skarn and mesothermal deposits are all recognised in the LFB. In this regard it is comparable to other world magmatic Au-Cu districts (Cooke et al., 1998). Corbett (1998) provided a detailed assessment of structural features in the LFB. It comprises mainly N-S arc parallel structures, some of which occur as terrain boundaries and host ore systems: the Gilmore Suture hosts the Mt Adra, Gidginbung, and Wyalong deposits. At the deposit scale in the LFB, almost all the mineralised vein systems display WNW orientations and are constrained between N-S arc parallel structures. The same type of relationships is often evident at the larger scale where mineralisation often appears associated with a perturbation episode that is atypical of the main structures. For example, mineralization along the N-S Gilmore Suture occurs within WNW-NW flexures.

Major porphyry deposits generally develop under conditions of rapid emplacement where dilatant fractures facilitate the continued evolution of large volumes of magmatic fluids to shallow levels until mineral deposition is promoted by cooler conditions. At Cadia (Cadia Hill deposit), such a strongly dilatant environment is

evidenced by the sigmoidal-shaped sheeted-vein system with a pronounced down-dip continuation formed as a jog between two N-S structures (Corbett, 1998). Despite this typical porphyry structural feature, the Cadia Hill deposit is a southwest dipping (65 deg) tabular body of sheet quartz veins rather than the typical upright cylindrical form of many deposits of this class (Fig. 1.4).

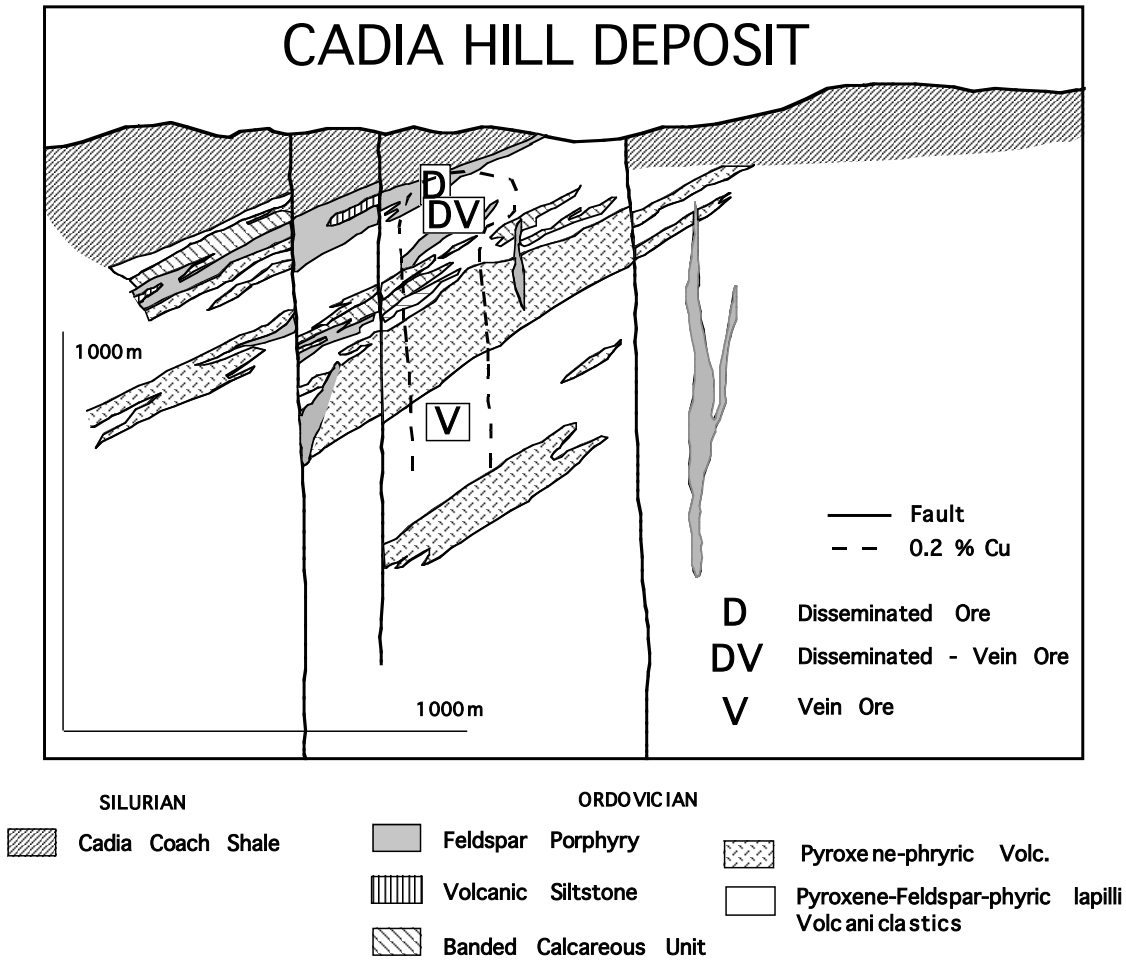

Figure 1.5 A simplified cross-section of the Cadia Hill deposit illustrating the difference in form and ore distribution relative to a southwestern USA model (Fig. 1.3). Adapted form Holliday et al. (2002).

Andesitic volcanism and porphyritic diorite to quartz diorite intrusions characterise most of the Philippines and Indonesian porphyry deposits (Cooke et al. 1998). A range of rock types also hosts the LFB deposits. The Cadia deposit is hosted by a monzonite intrusion that is relatively unusual in terms of its shoshonitic K-enrichments (Holliday et al. 2002), which are not common for other large deposits of the Pacific region (e.g., the low-K tholeiite to calc alkaline eastern Bismark intrusions of PNG: Hill et al., 2002).

1.8 RESEARCH METHODOLOGY

The LFB and its gold deposits share many features with younger gold districts. However, very few high-precision analyses are available for the gold deposits of NSW. Accordingly, igneous complexes associated with a world-class deposit (Ridgeway) and relatively minor (Copper Hill, Cargo, Fairholme) LFB gold deposits were selected for a new study. Cadia data, from the unpublished study of Green (2001), was also compared with the new Ridgeway data. In broad terms, the study was designed to assess whether the nature and geologic setting of magmatism could be correlated with the scale of gold mineralisation.

More specifically, a total of 94 new samples were collected in order to assess the nature of Ordovician magmatism in the LFB and characterise possible variations in magma evolutionary trends with respect to a) a major transverse structure (the Lachlan Transverse Zone) and b) gold deposit size and mineralisation style. Samples were subject to whole rock chemical analysis by the commercial facilities of Actlab Pacific Pty of Perth (WA) using a combination of Inductively Coupled Plasma (ICP) for major elements and ICP Mass Spectrometry for trace elements. The wide range of elements analysed by ICP-MS included many that are relatively immobile (Rollinson, 1993) during the moderate weathering of the host rocks typically present in NSW deposits. As a result, differences between igneous systems at the various study sites could be assessed despite weathering effects. Disturbance of primary chemical signatures was evident in strongly veined samples, however, and these effects were taken into account during interpretation of results. Petrographic and electron microprobe studies were carried out on polished thin sections corresponding to whole rock chemical samples in order to characterise igneous rocks and crystal fractionation processes as well as to identify mineralisation-related alteration or weathering effects.

CHAPTER 2
STUDY LOCALITIES AND SAMPLE PETROGRAPHY

2.1 INTRODUCTION

This study examines Ordovician igneous suites of the LFB at the Cargo gold deposit, the Copper Hill gold deposit, the Fairholme gold prospect, the Nasdaq gold prospect and the Ridgeway gold deposit. It summarises the field localities and provides descriptions of the sampled rocks along with their typical petrographic characteristics. Electron microprobe analyses were carried out on primary and secondary mineral phases in selected samples of the Bathurst, Cargo, Cadia, Copper Hill, Fairholme, and Ridgeway deposits (Appendix 1).

2.2. LOCALITIES AND SAMPLE DESCRIPTIONS

RIDGEWAY DEPOSIT

The Ridgeway deposit lies 500 m below the surface; 3 km northwest of the Cadia Hill open cut mine (Fig. 2.1), and was discovered in November 1996 by Newcrest geologists (Holliday et. al, 1999). It is a part of a Late Ordovician- Early Silurian porphyry alteration mineralisation system that extends over an area of at least 6 X 2 km within the Ordovician Molong Volcanic Belt of the Palaeozoic (Newcrest Mining Staff, 1999). The Ridgeway deposit is an upright bulbous body of stockwork quartz veining zoned about a small (50-100m-diameter) plug with an elliptical, pipelike geometry elongated along a west-northwest-striking axis of the Cadia Hill Monzonite porphyry. The horizontal dimensions of this stockwork are approximately 150 x 250m by at least 600m vertically (Fig. 2.2; Newcrest Mining Staff, 1998, Wilson et al., 2004). The plug was intruded into the relatively flat lying Forest Reefs Volcanic and Weemalla Formation to the west of the main Cadia intrusion. The Weemalla Formation is the stratigraphically lowest unit recognised at Ridgeway and comprises fine-grained, planar-laminated siltstone with minor beds of volcanic sandstone. Mineralisation at Ridgeway is spatially related to three groups of monzonite intrusions (early, inter, and late mineral), all of which postdate the emplacement the monzodiorite (Wilson et al., 2004) Spatially related pre-mineral intrusions include monzodiorite and pyroxene porphyry dykes.

The most intense stockwork veining and alteration and the highest Au and Cu grades occur immediately adjacent to the monzonite porphyry. The richest part of the ore body, 3.20g/t Au (Holliday et al. 2002), occurs above the porphyry and lower grade, 2.30-1.30g/ Au (Holliday et al. 2002) occurs along the margins of the intrusion. The intensity of veining and alteration declines both outwards and inwards from the monzonite porphyry margin. This results in a small low-grade central portion in the monzonite porphyry (Holliday et al, 1999).

The Ridgeway samples encompass the range of lithologies present within the deposit and include dioritic to monzonitic mafic units as well as intermediate rocks. The mafic lithology is typically fine to medium grained, green-grey porphyritic chlorite-sericite altered diorite with feldspar and abundant pyroxene phenocrysts. The more evolved monzodiorites and quartz monzonite porphyry are generally porphyritic and pink coloured. Samples for this study are moderately to strongly mineralised and therefore secondary sulphides and veining are commonly present.

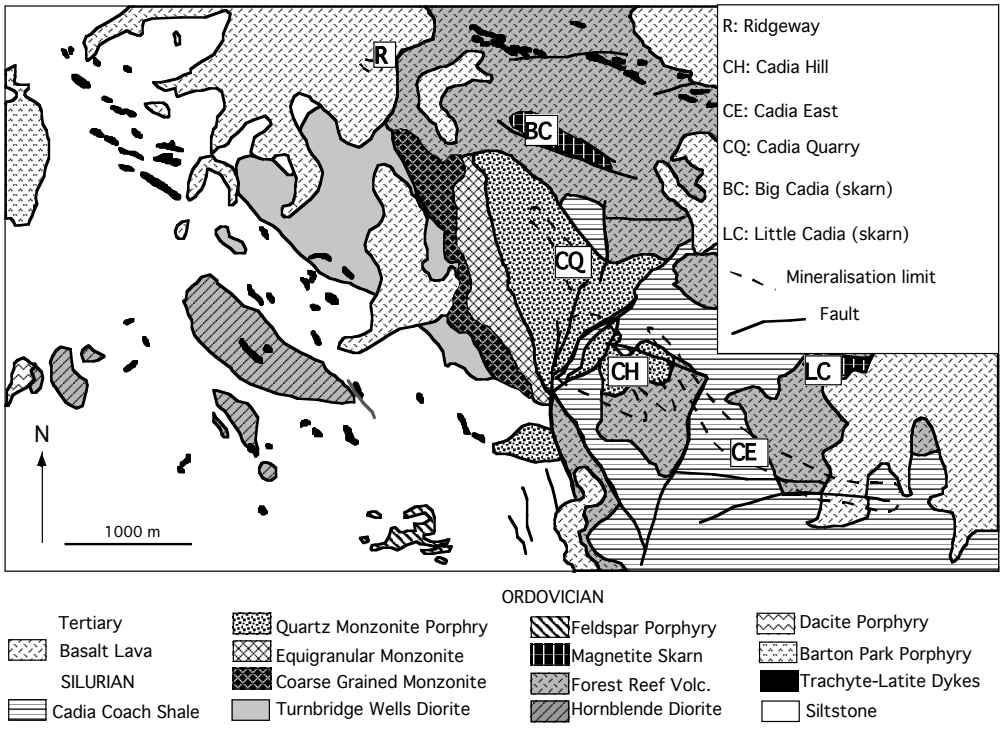

Figure 2.1 Simplified geological map of the Cadia area showing main rock types, faults and the location of gold (porphyry) and iron (skarn) mineralisation. For location of the Cadia-Ridgeway deposits in the Lachlan Fold Belt of NSW see Figure 1.1. Adapted from Holliday et al. (2002).

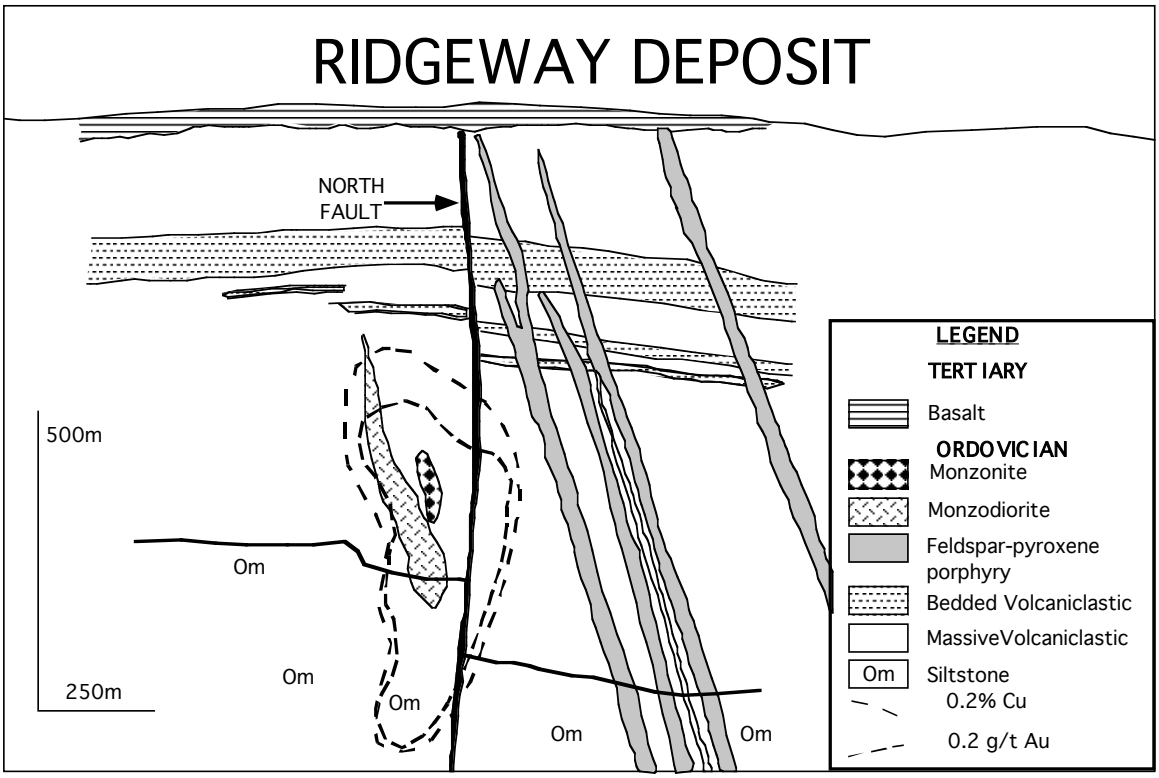

Figure 2.2. Cross section of the Ridgeway deposit illustrating mineralisation associated with monzodiorite and monzonite intrusive phases. Adapted from Holliday et al. (2002).

In thin section (Fig. 2.3) the diorites are porphyritic with euhedral to subhedral phenocrysts of pyroxene (Fig. 2.3A) and feldspar (Fig. 2.3B). The pyroxene is clinopyroxene (0.1 to 3.5 mm) and is generally altered to chlorite, epidote, magnetite and hematite but relatively fresh zones are preserved in some crystals (Fig. 2-3A, 2.4D).

The pyroxenes of the Ridgeway diorite, monzodiorite and monzonite porphyry range in composition from augite to Fe rich augite. They have limited variations in Al, Ca, Fe and Mg contents (1.7 to 2.4 wt. % Al_2O_3; 20 to 22 wt. % CaO; 5.2 to 6.36 wt. % Fe_2O_3 and 14.5 to 15.8 wt. % MgO (Appendix 1).

By comparison, the pyroxenes of the Cadia diorite, monzodiorite, synogranite, quartz monzonite and volcanic porphyry are augite and diopside (Green, 2001). Their MgO contents are lower than the Ridgeway samples and vary around 13.5 wt. %. However, their Al_2O_3 contents are higher than the Ridgeway and have a wider variation, 0.7 to 5.1-wt % (Green, 2001). The Cadia and Ridgeway pyroxenes have similar CaO contents.

Euhedral 0.2 to 1.8 mm secondary amphibole, possibly after hornblende, has itself been partially altered to chlorite and epidote. The Ridgeway and Cadia amphiboles are all actinolitic amphibole with Ca >> Na (11.7 to 12.5 wt. % CaO and 1.2 to 1.6 wt. % Na_2O) (Appendix 1; Green, 2001). They are aluminium poor amphiboles but distinct Al_2O_3 contents of 1.1 to 3.1 wt. % for the Ridgeway diorite and monzodiorite versus 2.4 to 6.0 wt. % for the Cadia volcanic porphyry reflect differences in primary rock compositions.

Subhedral plagioclase, 0.3 to 4.0 mm wide (Fig. 2.3B), is sericitised and chloritised. Euhedral to subhedral orthoclase, 0.3 to 2mm, has undergone potassic and sericitic alteration and relict grains now contain crystals of magnetite and chalcopyrite at the Ridgeway and Cadia deposits.

Quartz occurs as subhedral 0.1 to 0.5 mm secondary crystals indicative of hydrothermal overprinting. Magnetite, chalcopyrite and pyrite (Fig. 2.5E, F) appear related to mineralisation and occur as disseminated crystals in the rock matrix and within hydrothermal veins. The hydrothermal veins comprise Ca carbonate, chlorite-epidote and chlorite-epidote-quartz-carbonate assemblages (Fig. 2.4A, B). Chlorite and sericite are the major alteration minerals throughout the groundmass of Ridgeway diorites.

One of several globally recognised porphyry-related alteration assemblages (Sillitoe, 1991), the Potassic alteration assemblage, is widespread at Ridgeway. It comprises biotite, orthoclase, actinolite and magnetite. As a result, Ridgeway is distinctive among the study areas in that iron oxides (see 4.6) are dominated by a non-magmatic, low-Ti, variety of magnetite (Appendix 1). Hematite at Ridgeway is also part of the porphyry-related hydrothermal system as a component of the propylitic type alteration (Appendix 1), rather than a late surface-weathering product. Locally in the deposit, a chromian muscovite (fuchsite) also occurs as a secondary mineral phase in RW 4 (1) 1(Appendix 1).

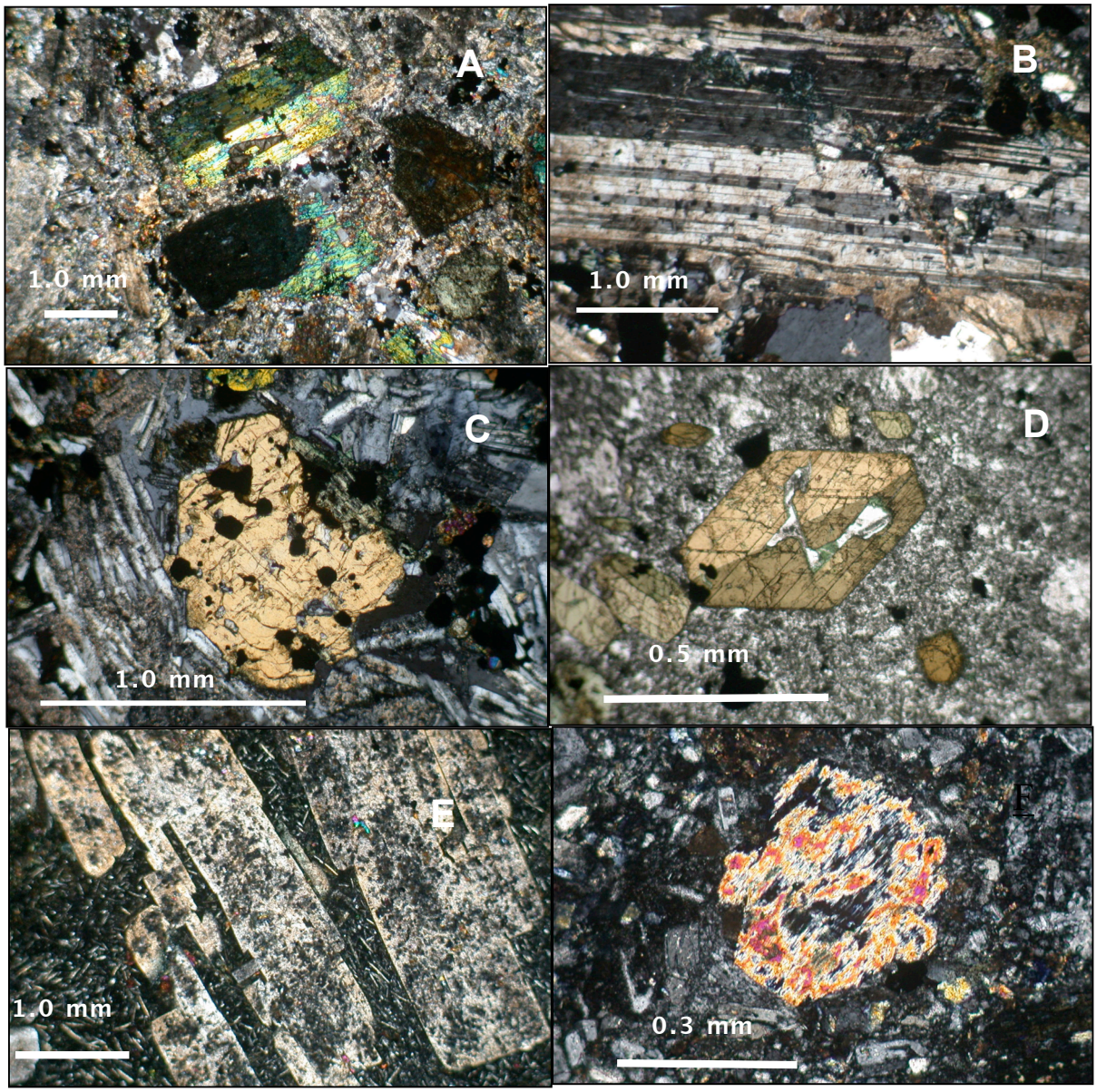

Figure 2.3. Igneous silicate minerals in LFB Ordovician igneous rocks. **A**. Slightly altered clinopyroxene - Ridgeway deposit (sample RW 13); **B**. Plagioclase, Ridgeway deposit (RW7); **C**. Clinopyroxene, Fairholme prospect (DR37-258); **D**. Unaltered Hornblende, Fairholme prospect (DR42-180); **E**. Sericitised plagioclase, Nasdaq ansdesite (NAS 3); **F**. Altered pyroxene, Nasdaq intrusive phase (NAS 1). All under crossed polars.

CARGO DEPOSIT

The Cargo deposit is located 10 km west of the Cadia-Ridgeway intrusive complex (Figs. 1.1, 1.2). A sequence of andesite to trachyandesite lavas, pyroclastic and epiclastic sediments of the Cargo Andesite formation have been intruded by the Cargo Intrusive Complex comprising coeval calc-alkaline diorite, quartz diorite and dacite porphyries. The complex is localised at a major structural intersection (Golden Cross Resources, 2001).

Subsequent intrusions into the structural zone by a differentiated alkalic suite developed a zoned complex of monzodiorite, quartz monzonite, monzonite and local syenite (Golden Cross Resources, 2001). Cargo is a large gold-copper mineralised porphyry system approximately 3 km by 2 km in size. It hosts 14 gold reefs mined at the turn of last century (Golden Cross Resources, 2001).

The Cargo samples were collected from diamond drill cores at several locations (Fig.2.4) in order to maximise coverage of the compositional spectrum of the complex. Collected samples include both intrusive and volcanic rocks and exhibit a large degree of compositional variation. The intrusive rocks are diorite, monzonite and granodiorite. They are typically massive porphyritic.

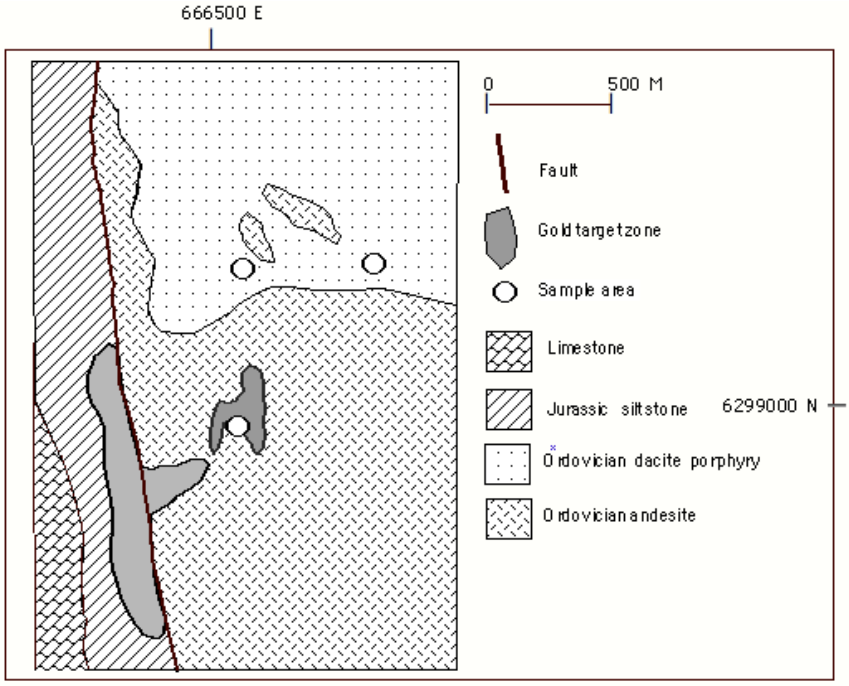

Figure 2.4 Simplified geology of Cargo deposit. Modified after Golden Cross Resources Ltd (2002). See Figure 1.1 for location.

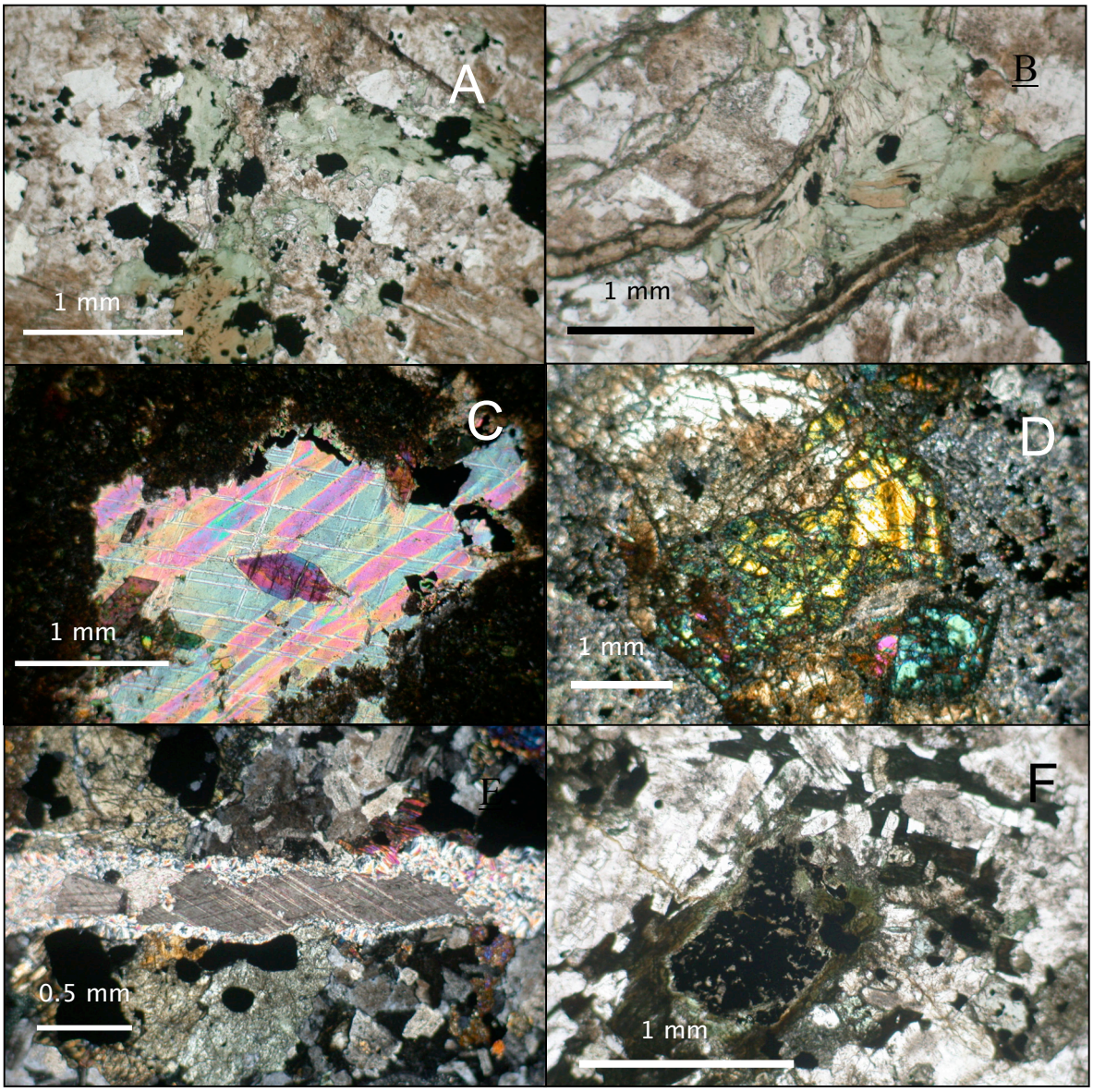

Figure 2.5. Alteration-related silicate and carbonate minerals in LFB Ordovician igneous rocks. A. & B. Chlorite after mafic minerals under plane-polarised light, Ridgeway (RW9). C. Calcite with epidote (centre) under crossed polars, Fairholme (DR42-119). D. Epidotised clinopyroxene under crossed polars, Ridegway (RW13). E. Carbonate – muscovite vein under crossed polars, Cadia Hill deposit (CD10). F. Green secondary biotite with magnetite replacing igneous mafic minerals under plane polarised light, Fairholme (DR 37-258).

The alteration mineralogy consists of K-feldspar, chlorite, epidote, sericite and carbonate. Alteration in the samples varies from disseminated secondary minerals, through to spots or clots of secondary assemblages, to distinct selvages on veins and pervasive overprinting of primary assemblages in the most intensely mineralised samples. The hydrothermal veins consist mainly of carbonate, quartz, chlorite, magnetite, pyrite and chalcopyrite.

The volcanic rocks include basalt, andesite, latite, dacite and rhyodacite. They range from glassy and aphyric, to porphyritic, and a few of them are brecciated. The alteration mineralogy includes chlorite, actinolite, silica, sericite, carbonate, epidote and K-feldspar. Alteration varies from disseminated secondary minerals to distinct vein selvages and pervasive overprinting of primary features. Hydrothermal veins consist of carbonate, quartz, epidote, chlorite, epidote-chlorite, quartz-epidote and pyrite.

In thin section the intrusive samples show porphyritic texture with relatively uniform distribution of phenocrysts. Euhedral clinopyroxene, 0.3 to 3 mm, has been partially to completely altered to chlorite, epidote, magnetite and hematite. Chlorite and magnetite replace hornblende amphibole.

Euhedral to subhedral plagioclase, 0.3 to 4 mm, has been partially to completely altered to sericite, carbonate, actinolite, chlorite, magnetite and pyrite. Euhedral to subhedral orthoclase, 0.4 to 1 mm, has altered to secondary K-feldspar and magnetite. Epidote, chlorite, K-feldspar and magnetite replace biotite. Euhedral actinolite, 0.1 to 0.5 mm, forms single crystals after other phenocrysts. Early chlorite occurs as interstitial grains. Subhedral quartz and carbonate, 0.2 to 0.8 mm, occur as disseminated secondary minerals and in veins. Disseminated chalcopyrite is associated with chlorite veins. Magnetite and pyrite are associated with chlorite-epidote-altered zones (Fig. 2.5D).

The volcanic samples display porphyritic texture but have variable phenocryst content. In thin section, chlorite, epidote, pyrite, chalcopyrite, silica, magnetite and hematite strongly replace ferromagnesian crystals. Feldspar, plagioclase and sanidine, 0.4 to 4 mm, have altered to sericite, carbonate, actinolite and pyrite. Quartz and carbonate, subhedral, 0.2 to 1mm, occur as magmatic and as hydrothermal veins. The groundmass is composed of quartz, carbonate, biotite, feldspar, magnetite, chlorite and sericite. Magnetite, pyrite and chalcopyrite are associated with chlorite-alteration zone (Fig. 2.5C).

COPPER HILL DEPOSIT

Copper Hill, the site of the first copper mine in NSW, is located approximately 40km north of the Cadia mine (Figs. 1.1, 1.2). It is a part of the Late Ordovician- Early Silurian porphyry alteration mineralisation system of the Ordovician Molong Volcanic Belt.

Intermediate to mafic volcanic rocks and volcanically derived sediments of the Lower Ordovician Fairbridge Volcanics suite are overlain by the Reedy Creek limestone of Middle Ordovician age. Quartzite, sandstone and andesite of the Upper Ordovician Cheeseman's Creek Formation occur conformably above the Reedy Creek limestone. The Ordovician sequence has been intruded and overlain by an igneous complex consisting of sub-volcanic intrusive dacite and diorite.

A moderate to strong hydrothermal alteration accompanied the intrusive phase. To date, exploration has identified one main zone of mineralisation 300m long, 50m wide and up to 200m deep. It hosts porphyry-style quartz-magnetite sheeted veins and stockwork related to an early phase of magmatic, potassic alteration (Golden Cross Resources, 2001)

Golden Cross Resources (2004) reported estimate resource from various companies, and also undertake it own geostatistical resource estimation to give a feel for the possible mineral resource inventory of the Copper Hill (Table 2.1)

Company	Tonnes (millions)	Copper (%)	Gold (g/t)	Palladium (g/t)
Anaconda	134.00	0.17		
Cyprus	22.90	0.51	0.69	
Golden Cross Operations	6.60	0.80	0.80	
Golden Cross Operations	1.90	0.85	1.74	
ComputerAidedGeoscience	0.48	1.20	1.05	0.04
ComputerAidedGeoscience	18.50	0.55	0.55	0.02

Table 2.1 Copper Hill mineral resources. Adapted from Golden Cross Resources Ltd (2004).

The Copper Hill samples were collected from diamond drill holes NCH6 and NCH8 in the vicinity of the Copper Hill open cut (Fig. 2.6). The samples comprise intrusive rocks varying from diorite to monzonite and volcanic rocks ranging from basalt

to dacite. The intrusive lithologies are typically porphyritic, green-grey and pink-grey, diorite, quartz diorite and monzonite. The volcanic lithologies are also commonly porphyritic, dark brown, grey brown and pink-grey, basalt, andesite and dacite. The intrusive and volcanic rocks contain varying amounts of secondary of sericite, chlorite and potassium feldspar.

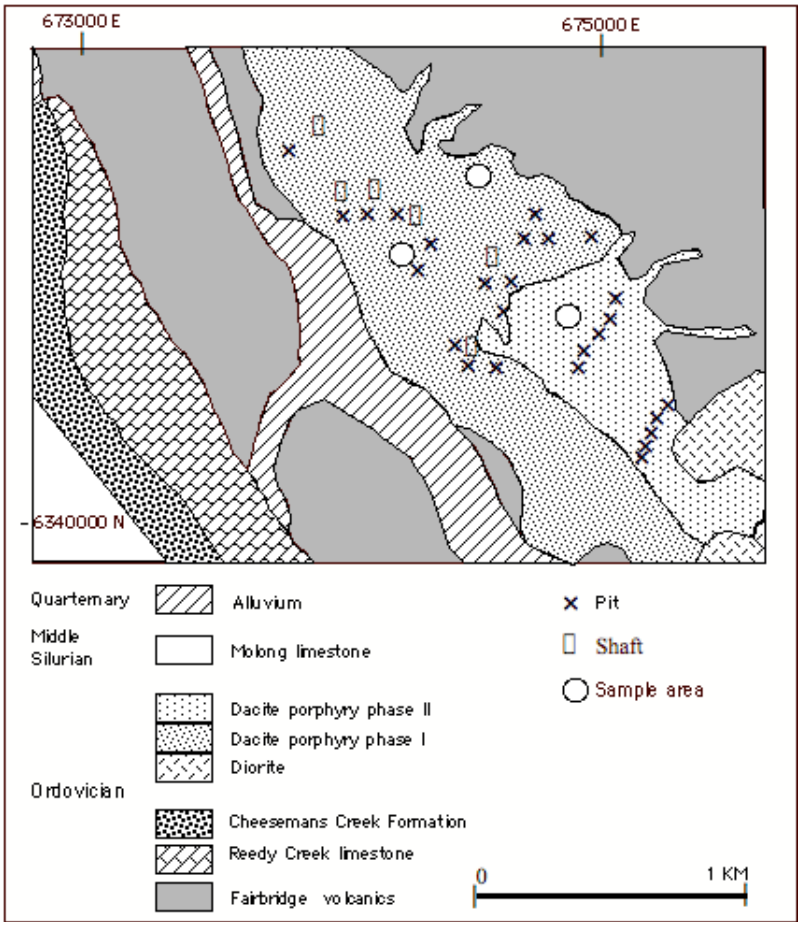

Figure 2.6 Simplified geology of Copper Hill deposit. Modified after Golden Cross Resources Ltd (2002). See Figure 1.1 for location.

In thin section, the intrusive samples are porphyritic with euhedral to subhedral feldspar phenocrysts mainly 0.4 to 1mm orthoclase with about 16 wt.% K_2O (Appendix 1). They have altered to sericite, carbonate, chlorite, secondary K-feldspar, quartz, epidote, chalcopyrite and pyrite (Appendix 1). Euhedral to subhedral epidote, 0.4 to 1 mm, occur as single crystals or as aggregates of crystals.

Pyroxene, amphibole and biotite are often completely replaced by chlorite, epidote, quartz, carbonate, chalcopyrite, pyrite, magnetite, galena and hematite (Fig. 2.5H). Quartz occurs as disseminated, subhedral 0.2 to 0.5 mm crystals, and as hydrothermal veins. Magnetite, chalcopyrite and pyrite are disseminated in the rock matrix but are more abundant in or near hydrothermal veins and veinlets that mainly consist of carbonate-epidote-quartz assemblages.

The basaltic volcanic rocks are porphyritic with euhedral to subhedral feldspar phenocrysts. Feldspar includes both 0.3 to 2mm plagioclase and 0.2 to 0.8 mm K-feldspar. Their groundmass is typically altered to assemblages of sericite and secondary K-feldpsars, quartz, epidote, carbonate and magnetite.

Chlorite, carbonate, epidote, quartz, actinolite, magnetite and pyrite partially to completely replace pyroxene, amphibole and biotite. Quartz occurs as disseminated, 0.3 to 4 mm, crystals and as hydrothermal veins. Carbonate and quartz-carbonate-chalcopyrite-pyrite veins also occur.

Hematite subtypes can be distinguished at Copper Hill on the basis of compositions determined by microprobe analysis. Three subtypes include Fe-Ti-Mn, Fe-Ti and Fe varieties (Appendix 1). The latter occurs in veins whereas the other two types occur within the rock matrix and may reflect compositions influenced by a range of primary minerals such as pyroxenes and amphiboles.

FAIRHOLME PROSPECT

The Fairholme prospect is located 20 km north-northwest of the Cowal gold deposit (Figs. 1.1, 1.2). It covers the Late Ordovician Fairholme igneous complex of the Ordovician Junee Narromine Volcanic Belt of the LFB. The deposit consists of andesitic-basaltic vesicular lavas, volcaniclastics and fine-grained argillaceous sediments. Intruding this sequence are latite porphyries, andesite porphyries, microdiorite and diorite. All of these units belong to the Ordovician Fairholme igneous complex.

The Ordovician units are overlain by up to 120m of Quaternary cover. Drilling has delineated three zones of alteration and low Cu/Au mineralisation: the Boundary Prospect, 800 x 500m, the Gateway Prospect, 2 km x 500m, and the Dungarvan Prospect, 2 km x 700m (Newcrest mining Limited staff, unpublished report).

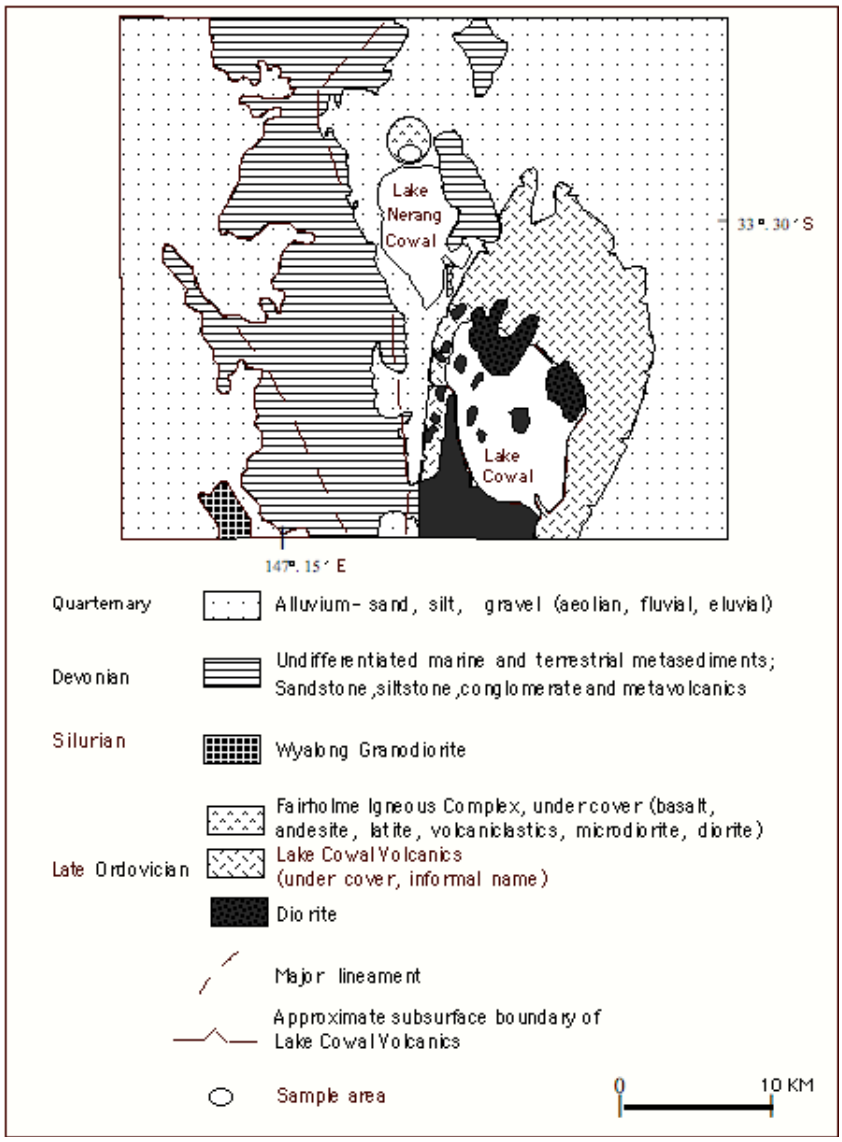

Figure 2.7 Simplified geology of Fairholme deposit. Modified after North Ltd (1995) and Newcrest Mining Ltd (1997). See Figure 1.1 for location.

Collected samples (Fig.2.7) at the three prospects are either chips from Reverse Circulation drilling or core samples from diamond drilling and include both intrusive and volcanic rocks. The intrusive rocks are weakly mineralised and are commonly porphyritic. They contain sericite-carbonate-chlorite-epidote-actinolite-silica and potassic alterations. They are, massive, grey and dark grey diorite and granodiorite. Hydrothermal veins include carbonate and quartz.

The porphyritic and foliated volcanic rocks are more strongly mineralised than the intrusive rocks. They range from basalt to andesite and latite. The alteration mineralogy is

sericite, carbonate, silica, epidote, chlorite, actinolite and potassic. The alteration types include patchy, disseminated, spotted, nodular and pervasive. Hydrothermal veins comprise carbonate, biotite, quartz and chlorite-actinolite.

In thin section, the intrusive samples are typically porphyritic with euhedral to sudhedral phenocrysts of clinopyroxene (Fig. 2.3C), 0.7 to 1.9mm that are mainly altered to chlorite, epidote, magnetite, hematite, pyrite and silica. They are also commonly pseudomorphed by assemblages of chlorite, actinolite, epidote and magnetite.

The Fairholme amphiboles are Ca-Mg-Fe and Ca amphiboles, tremolite and hornblende. The tremolite contains 10.40-12.25 wt % CaO; 9.81- 12.11 wt % MgO and 5.9- 8.37 wt % Fe_2O_3 (Appendix 1). Euhedral to subhedral hornblende amphibole, 0.3 to 0.6 mm, contains 11.8- 12.1 wt % CaO and 1.9- 2.1 wt % Na_2O; 12.4 –13.7 wt % MgO; 4.4 –7.3 wt % Fe_2O_3; 12.5 –12.9 wt % Al_2O_3 (Appendix 1). The hornblende is commonly altered to tremolite (they are distinct in Al_2O_3 content, 1.5–2.0 wt.% for tremolite and 12.5 –12.9 wt % for hornblende), or a mixture of epidote, chlorite and magnetite.

Euhedral to subhedral plagioclase (10 – 14 wt.% CaO) and orthoclase, 0.3 to 1 mm and 0.4 to 1.8 mm, have altered to sericite, carbonate, epidote, chlorite, actinolite and secondary K-feldspar. Subhedral biotite is replaced by epidote, chlorite, magnetite, hematite and silica. Subhedral quartz, 0.2 to 0.4 mm, occurs as disseminated crystals and in hydrothermal veins. Carbonate forms as both interstitial and hydrothermal vein types. Disseminated magnetite is associated with epidote-chlorite altered zones.

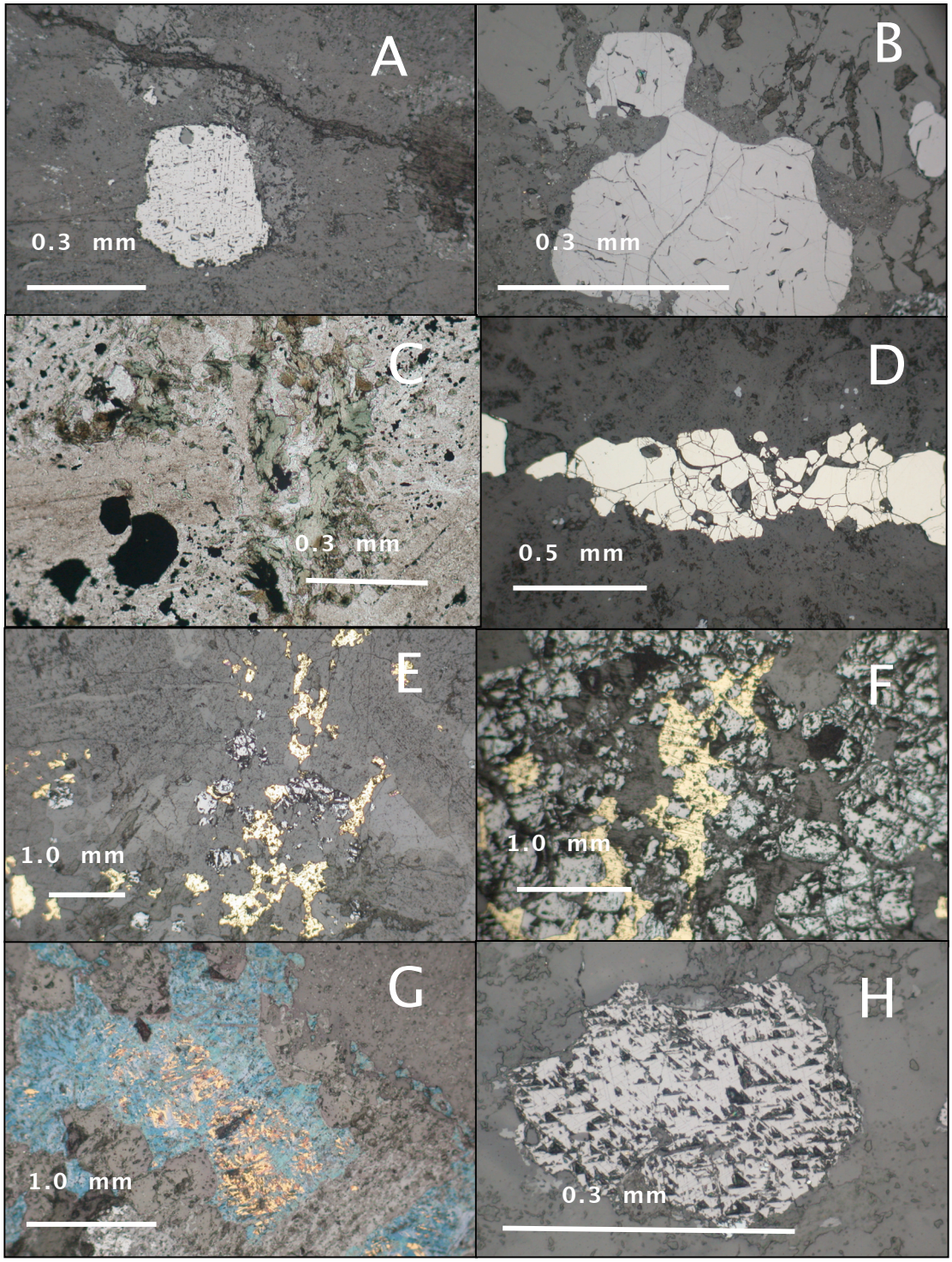

Figure 2.8 Primary and alteration-related opaque minerals in LFB Ordovician igneous rocks. **A.** Igneous magnetite, Cadia (CD 12); **B.** Secondary magnetite, Cadia (CD 8); **C.** Magnetite with chlorite after breakdown of mafic minerals, Cargo (CN1-195-6); **D.** Magnetite veinlet, Cargo (CN11-43.8); **E. & F.** Pyrite and magnetite (RW9); **G.** Bornite with chalcopyrite, Ridgeway (RW1); **H.** Galena, Copper Hill (NCH6-119.70).

Microprobe analyses identify a range of Cr and Ti contents (Appendix 1) in hematite compositions at Fairholme. Chromium haematite (1.7-4.2 wt. % Cr_2O_3, 0.001-0.02 wt. % TiO_2 and 52.3-52.6 wt. % Fe_2O_3) occurs as inclusion in mafic minerals whereas comparatively Ti-rich haematite (0.03-0.09 wt. % Cr_2O_3, 5.3-6.9 wt. % TiO_2 and 52.5-61.5 wt. % Fe_2O_3) occurs in the groundmass.

The porphyritic basaltic volcanic samples range from massive to foliated. Primary clinopyroxenes are euhedral to subhedral, 0.4 to 2.5mm, prismatic to elongate. Fresh zones in the pyroxenes of the basalt porphyry are augite and diopside. They contain higher CaO contents than Cadia or Ridgeway 23.0 to 24.1 wt %. Secondary minerals replacing or overprinting pyroxene include epidote, chlorite, silica, actinolite, magnetite, hematite, chalcopyrite and pyrite.

Euhedral to subhedral amphibole, 0.4 to 1 mm, prismatic to elongated (Fig. 2.3D), has commonly been altered to epidote, chlorite and magnetite. Subhedral biotite, 0.6 to 1 mm, tabular to elongate, has altered to epidote, chlorite, silica and magnetite. Sericite, chalcopyrite and pyrite replace subhedral plagioclase, 0.3 to 1 mm, tabular to elongate.

Subhedral quartz, 0.2 to 0.3 mm occurs as disseminated crystals and in hydrothermal veins. The Groundmass comprises sericite, plagioclase, quartz, carbonate, magnetite, pyrite and chalcopyrite. Carbonate, actinolite, pyrite, chlorite and epidote fill cavities (Fig. 2.4C). Pyrite, chalcopyrite and magnetite are disseminated in the chlorite-epidote-altered zone. Disseminated chalcopyrite is associated with carbonate veins.

NASDAQ PROSPECT

The Nasdaq Cu - Au prospect is located approximately 30 km north of the town, Boorowa, south of the Cadia-Ridgeway mines (Fig 1.1). It occurs in Late Ordovician intermediate intrusive rocks, diorite, and intermediate volcanic rock, andesite, which belong to the Carbonne group of the Palaeozoic Lachlan Fold Belt.

The Carbonne group includes limestone, aphyric basalt, interbedded volcanic mudstone-siltstone and volcaniclastic sandstone, volcanolithic sandstone, chert pebble conglomerate, volcanic conglomerate, massive basalt and andesite and undifferentiated Kenyu formation (Geological Survey of NSW, 2002). Exploration has delineated a 320m Cu – Au mineralised zone along strike (DMR, 2002b).

Nasdaq samples were collected from outcrops at the prospect and include dioritic intrusive rocks and andesite (Fig. 2.9). The intrusive rocks are cryptocrystalline, massive, dark apple green-grey, mineralized micro diorite. Hydrothermal chlorite-epidote veining crosscuts the intrusive rocks.

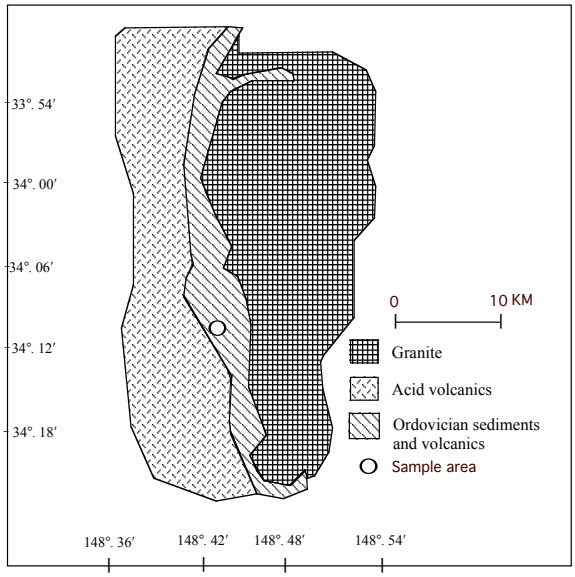

Figure 2.9 Simplified geology of Nasdaq prospect. Modified after Gateway mining (2004). See Figure 1.1 for location.

In thin section, the intrusive samples are commonly porphyritic. Euhedral clinopyroxene (Fig. 2.3F), 0.5-0.8 mm, has been altered to chlorite, magnetite, hematite, pyrite, and chalcopyrite. Chlorite, epidote, magnetite, hematite, pyrite and chalcopyrite completely replace amphibole.

Euhedral- subhedral feldspar (plagioclase and orthoclase), 0.1- 1 mm, has been altered to sericite, chlorite, epidote, actinolite, K-feldspar, pyrite and chalcopyrite. Chlorite, hematite magnetite and pyrite replace subhedral- euhedral, 0.1 to 0.5 mm biotite. Subhedral, 0.1 to 0.2-mm quartz, occurs as interstitial crystals. Chalcopyrite, pyrite and magnetite are disseminated in the rock matrix, particularly in the chlorite-K-feldspar altered-zone and in chlorite-epidote veins.

The Nasdaq andesite is strongly feldspar porphyritic (Fig. 2.3E). The feldspars (plagioclase and sanidine) are euhedral to subhedral and 1 to 4 mm wide. Both feldspars may be strongly altered to sericite, epidote, actinolite, silica, hematite, chalcopyrite and pyrite. Chlorite, epidote, hematite, pyrite and chalcopyrite completely replace

ferromagnesian crystals. The groundmass consists of plagioclase, sanidine, quartz, chlorite and pyrite.

2.3 SUMMARY

Petrographic analysis and microprobe results establish a wide range of primary and secondary features within the Ordovician rocks examined in this study. For example, calc alkaline to shoshonitic affinities are supported by the variable abundance of primary K-feldspars. Primary mineral phases such as pyroxenes and igneous magnetite provide an indication of the fractionating mineral assemblages responsible for igneous trends in magma chemistry assessed in the following chapters.

The most pervasive alteration is associated with highly mineralised shoshonite Ordovician rocks at Ridgeway and Cadia. The less mineralised calc alkaline Ordovician rocks at Cargo, Copper Hill and Fairholme, are less altered overall, although secondary mineral assemblages are locally abundant.

The hydrothermal mineral assemblages documented in these LFB deposits are characteristic of younger Cu-Au Porphyry style mineralisation (Sillitoe, 1991). Subtle variations within deposits and differences between study areas are more readily observed in thin section than in hand specimen. For example, several varieties of chlorite occur at several sites. Fe- and Mg-rich chlorite occurs at Ridgeway, Fe-rich chlorite at Cadia and in Bathurst regional samples, and Fe- and Mg-poor chlorite are present at Copper Hill, Cargo and Fairholme (Appendix 1).

The high Ti-Mn-Cr content of iron oxides in the Bathurst, Fairholme and Copper Hill are indicative of a primary, magmatic, origin. In contrast, the low abundance of these elements in the Ridgeway iron oxide indicates a hydrothermal source typical of porphyry-related alteration (Guilbert and Park, 1986). The variable content of Ti, Mn, and Cr in Cadia iron oxides suggests a combination of magmatic and hydrothermal magnetites.

Many varieties of carbonates are observed at the different study localities. For example, Ca-carbonate at Ridgeway and Cadia (Fig. 2.4E) (a few Ca-Fe-Mg carbonates were found in association with iron oxides at Ridgeway) and various Ca, Ca-Fe, Ca-Fe-Mn carbonates are observed at Bathurst, Fairholme and Copper Hill (Appendix 1).

CHAPTER 3
MAJOR ELEMENT CHEMISTRY

3.1 INTRODUCTION

This chapter examines the major element chemistry of Ordovician igneous suites in the LFB. New data is reported for rocks of the Cargo, Copper Hill, Fairholme, Nasdaq and Ridgeway deposits located inside and outside the Lachlan Transverse Zone.

The Ridgeway and Cadia samples are closely associated and occur in the Cadia igneous complex. Together with the Cargo igneous suite they are located inside the LTZ. In contrast, Copper Hill, Fairholme and Nasdaq igneous suites occur outside the LTZ.

Additional data for Cadia and Ridgeway for samples described as unaltered by Holliday et al. (2002) and Blevin (2002) are included in the database. Samples from the Cadia mine and the Bathurst region from Green's (2001) Honours thesis are also included in chemical plots for comparative purposes.

3.2 VARIATION DIAGRAMS

The major element oxides are first plotted on variation diagrams against Al_2O_3/TiO_2 because 1) this ratio effectively monitors igneous fractionation, 2) the ratio consists of two element oxides that are immobile under a wide range of alteration and weathering conditions, and 3) a ratio is not susceptible to the effects of mass addition or loss associated with the movement of mobile elements.

These and other bivariate graphs or scattergrams are used to assess the interrelationship between elements in the data set in order that geochemical processes such as crystal fractionation may be characterised (Rollinson, 1993). The evolution of the various Ordovician igneous suites can then be assessed to evaluate possible links between magma sources or magma evolution versus gold (± copper) mineralisation.

Maximum Al_2O_3/TiO_2 values for each locality provide an indication of the degree of magma evolution in each area. For example, maximum Al_2O_3/TiO_2 values obtained in this study correspond to felsic rocks at Cargo, which possess silica contents in excess of 70 wt. %. Given that Ordovician intrusions in the LTZ encompass more evolved compositions than those found outside the LTZ, Al_2O_3/TiO_2 values are trend to higher values within the regional structure (LTZ).

Discussion of the major elements in the following sections is grouped according to whether their behaviours are typically compatible (i.e., preferentially concentrated in solid phases) or incompatible (i.e., tend to concentrate into magma melts).

3.2.1 COMPATIBLE MAJOR ELEMENT VARIATION DIAGRAMS

The major elements Ca, Fe, Mg, Mn, P and Ti tend to decrease in abundance in a magma as it evolves because they have higher concentrations in the early-formed minerals, such as plagioclase, pyroxene, amphibole and magnetite, than in the associated magma. The Cadia, Ridgeway, Fairholme and Nasdaq samples are restricted to mafic – intermediate compositions and therefore occur at low Al_2O_3/TiO_2 values. The regional Bathurst dataset, Cargo, and Copper Hill samples include more evolved magmas and extend over a correspondingly larger range of Al_2O_3/TiO_2.

The CaO contents of Fairholme, Copper Hill, Ridegway and Cadia samples tend to higher values at lower Al_2O_3/TiO_2 (Fig. 3.1A) but igneous trends are not well preserved. This behaviour suggests that igneous trends caused by the removal of the plagioclase, pyroxene, and amphibole were partially disturbed by the widespread carbonate alteration observed in thin sections.

The intrusive and volcanic samples show similar relatively well-defined Fe_2O_3 trend (Fig. 3.1B). As expected, Fe_2O_3 contents decrease with rising Al_2O_3/TiO_2 values, indicating that iron was removed from mafic silicates and magnetite. Some samples, mainly from Cadia and Ridgeway appear to define a Fe-rich sub-trend above the main trend that may reflects magnetite accumulation or hydrothermal magnetite formation that is supported by petrographic evidence and microprobe data showing low-Ti compositions (see 2.2). The Bathurst, Cadia, Copper Hill, Fairholme, Nasdaq and Ridgeway samples extend to low Al_2O_3/TiO_2 values and therefore include lower Fe contents.

The MgO contents of all data sets decline with increasing Al_2O_3/TiO_2 values because of fractional crystallisation process involving the removal of olivine, pyroxene, amphibole and biotite. The volcanic and intrusive samples have similar relatively well-defined trends (Fig. 3.1C).

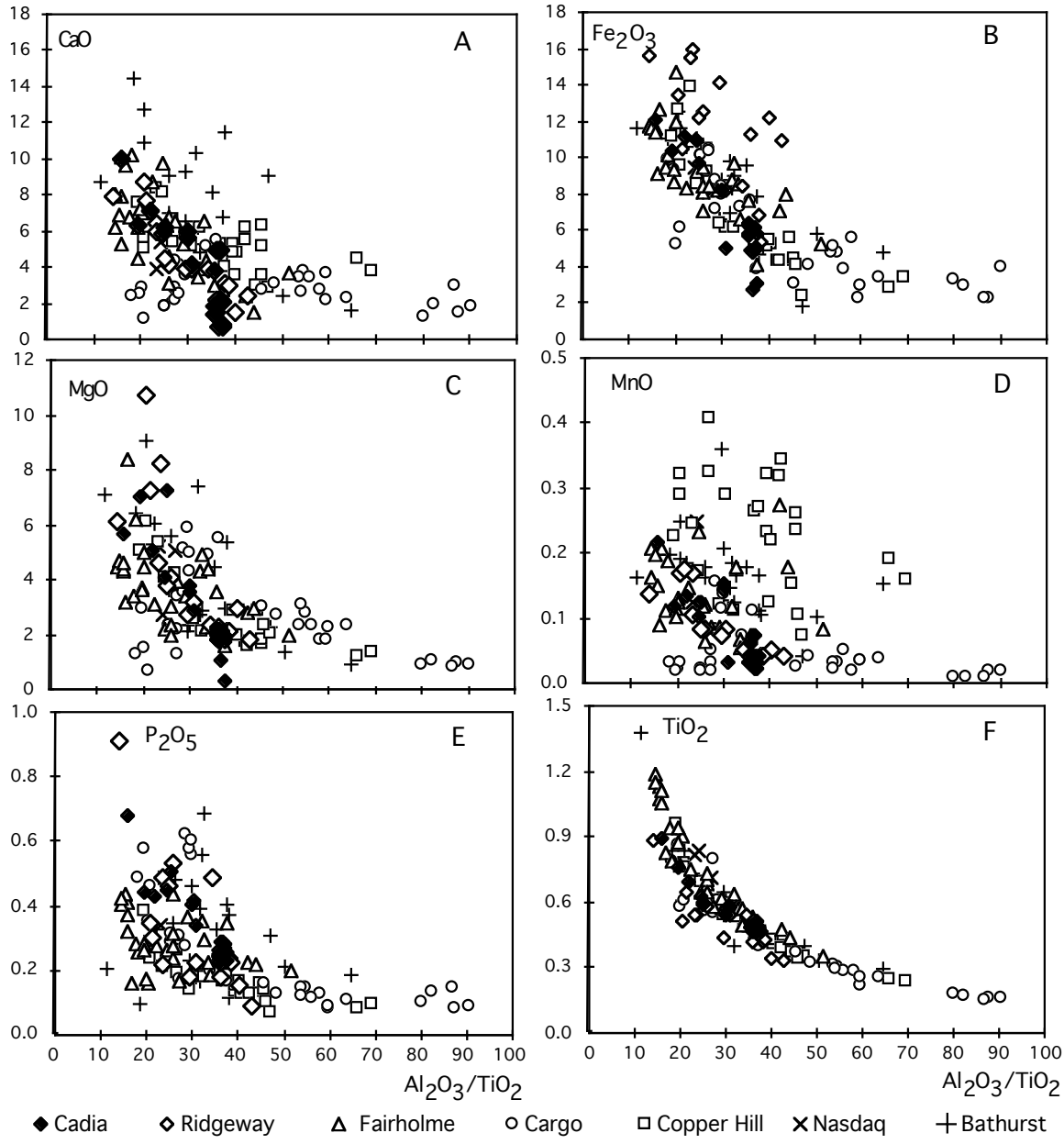

Figure 3.1. Variation diagrams for compatible major elements (as weight % oxides) versus Al_2O_3/TiO_2 in Ordovician igneous rocks of the Lachlan Fold Belt in NSW.

The intrusive and volcanic samples display relatively broad scatter in the MnO trend (Fig. 3.1D). The Copper Hill samples are characterised by high MnO contents. The P_2O_5 trend of intrusive samples is similar to the P_2O_5 trend of volcanic samples (Fig. 3.1E). The fact that P_2O_5 contents drop with increasing Al_2O_3/TiO_2 values indicates apatite fractionation occurred. However, a few of Ridgeway and Cadia samples have high P contents, with maximum abundances of 0.9 wt % P_2O_5, compared to other Ordovician rocks with similar Al_2O_3/TiO_2, possibly as a result of hydrothermal processes.

As expected, TiO_2 contents decrease with increasing Al_2O_3/TiO_2 values. The intrusive and volcanic samples both exhibit a well-defined TiO_2 trend (Fig. 3.1F). The Cargo samples display maximum variation in TiO_2 and Al_2O_3/TiO_2 values. A sub-group of Fairholme samples at high TiO_2 contents define a tight trend suggesting they are closely related. Some Cadia – Ridgeway samples fall beneath the main trend between Al_2O_3/TiO_2 = 20 to 40.

All of the Ordovician igneous suites, both inside and outside the LTZ, have similar compatible major element variation trends. The compatible element data does not provide a particularly effective means to discriminate between the various igneous suites. Some distinctive features such as high Fe contents, or relatively low Al contents (giving low Al_2O_3/TiO_2 values), among Ridgeway and Cadia samples may reflect atypical fractionation involving comparatively more magnetite accumulation or greater amounts of feldspar removal. For the most part alteration is moderate and only samples collected adjacent to, or including, hydrothermal veins have been strongly altered.

3.2.2 INCOMPATIBLE MAJOR ELEMENTS DIAGRAMS

A plot of Al_2O_3 versus Al_2O_3/TiO_2 (Fig. 3.2A) provides additional information versus Figure 3.1F. The low Al content of Cadia – Ridgeway samples accounts for the off-trend samples in the previous figure. Intermediate volcanic rocks from Fairholme, Cargo, and the Bathurst region display high Al contents but Fairholme intrusive rocks show a much greater range of Al_2O_3 contents over a narrow Al_2O_3/TiO_2 and therefore are unlikely to have undergone much Fe-oxide fractionation. Conversely, Copperhill exhibits a narrow range of Al_2O_3 contents over a wide range Al_2O_3/TiO_2, which probably results from magnetite fractionation and the removal of Ti. Cargo exhibits a similar wide range of Al_2O_3/TiO_2 values although Al_2O_3 contents are more variable and peak at ~ 21% Al_2O_3.

The behaviour of Na_2O (Fig. 3.2B) varies between the study areas but no strong patterns are evident. Overall, the distribution of Na_2O is likely to reflect a combination of processes including 1) fractionation of several Na-bearing minerals such as albitic feldspars, pyroxene, and amphibole, 2) alteration linked to mineralization, and 3) weathering of some near-surface samples.

The distribution of K_2O is similar to that of Na_2O, with no strong correlations with Al_2O_3/TiO_2 evident for particular sites (Fig. 3.2C). However the overall data set does suggest two main trends (ie, a High- and Low-K trend) that are also present in the

regional Bathurst sample set. The result suggests that two igneous suites may be present at individual localities, which could obscure correlations for some elements. The subject of multiple suites at individual localities is discussed further on the basis of trace element geochemistry in Chapter 4. The intrusive and volcanic samples of all study areas exhibit positive correlations between SiO_2 and Al_2O_3/TiO_2. Silica-rich Cargo samples at low Al_2O_3/TiO_2 (~ 22) are the products of non-igneous quartz veining (Fig. 3.2D).

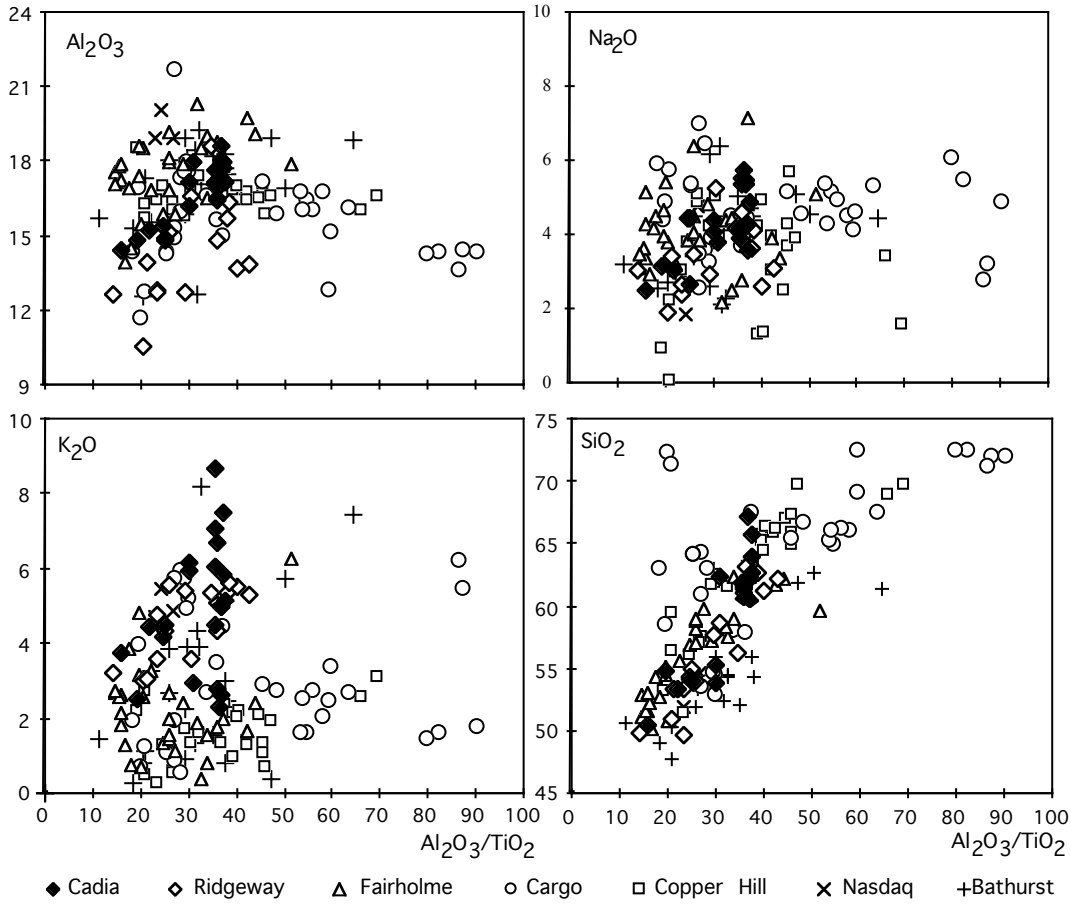

Figure 3.2. Variation diagrams for incompatible major elements (as weight % oxides) versus Al_2O_3/TiO_2 in Ordovician igneous rocks of the Lachlan Fold Belt in NSW.

In summary, the incompatible major element variation diagrams suggest distinct trends among Ordovician rocks inside and outside of the LTZ. Potassium contents in particular suggest two trends. Other results highlight sporadic alteration in the sample set. Major element oxide discrimination plots from the literature are considered below. These have two purposes: the can be used to characterize individual samples and to characterize igneous suites based on trends defined by sets of samples. Accordingly, the plots establish a preliminary classification of the samples.

3.3 CHEMICAL CLASSIFICATIONS

3.3.1 K_2O VERSUS SiO_2 CLASSIFICATION

Rock samples are classified in (Fig. 3.3) according to the K_2O vs. SiO_2 diagram of Rickwood (1989) and Le Maitre et al. (1989) that assigns samples to particular igneous suites. They exhibit considerable variation in compositions that range from low K tholeiitic, calc-alkaline, high-K calc alkaline and to shoshonite series.

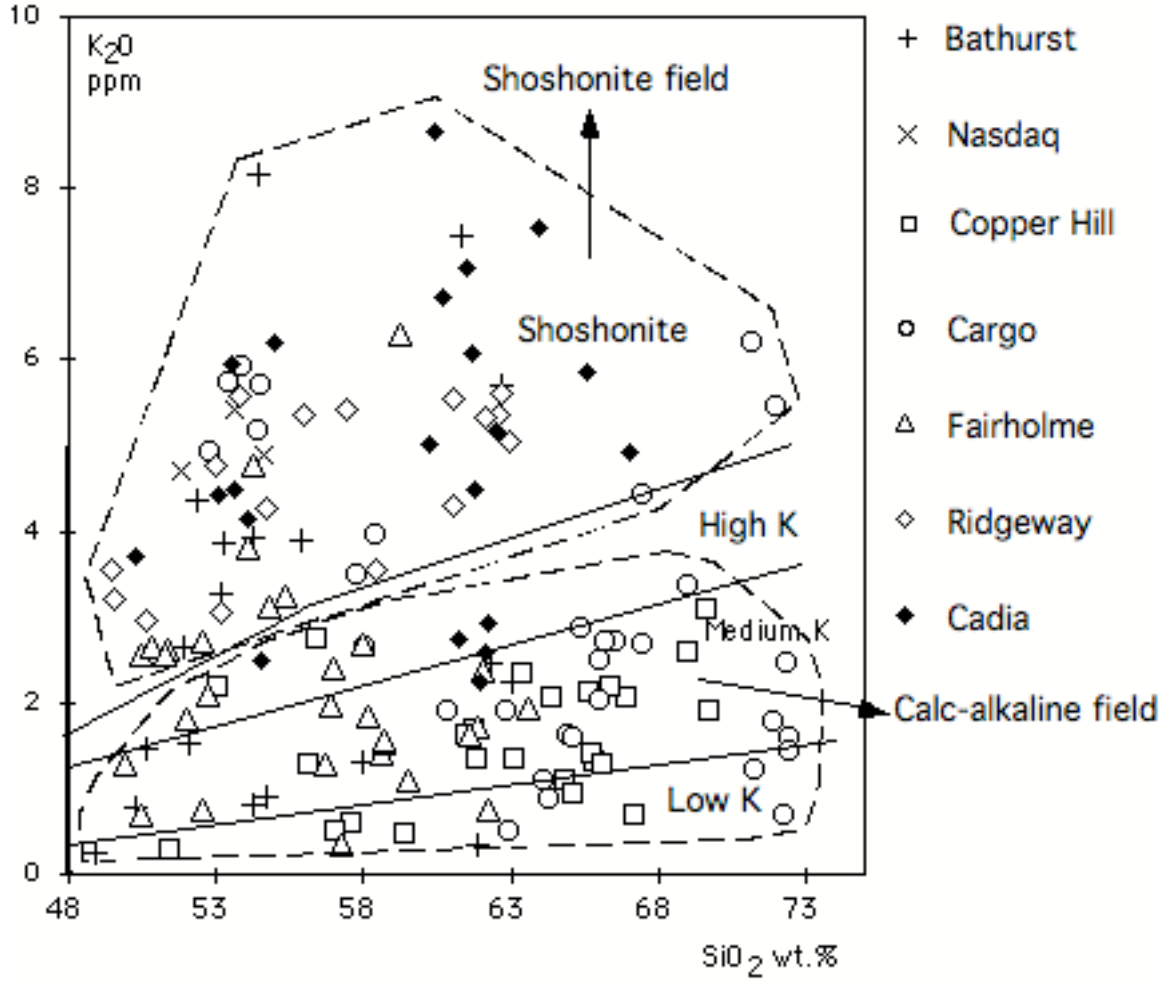

Figure 3.3. A K_2O versus SiO_2 classification plot for Ordovician igneous rocks of the Lachlan Fold Belt in NSW. Adapted from La Maitre et al. (1989) and Rickwood (1989). Medium K and Low K are also termed calc alkaline and tholeiite series respectively.

The Cadia and Ridgeway samples plot as high-K calc-alkaline to shoshonite in composition. They define a clear trend although a few Cadia samples that lie off the trend, as a result of hydrothermal alteration. The Cargo, Bathurst and Fairholme sample sets each plot in several fields extending from tholeiitic to high-K calc-alkaline series and

shoshonite series. The Copper Hill samples range form tholeiitic to calc-alkaline in composition. Based on the plot of K_2O versus Al_2O_3/TiO_2 (Fig. 3.2C), this broad range of data may be tentatively subdivided into two main trends as indicated by the dash fields added to the K_2O vs. SiO_2 plot.

Although susceptible to alteration, this plot confirms the Ordovician magmas were generally derived from sources rich in K_2O, consistent with a subduction-hybrid mantle (Blevin, 2002).

3.3.2 TAS CLASSIFICATION

Rocks samples are classified by their total alkalis (K_2O + Na_2O) vs. SiO_2 content on the TAS diagram of Le Maitre et al. (1989). The plot is mainly used to classify samples as particular rock types rather than assigning them to suites (Fig. 3.4).

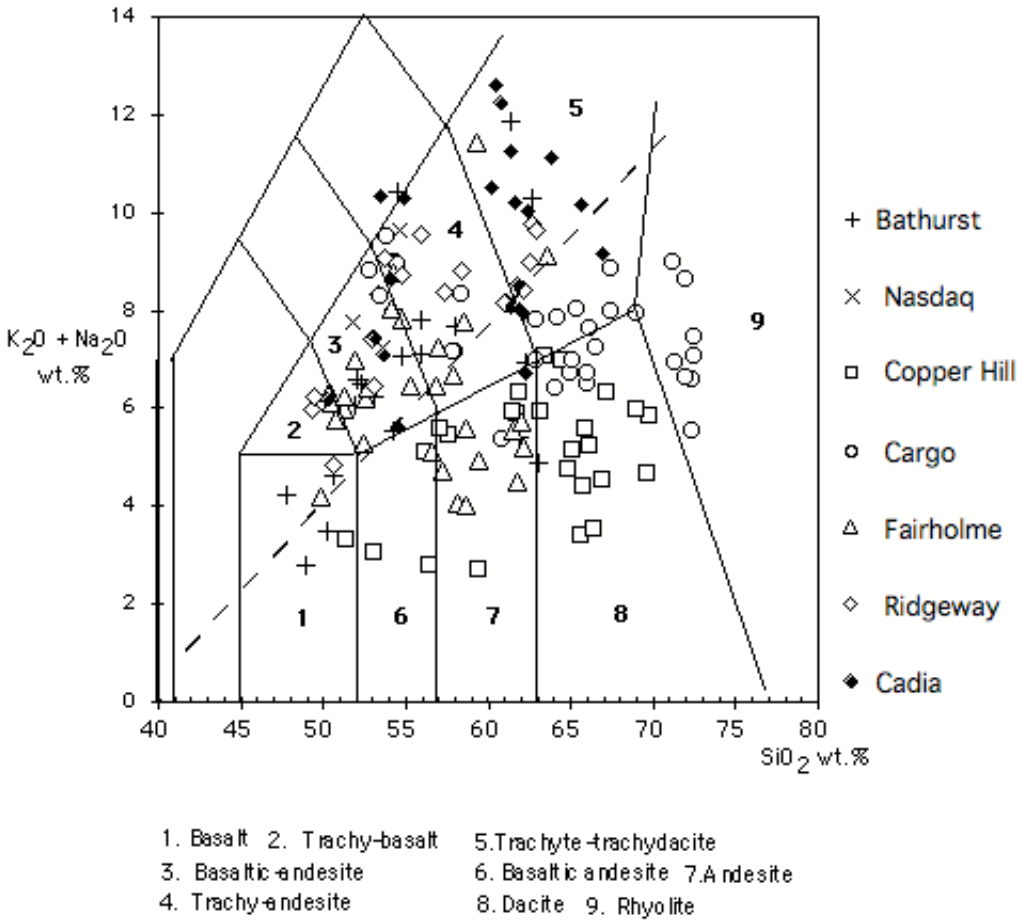

Figure 3.4. A total alkali (Na_2O + K_2O) versus Silica diagram (TAS) for Ordovician igneous rocks of the Lachlan Fold Belt in NSW. Dashed line indicates boundary between alkalic and tholeiite fields according to MacDonald (1968). Rock type fields from Le Maitre et al. (1989).

The Cadia, Copper Hill, Ridgeway, Fairholme and Nasdaq samples define clear trends that are more distinct than that defined by Na_2O alone (e.g. Fig. 3.2B). Ridgeway and Cadia fall within the trachy-basalt to trachydacite-trachyte fields (Fig. 3.4) whereas the Copper Hill samples are less alkali-rich and extend from the basalt to dacite fields. The regional set of Bathurst samples defines two compositional fields that correspond to similar alkali-rich and alkali-poor trends: trachy-basalt to trachydacite-trachye and basalt to rhyolite. Although multiple trends are expected in the regional data set, two trends are also observed in the Cargo and Fairholme data, indicating that two distinct phases of magmatism are present at the deposits.

The total alkali (K_2O + Na_2O) versus SiO_2 subdivision of volcanic rock series (MacDonald, 1968) (Fig. 3.4) can be used to classify samples into one of two broad categories. A line marks the fields of tholeiitic or "alkalic" rocks on this plot. The latter category corresponds to multiple suites on the previously described K_2O vs. SiO_2.

The impact of hydrothermal alteration and weathering is moderate on most of the new samples used in this study. For example the Cadia, Copper Hill and Ridgeway igneous samples plot in the same compositional fields (K_2O vs. SiO_2 and TAS) as the unaltered or weakly altered samples of Holliday et al. (2002), and Blevin (2002) from the same areas. The deeply buried Fairholme samples display igneous trends on the major element and geochemical classification plots indicate that they are less affected by alteration and weathering.

3.4 SUMMARY

Most of the studied samples are only weakly altered. They illustrate good primary igneous trends representing AFC (assimilation and fractional crystallisation), although a few samples lie off of certain trends as a result of post magmatic processes such as mobilisation during hydrothermal veining.

The studied igneous samples provide a good example of subduction environment magmatism. They include K_2O enriched igneous trends that are consistent with subduction-modified mantle wedge sources. A few effects, such as the high Fe_2O_3 contents of some Ridgeway samples probably reflect porphyry-style hydrothermal alteration processes.

The Ordovician rocks define two main trends that cut across Low K (tholeiite), Medium K (calc alkaline), High K and shoshonite fields on a widely used K_2O versus Silica plot. However, two main trends are evident on the plot that correspond to more general alkalic and tholeiitic subdivisions of the TAS diagram. The results emphasize that Cadia-Ridgeway rock samples are distinct from other study areas in being entirely alkalic. In contrast, Copper Hill samples are all tholeiitic. Cargo, Fairholme and Bathurst regional samples include both types of magmas which indicate that alkalic magmas, often considered favorable for gold (Müller and Groves, 1997), are widespread in the fold belt. If these rocks are to be distinguished more thoroughly then trace element characteristics must be determined.

CHAPTER 4

TRACE ELEMENT CHEMISTRY

4.1 INTRODUCTION

A trace element may be defined as an element which is present in a rock at a concentration of less than 0.1 wt %, that is less than 1000 parts per million (ppm). Some trace elements may form mineral species in their own right but most commonly they substitute for major elements in the rock-forming minerals. Trace element analyses are particularly useful for assessing processes involving crystal-melt or crystal-fluid equilibria (Rollinson, 1993).

This study has greatly increased the amount of high quality trace element data available for several of the study areas including Ridgeway, Copper Hill, Cargo and Fairholme. In addition, the quality of the ICPMS data exceeds that available from published sources (Holliday et al., 2002; Blevin et al., 2002) and is more comprehensive in terms of the number of elements analysed.

The trace elements systematic of LFB Ordovician igneous suites are first examined in order to establish the number and distribution of distinct magmatic systems. The petrogenetic significance of the data is then considered in terms of sources, magma evolution, tectonic setting and ore deposit genesis.

As noted in the previous chapter, elements that preferentially concentrate in mineral phases rather than in the magma liquid are described as compatible. Compatible trace elements include Ni, Co, Cr, Sc and V.

Incompatible trace elements are subdivided into two groups on the basis of their charge/size ratio. This property is often described as field strength and may be thought of as the electrostatic charge per unit surface area of the cation. Small highly charge cations are known as high field strength cations (HFSE) and large cations of small charge are known as low field strength cations. Low field strength cations are also known as large ion lithophile elements (LILE).

High field strength elements, HFSE, include Hf, Nb, Pb, Ta, Th, Ti, U, Y, Zr, and the lanthanides or rare earth elements (REE). Low field strength elements, LILE, include Cs, Rb, K and Ba. To these may be added Sr, divalent Eu and divalent Pb (Kerrich and Wyman, 1996; Rollinson 1993).

4.2 TRACE ELEMENT VARIATION DIAGRAMS

The following sections consider the behaviour of compatible trace elements, large ion lithophile elements (LILE) and high field strength elements (HFSE) which are plotted on Harker variation diagram x-y plots (Rollinson, 1993), against Ni, K_2O, or Zr respectively. on the x-y plots because Ni and Zr are relatively compatible and incompatible trace elements respectively (Rollison, 1993). Potassium is commonly used in the literature, therefore trace elements are plotted against it for comparison purposes.

4.2.1 COMPATIBLE TRACE ELEMENTS

As expected, Co concentrations in the samples of this study fall with decreasing Ni values (Fig. 4.1A). The intrusive and volcanic samples define a relatively well-defined trend with two different slopes: sub-vertical and shallow slopes. Several Bathurst Ni-rich olivine cumulate-bearing samples are not shown on the plots because they compress the scale of other samples.

The Copper Hill, Fairholme and Nasdaq samples show a good sub-vertical trend at low Ni values, 0 to 45 ppm. The Bathurst and Cargo samples define two trends: sub vertical at 0 to 45 ppm Ni and scattered at Ni values higher than 45 ppm. The Cadia and Ridgeway samples show good trends. They fall in both sub-vertical and shallow slope trends. They define a sub-vertical trend at low Ni values, 0 to 45 ppm, and shallow-sloped trend at high Ni values, 45 to 200 ppm. They exhibit an inflection from sub-vertical slope trend at about 40 – 60 ppm Ni.

The distribution of Sc is similar to the Co distribution, with Cargo and Bathurst samples scattered at Ni values higher than 70 ppm (Fig. 4.1B). At low Ni values, < 70 ppm, the intrusive and volcanic samples of all igneous suites show a good correlation trend with Sc. Vanadium shows a similar correlation with Ni although Bathurst and Cargo samples define a near vertical trend at Ni values higher than 70 ppm (Fig. 4.1C). Chromium and Co exhibit similar co-variations at low Ni and are also more scattered at higher Ni abundances (Fig. 4.1D).

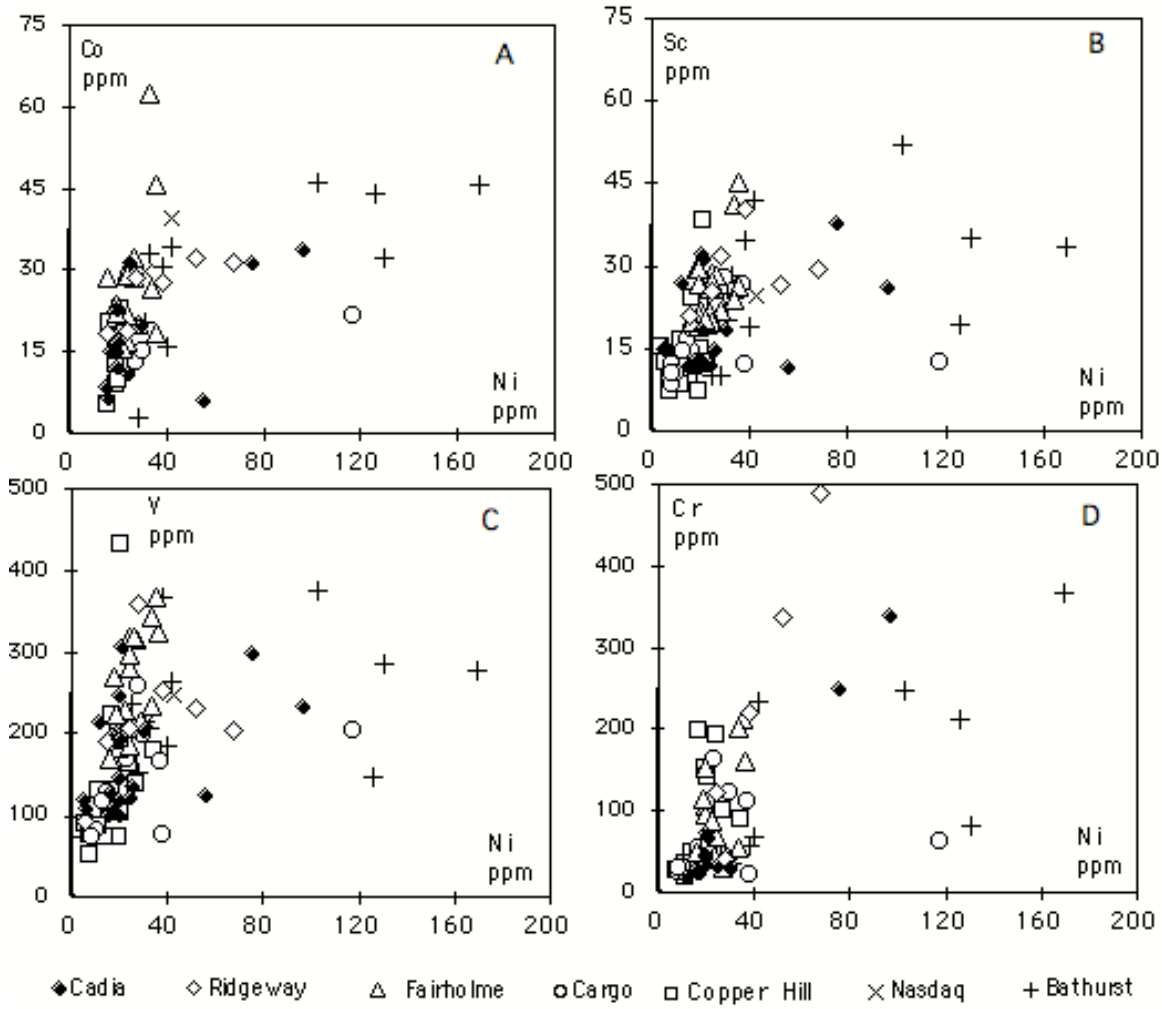

Figure 4.1. Compatible element variation diagrams for Ordovician magmas of the Lachlan Fold Belt in NSW.

In summary, the compatible trace element data indicates that all igneous suites have similar compatible trace element trends. Most data lie on trends with steep slopes at Ni contents that correspond to intermediate to evolved compositions. There are differences, however, between Fairholme and Cadia-Ridgeway and the regional Bathurst samples that reflect differing extents of magma evolution between these suites. Higher Ni contents are generally associated with samples of the regional Bathurst set, which does not constitute a single magma and may include examples of cumulate material in some cases.

4.3 INCOMPATIBLE TRACE ELEMENTS

4.3.1 LARGE ION LITHOPHILE ELEMENTS (LILE)

The LILE include Ba, Rb, Sr, and Cs. Cesium abundances are below detection limits for many samples and are not considered further.

Barium and Rb concentrations in all igneous suites positively correlate with K_2O values and display well-defined trends (Fig. 4.2A and B). In contrast to Ba and Rb, Sr does not display strong correlations with K (not shown). This differing behaviour among the LILE is most plausibly accounted for by K-feldspar control of Ba and Rb and multiple phases controlling Sr (e.g. plagioclase in addition to K-feldspar). The LILE variation diagrams indicate that most samples collected for this study retain magmatic or near-magmatic concentrations of these mobile elements, indicating they are relatively unaffected by weathering.

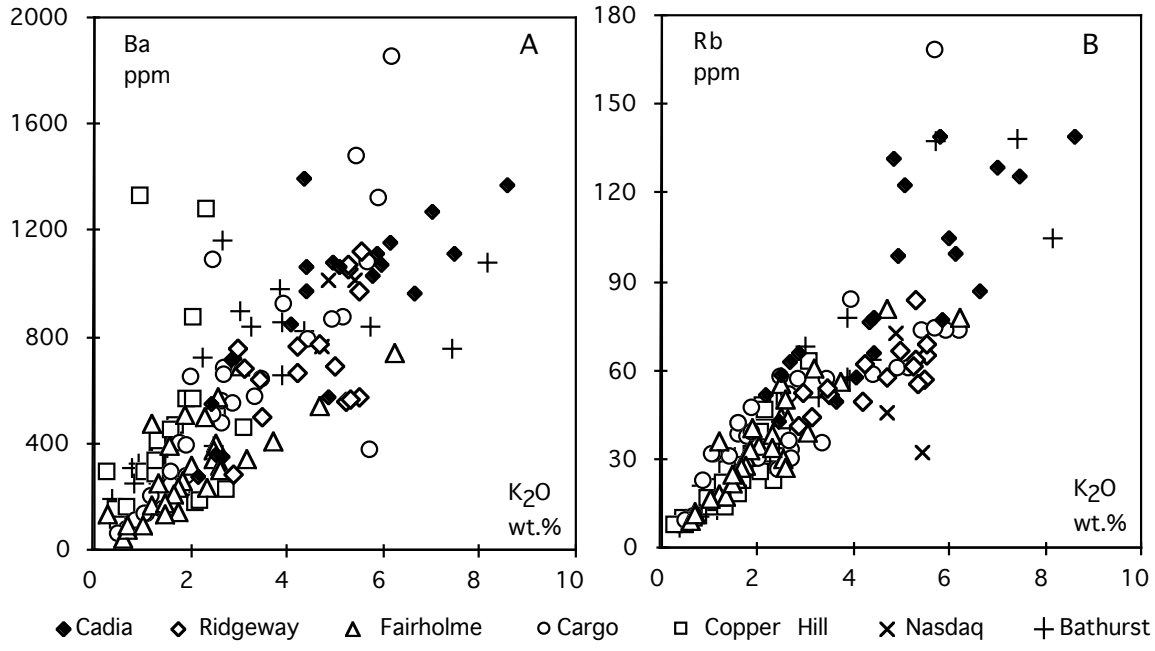

Figure 4.2. LILE variation diagrams for Ordovician igneous rocks of the Lachlan Fold Belt in NSW.

4.3.2 HIGH FIELD STRENGTH ELEMENTS (HFSE)

The trace elements Hf, Nb, Pb, Ta, Th, U, Y and Zr occur as small ions (< 1.2 Å radius) with high charges (+3 to + 6) under geological conditions and are termed the high field strength elements (HFSE). If two incompatible elements are plotted on a variation diagram then they should define strong trends because both elements are concentrated in the melt. Therefore, the least mobile and most incompatible of the HFSE (Hf, Nb, Ta, Th) are plotted against Zr in order to distinguish between distinct magma evolutionary paths among the study sites. The choice of Zr is based on the fact that it is readily analysed and is immobile. It behaves incompatibly in magmatic systems unless or until Zr-bearing phases such as zircon are formed.

All igneous suites display similar linear Hf trends (Fig. 4.3A); that reflects the incompatible nature of Hf and its strong chemical similarities with Zr. A few Cadia Quartz Monzonite Porphyry samples cluster slightly off of the main trend. The significance of this cluster is not obvious, although these samples have been overprinted by potassic alteration.

Correlations also exist between Zr and Nb (Fig. 4.3B) although the trends are not as pronounced as those defined by Hf. Both intrusive and volcanic rocks from Fairholme define a high Nb trend that is distinct from the bulk of the data. This observation strongly suggests that Fairholme intrusive rocks (apart from one sample of feldspar porphyry intrusion) are part of the same magma series as the volcanic rocks and may be considered a feeder system for the volcanic rocks.

A plot of Th versus Zr (Fig. 4.3C) displays a broad correlation between the two incompatible elements. In detail, a trend for Copper Hill samples is offset to higher Zr values than the main trend. Fairholme samples do not define a clear trend and contribute scatter to the plot as a whole. Two Cargo magma suites are evident in Th-Zr plot. They define high and low-Th trends. Cadia-Ridgeway samples span a wide range of Zr and Th contents but many of these samples define the high end of a distinct Th-Zr trend within the dataset.

Although Ta is widely considered to be the chemical twin of Nb because of similar sizes and charge characteristics, its distribution differs somewhat from Nb in the Ordovician magmas. At high abundances, Nb and Ta exhibit different trends for Fairholme samples on Zr variation diagrams. This differing behaviour demonstrates that significant variations in Nb/Ta ratios are possible among igneous rocks as a result of

different fractionation and crustal assimilation paths, as discussed in Chapter 5. Most Cargo samples follow the main trend but five latite and Quartz-feldspar porphyry samples define a distinct low-Ta trend, consistent with the suggestion (Chapter 3) that two separate magma suites occur at the deposit.

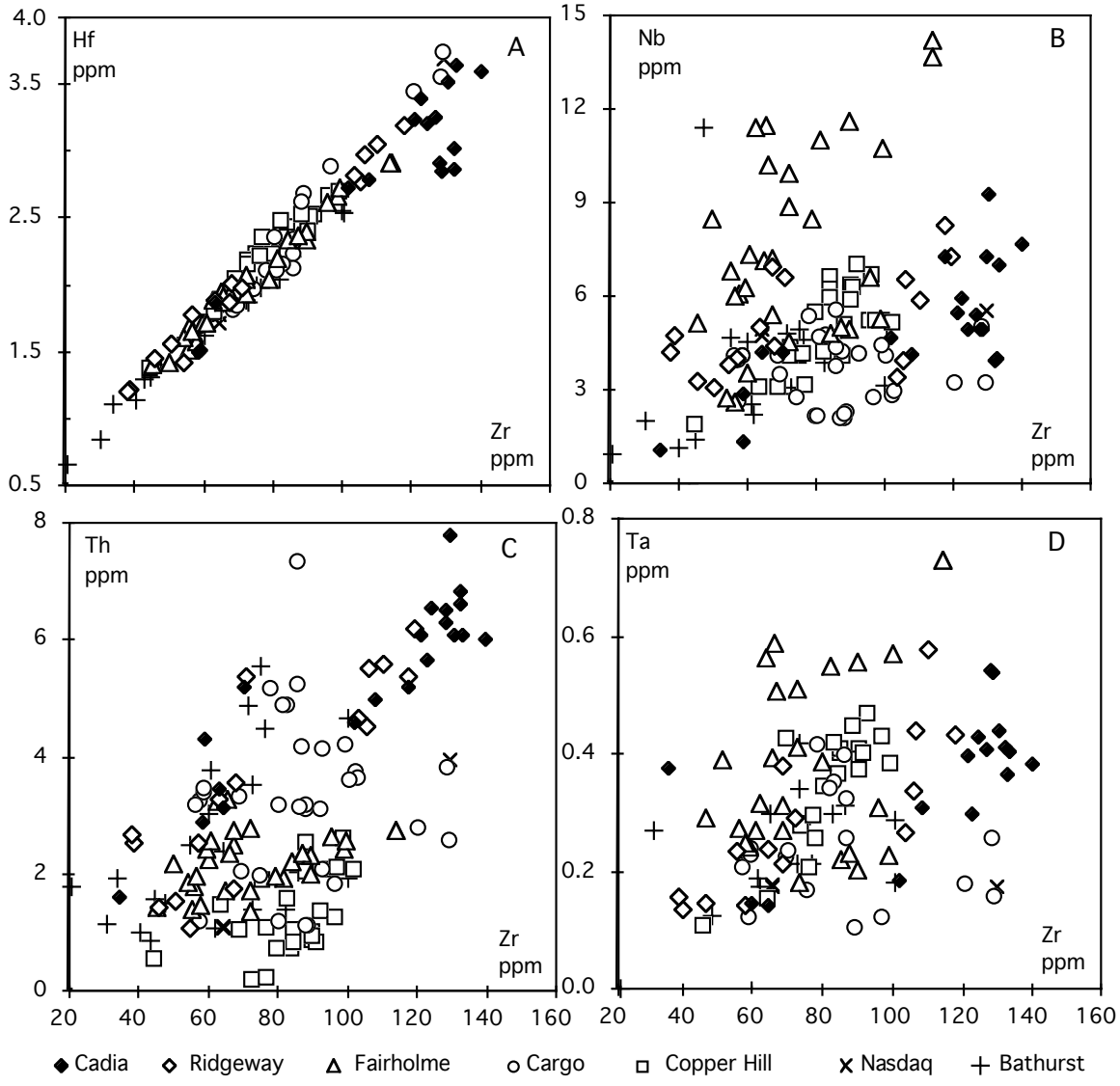

Figure 4.3 HFSE variation diagrams for Ordovician igneous rocks of the Lachlan Fold Belt in NSW.

On the Nb-Y tectonic discrimination plot (Fig. 4.4, Pearce et al. 1984) the Ordovician rocks samples exclusively fall in the field of volcanic arc granite or syn-collisional granites (VAG + syn-COLG). The result is consistent with the inferred setting

of the LFB during the late Ordovician. However, the plot does not provide a clear means of distinguishing Cadia-Ridegway magmas from those associated with smaller deposits.

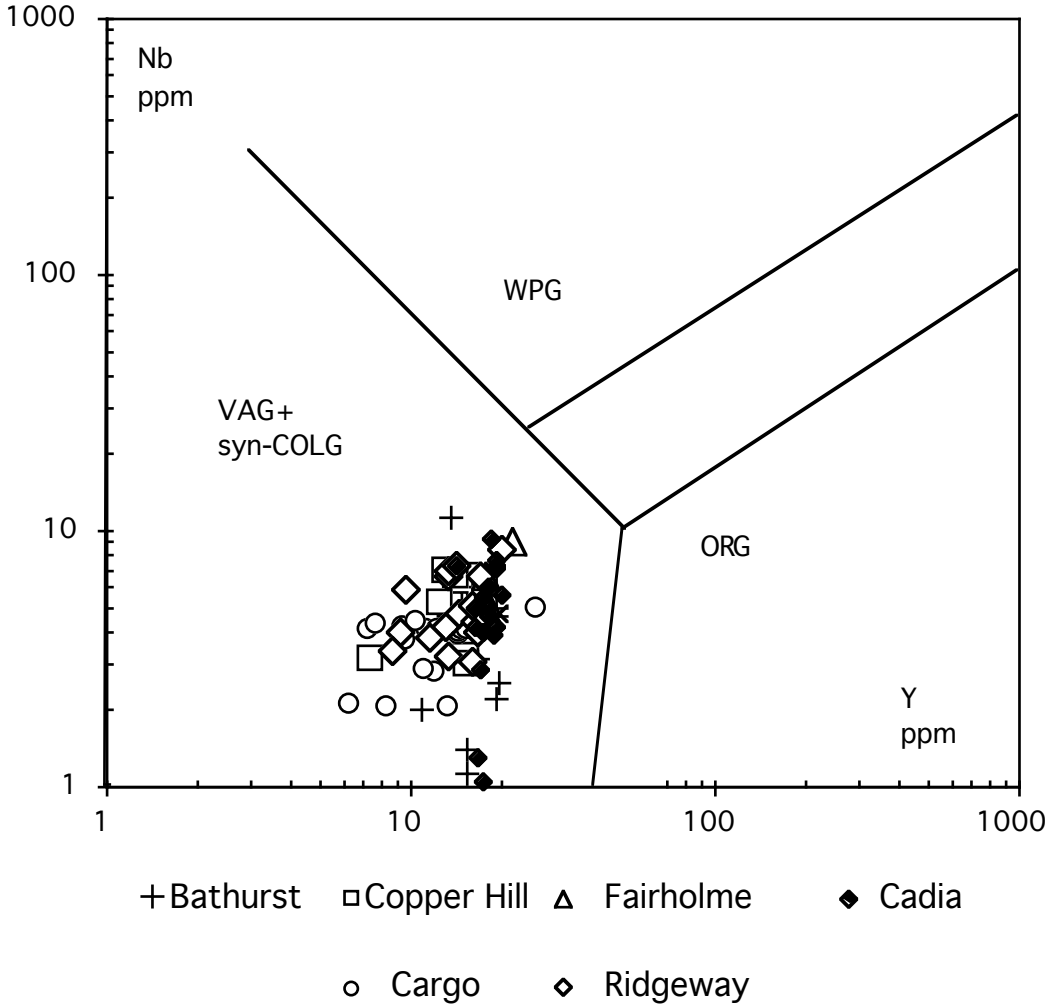

Figure 4.4 A Nb versus Y tectonic discrimination plot for granites (Pearce et al., 1984) showing a subduction-related setting for intrusive samples of the Ordovician magmas of the Lachlan Fold Belt in NSW.

4.4 RARE EARTH ELEMENTS (REE)

The rare earth elements (REE) comprise the series of elements with atomic numbers from 57 to 71 – La to Lu. The REE all form stable +3 ions and are of similar size. As a result, they have similar chemical and physical properties that differ slightly as a result of a steady decrease in ionic size with increasing atomic number.

Typically the low –atomic number members of the series are termed the light rare earths (LREE: La - Nd), those with higher atomic numbers the heavy rare earths (HREE Er - Lu) and the elements Sm to Ho are known as the middle rare earth elements (MREE) (Rollinson, 1993). Lutetium was used as an internal reference during ICPMS analysis of these samples at Actlabs Pacific and therefore is not shown on the REE plots.

The REE are amongst the least soluble trace elements and are relatively immobile during low-grade metamorphism, weathering and hydrothermal alteration (Rollinson, 1993). They have very similar chemical and physical properties (stable 3^+ ions of similar size) but they differ in chemical behavior because of the small but steady decrease in ionic size with increasing atomic number. These differences result in varying behaviour during petrological process, which cause the REE to fractionate relative to each other. (Rollinson, 1993).

In general terms, all igneous suites inside and outside the LTZ have similar REE patterns on the Chondritic plots. They exhibit REE fractionation with LREE enrichment that is characteristic of subduction related magmas as expected of their tectonic setting in the Lachlan Fold Belt.

The REE systematics of samples in this study range from almost unfractionated to strongly LREE-enriched. There is a good correlation between La abundance and MREE - HREE fractionation ($[Gd/Yb]_{cn}$) (Fig. 4.5A) and therefore between La and the degree of overall REE fractionation ($[La/Yb]_{cn}$) (Fig. 4.5B). However, La versus LREE fractionation ($[La/Sm]_{cn}$) (Fig. 4.5C) differs between study sites. It is notable that the Ridgeway samples define a distinct trend from the nearby Cadia samples, suggesting that the different modes of emplacement at the two sites produced distinct magma evolutionary paths involving differing proportion of the crystallising phases or assemblages involving different minerals.

Europium does not display large anomalies in the samples, with most analyses falling between 0.8 and 1.1 (Fig. 4.5D). Higher Eu/Eu* values for some Copper Hill samples do not correlate with Al_2O_3/TiO_2, a monitor of feldspar fractionation. Therefore, these samples are likely to reflect local mobilization of Eu rather than an igneous process.

Rare earth element concentrations in rocks are usually normalised to a common reference standard for plotting purposes. The most commonly used normalising values are those for chondritic meteorites (Rollinson, 1993). Parallel REE patterns for a group of spatially associated igneous rocks are consistent with evolution of a single magma by crystal fractionation with or without progressive crustal assimilation. The range of REE

concentrations defined by the samples is indicative of the extent of fractionation in the magma. Where REE patterns for closely associated igneous rocks cross-cut each other, it is more likely that different magmas are present or that initially similar magma batches evolved in different way, The chondrite-normalised patterns of LFB Ordovician rock samples (Fig. 4.6) are indicative of multiple magmas at most study sites.

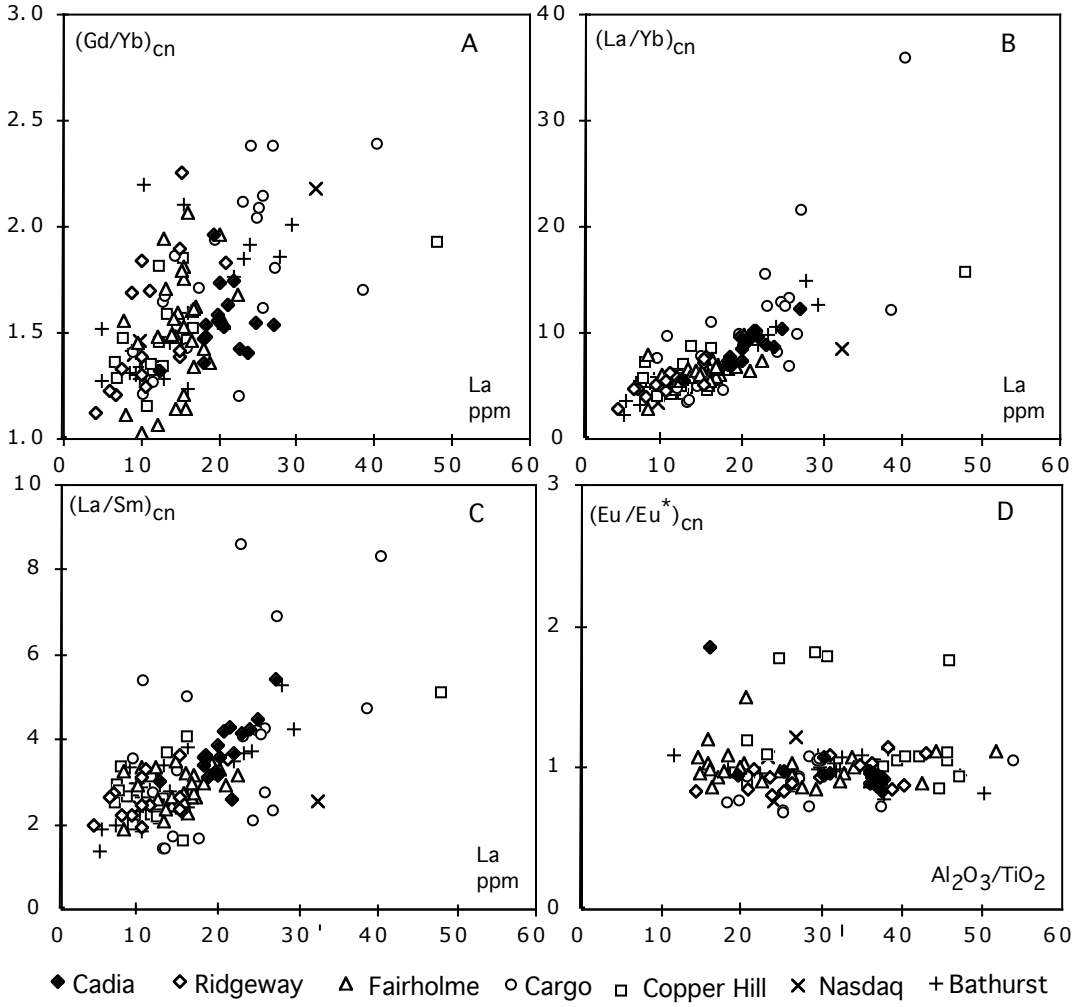

Figure 4.5 Rare Earth Element ratio variation diagrams for Ordovician magmas of the Lachlan Fold Belt in NSW.

For example, the narrow range of parallel Cadia plots (Fig. 4.6B) and broad range of parallel Fairholme plots (Fig.4.6C) indicate less fractionation between sampled magma at Cadia compared to extensive fractionation at Fairholme. The Cargo and Copper Hill sites display broad concentration ranges and crosscutting patterns that are reflective of a strong fractionation in two different magmas (Fig. 4.6 E and F).

On the Chondritic normalised plots (Fig. 4.6) the Yb to Ho segment, HREE, of the Ordovician rocks indicate low element abundances and little inter-element fractionation. The Ho to La segment, MREE-LREE, displays weakly to strongly positive trends indicating progressively greater enrichment of these elements to La. These features are characteristic of subduction zone magmatism. During dehydration or small degree melting of the subducting slab, HREE are left behind in the slab whereas the MREE and LREE are moderate to highly incompatible and mobilised in fluids and melts. As a result, these elements become enriched in the mantle above the subducting slab that is the source of the arc-related magmas (Munker, 1998).

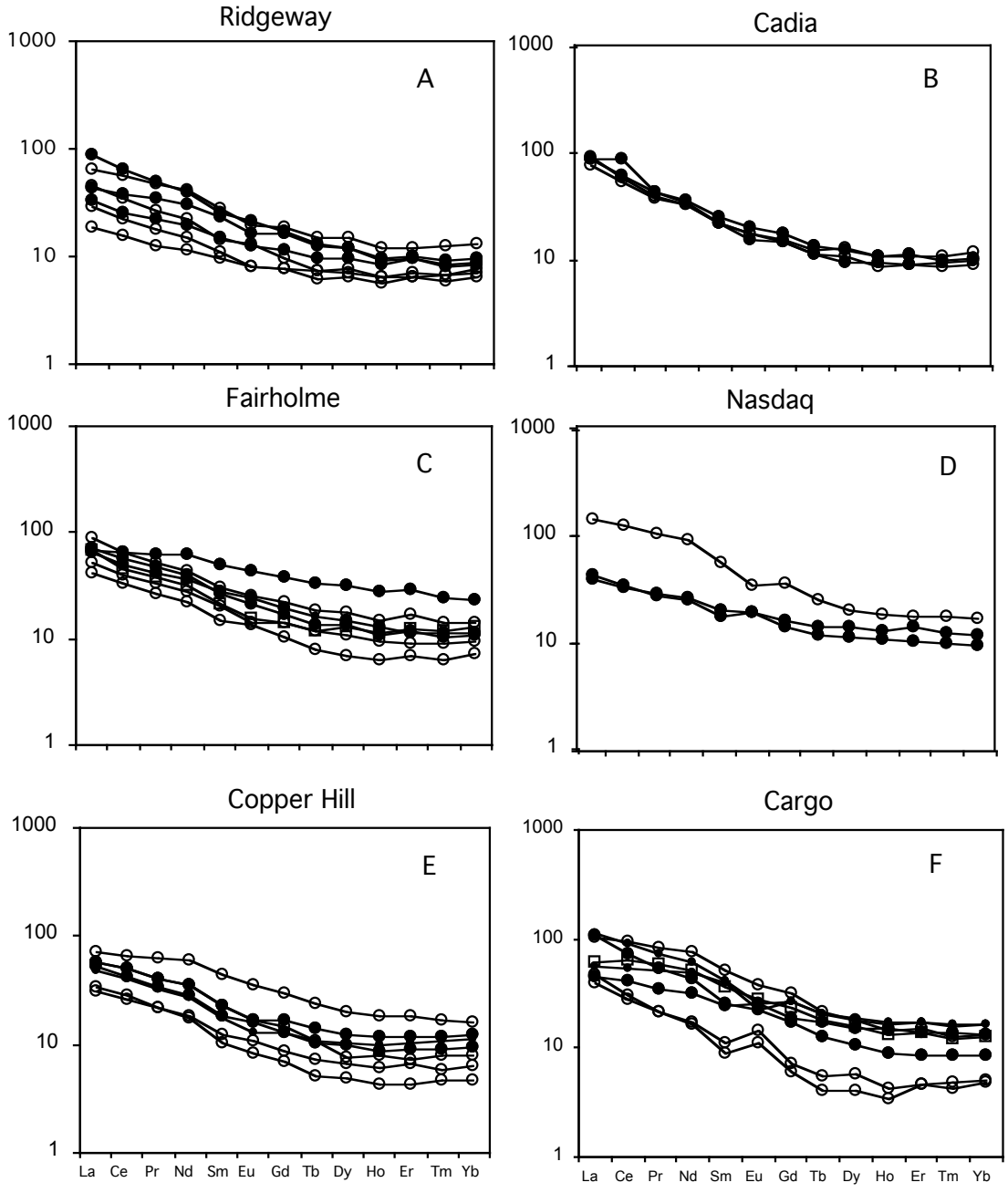

Figure 4.6 Chondrite-normalised rare earth element plots for Ordovician igneous rocks of the Lachlan Fold Belt in NSW. Normalising values from Sun and McDonough, 1989. Open circles are volcanic samples; closed circles are intrusive samples.

4.5 MULTI-ELEMENT PRIMITIVE MANTLE NORMALISED PLOTS

The primitive mantle is the inferred composition of the mantle before the continental crust formed. The multi-element, or Primitive Mantle-normalised, plots are an extension

of the more familiar chondrite-normalised REE plots in which other trace elements are added to the traditional REE plots (Rollinson, 1993).

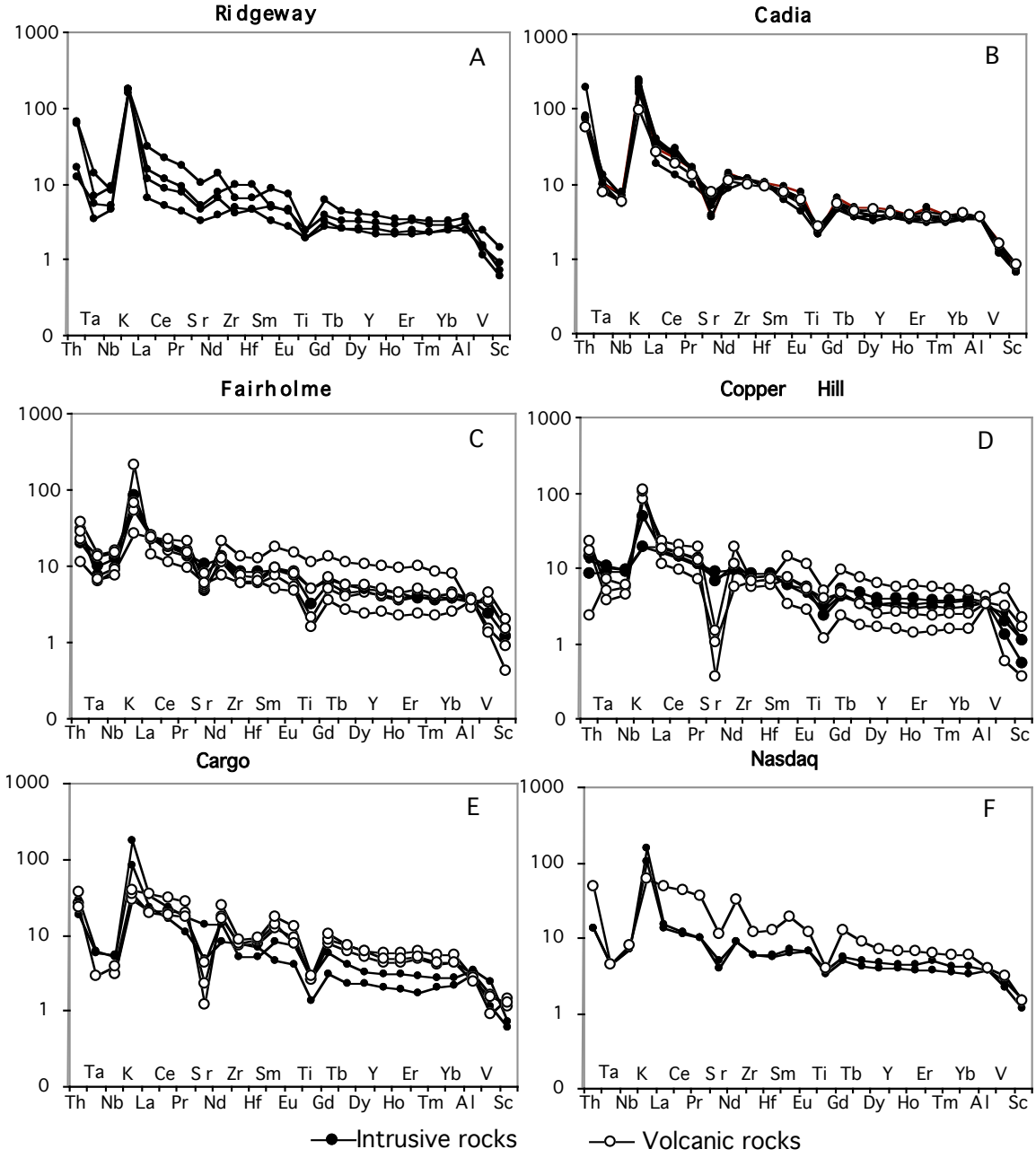

Figure 4.7 Primitive mantle-normalized plots for Ordovician igneous rocks of the Lachlan Fold Belt in NSW. Normalizing values from Sun and McDonough (1989).

The Ordovician rocks samples exhibit a broad range of trends on the Primitive Mantle plots but HFSE fractionation versus the LILE is seen in all cases (Fig. 4.7). In particular, there are negative anomalies for Ti, Nb and Ta, and sometimes at Zr and Hf. Strong enrichment in incompatible elements such as Ba, Rb, Th and K on the plots is

consistent with mantle metasomatism by slab-derived fluids in the subduction related setting of the Ordovician rocks.

All localities display Sr depletion in the patterns of some or all samples that reflect the variable removal of Sr during fractionation of plagioclase. Distinct magmas are evident in the plots. For example, a quartz-feldspar porphyry intrusion at Fairholme plots at higher HREE abundances and has only a small negative Ti anomaly. Also, the Nasdaq andesite has a very different plot than the nearby intrusive rocks, again indicating two distinct magmas. The extent of fractionation within an igneous suite can also be assessed on these plots. Copper Hill intrusions have only minor variations in trace element contents but volcanic rocks exhibit a wide range of trace element abundances. At Cargo, the volcanic rocks are more fractionated than the intrusive samples. Ridgeway samples record a larger amount of fractionation than Cadia samples, although the main features of the plots, such as K-enrichment or Ti depletion, are similar.

4. 6 DISTINCTIVE GEOCHEMICAL FEATURES OF THE LARGE RIDGEWAY – CADIA DEPOSITS

Several distinctive features of igneous rocks at the Ridgeway – Cadia deposits have been noted previously, such as their consistently high potassium contents and shoshonitic character (Chapter 3). The potassic nature of the magmas is also illustrated on the Primitive Mantle normalised plots of the Ridgeway and Cadia rocks. Potassium contents are consistently high but at other localities only a few samples have K > 100 time Primitive Mantle. In addition, the plots show that thorium abundances are generally high (~ 90 – 100 x PM) at both Cadia and Ridgeway, although several Ridgeway samples have lower (x 10 PM) contents. Most samples from other deposits have Th < 50 times Primitive Mantle. These features are more readily compared on an x-y plot as shown in Figure 4.8.

Other distinctive trace element features or notable relationships between major and trace elements are also best observed on x-y plots. An example is the behaviour of Fe, Ti, and V, all of which are found in igneous iron oxides such as magnetite. Figure 4.9 illustrates the unique trend of most Ridgeway samples. The offset trend defined by these rocks can be related to alteration events and the formation of hydrothermal magnetite with low Ti and V contents.

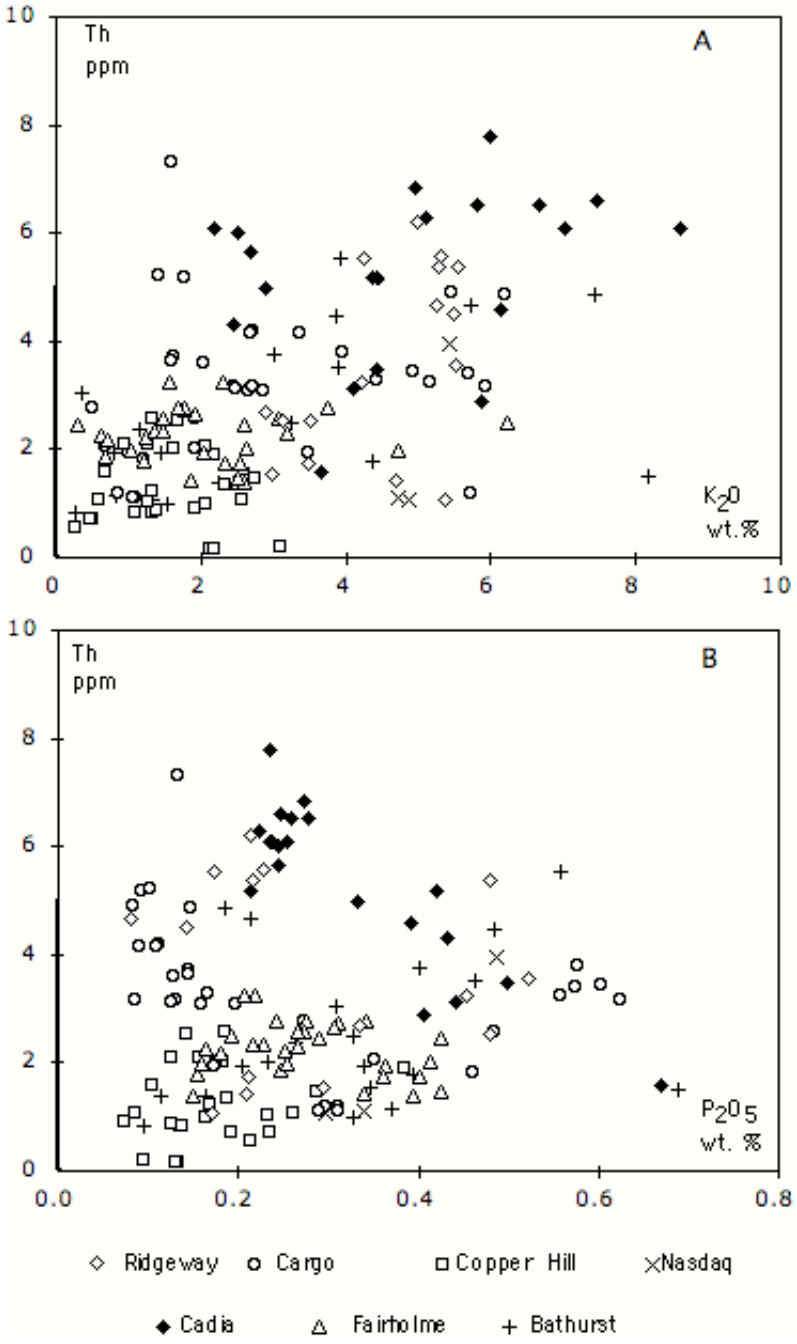

Figure 4.8 Th contents plotted against major element oxide abundances. **A.** Cadia – Ridgeway samples include those with the highest K contents. Most Cadia-Ridgeway samples also have high Th contents compared to other study areas. **B.** Many of the Cadia-Ridgeway samples define a distinct Th-P trend. This likely is the result of early apatite saturation in the Cadia-Ridgeway magmas which keeps P contents low compared to samples with high Th contents at other localities.

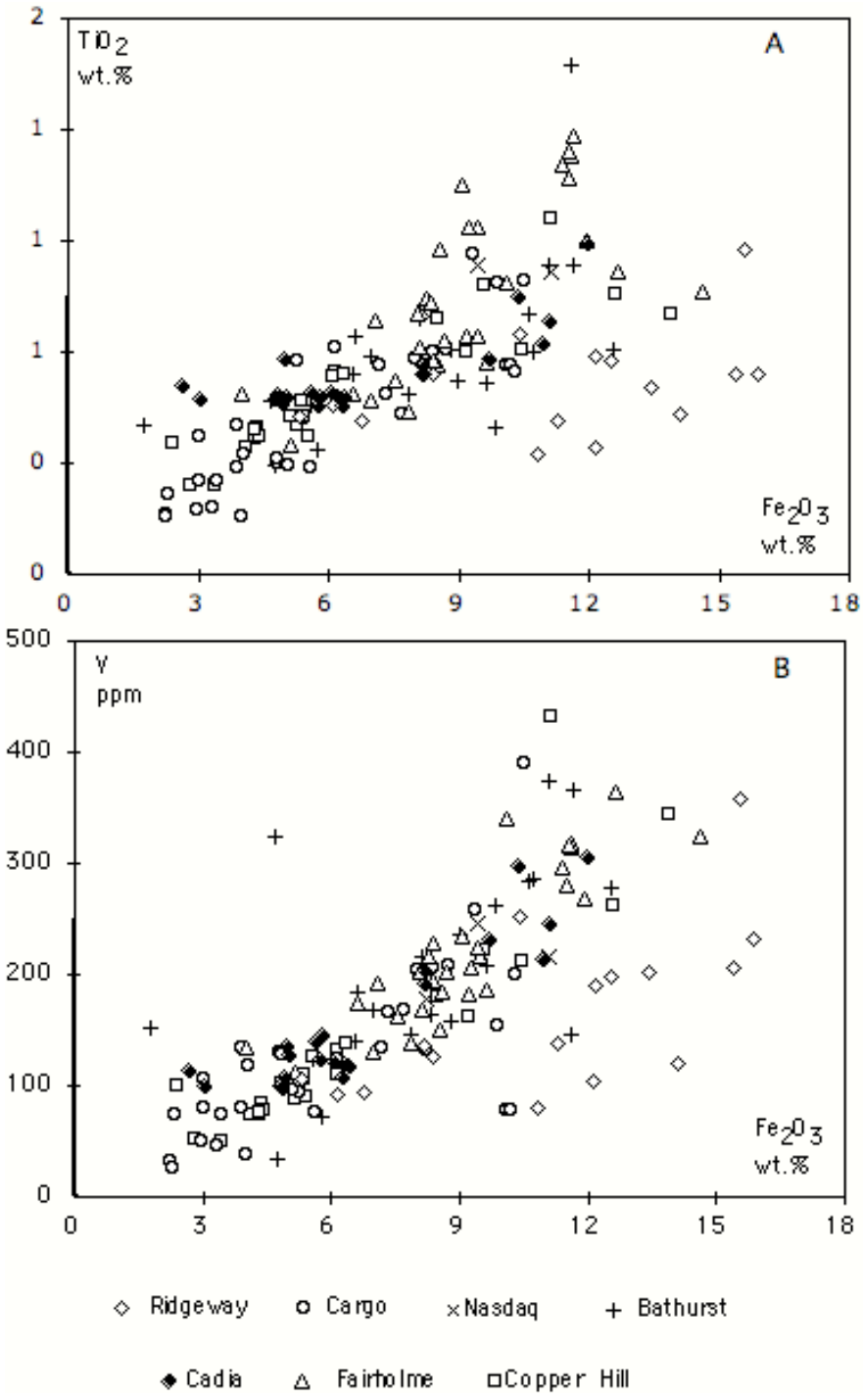

Figure 4.9 Variation diagrams for magnetite-associated elements. **A.** Many Ridgeway samples are offset to high Fe contents, probably as a result of the formation of hydrothermal magnetite that is Ti-poor. **B.** Similar patterns occur on a plot involving V because this element is abundant in igneous magnetite but is not concentrated in hydrothermal magnetite.

4.7 SUMMARY

Geochemical discrimination plots and the overall trace element characteristics of the NSW Lachlan Fold Belt igneous rocks, such as LREE- LREE and LILE enrichment and HFSE depletion (Nb, Ta and Ti) are consistent with a subduction-related tectonic setting in the Ordovician. In detail, differences in the HFSE and REE trends of the Ordovician rocks indicate several magma types are present in the belt. Crosscutting REE and multi-element trends indicate several magma types and (or) batches are also present at individual study areas.

Differences are also evident in the extent of magma fractionation at different sites. Ridgeway samples analysed in this study define a wider range of trace element concentrations than the Cadia quartz monzonite porphyry, monzodiorite, diorite, and syenogranite reported by Green (2001). Differences in fractionation processes can also be detected in the trace element plots. For example, Fairholme samples define a high Nb trend that is distinct from the main Nb-Zr main, probably because of magnetite.

The trace element chemistry results also have implications for mineral exploration as discussed in section 5.5 below. Trace element geochemistry shows distinctive features for the Cadia – Ridgeway deposits resulting from both igneous processes and more pervasive hydrothermal events.

CHAPTER 5
DISCUSSION - TECTONICS, MAGMA CHEMISTRY

5.1 INTRODUCTION

Much of our understanding of the characteristics of porphyry deposits comes from studies in the 1970s of the Laramide porphyry Cu systems, southwest USA, (Cooke et al., 1998). Porphyry copper deposits have been mined in bulk since 1906, when Bingham, Utah, came into production. Most of the world's gold-rich porphyry copper deposits are confined to the circum-Pacific region. However, deposits are also known in Alpine-Himalayan orogenic belts and elsewhere (Sillitoe, 1990).

In recent years, it has been recognised that Tertiary and Quaternary gold rich porphyry Cu deposits in the western Pacific and South East Asia have their own characteristics, which result from the distinctive tectonic setting and host rock lithologies found in island arcs (Sillitoe, 1997). These are typified by the Philippine systems such as Santo Tomas II, Dizon, and Far South East, but also include deposits such as Grasberg and Batu Hijau, Indonesia, and Ok Tedi, the Frieda River deposits, and Panguna, PNG, (Corbett and Leach, 1994).

Some of the oldest known porphyry Cu-Au deposits occur in the Ordovician volcano-sedimentary sequences of NSW, Goonumbla, Cadia, Copper Hill, Cargo, and Lake Cowal (Cooke et al., 1998). The Ordovician Cu-Au porphyry deposits of NSW and the circum Pacific porphyry provinces, while having a number of similarities, also have several distinctive characteristics. The following is a description and comparison of the tectonic setting, structure and magma chemistry of the circum Pacific and the Ordovician Cu-Au porphyry deposits of LFB (including the LTZ) and a discussion and comparison of Nb/Ta trends of the LFB porphyries and available data for other types of igneous systems.

5.2 TECTONIC SETTING OF PACIFIC RIM CU-AU PORPHYRIES

Most Pacific Rim Au-Cu mineralisation is associated with Tertiary subduction-related volcano-plutonism in island arcs developed at convergent plate boundaries (Sillitoe 1992). Various tectonic sub-settings styles are distinguished based on orthogonal or oblique convergence, intra arc rifting and back arc extension (Sillitoe, 1992).

Back arc settings may be the locus of intrusion of alkaline magmas possibly derived from deep melting. Major structures, commonly extensional, are required for melts of this type to rise to high crustal levels where rapid cooling and oxidation of magma occur (eg. porphyry-related Au mineralisation within the Tabar-Lihir-Feni chain, PNG or the Emperor Au mine Fiji; Corbett and Leach, 1994).

Major structures in subduction related Pacific Rim porphyry Cu-Au may be classified as accretionary, transfer and intra-plate rifts (Corbett and Leach, 1994). Accretionary structures develop parallel to the subducting plate margin and accommodate much of the movement as thrusts if the collision is normal. In settings of oblique subduction, arc parallel structures may form transcurrent faults that display predominantly strike slip components of displacement (e.g. the FSE, Philippines and Frieda River, PNG). Transfer structures are deep crustal breaks and so act as a focus for rising magmas to localise porphyry systems (e.g. Wati or Yandera, PNG). Intra-plate rifts localise the alkaline volcanism in the Tabar-Lihir island chain, PNG, and the associated porphyry-related gold mineralisation (Corbett and Leach, 1994)

5.3 LFB CU-AU PORPHYRIES VERSUS THE PACIFIC RIM: TECTONIC SETTING AND PETRO-CHEMISTRY

Many of the porphyry Cu-Au deposits of the Pacific Rim occur in association with alkaline volcano-plutonism (Sillitoe, 1979), and so have been classed by Bonham (1988), as alkalic gold deposits. The stocks that host the large Au-rich porphyry deposits are all of I-type and belong to the magnetite series, thereby indicating contributions from oxidised sub-crustal melts (Ishihara, 1981). The mineralised porphyry stocks are either calc-alkaline or high-K calc alkaline in petrochemical affiliation, with those at Bajo de La Alumbrera, Argentina, and Cadia Hill, NSW, also qualifying as members of the shoshonite suite (Sillitoe, 1997).

Moreover, volumetrically minor mafic alkaline and shoshonitic igneous rocks in the Bingham district, Utah USA, are modelled as parental to the porphyry Cu-Au stock (Keith et al., 1995). The mineralised porphyries span a broad compositional range: diorite through quartz diorite and dacite to monzodiorite, monzonite and quartz monzonite (monzogranite), (Sillitoe, 1997).

Most of the world's Au-rich porphyry copper deposits are confined to the circum-Pacific region. They typically range in age from Mesozoic, Tertiary to Quaternary

(Sillitoe, 1990). The oldest, however, are the Ordovician Cu-Au porphyry deposits of NSW porphyry provinces (Cooke et al., 1998). Porphyry Cu-Au deposits are also known in Alpine-Himalayan orogenic belts (Sillitoe, 1993), Oyu Tolgai, Mongolia (Ivanhoe Mines, 2004) and elsewhere. The following is a comparison of tectonic setting, structure and magma chemistry of these Ordovician Cu-Au porphyry deposits and the Pacific Rim porphyry Cu-Au provinces.

The LFB Ordovician porphyry Cu-Au deposits are subduction related (see Section 1.4), are associated with arc volcanic rocks and episodes of oblique convergence (Glen et al., 1997; Corbett and Leach, 1998). Therefore, their tectonic setting is similar to the tectonic setting of most of the Pacific Rim porphyry Cu-Au deposits as described by Sillitoe, 1992 (e.g. porphyry-related Cu-Au mineralisation at Misima, PNG; Acupa, Philippine; Lombok Tandai, Indonesia).

The state of subduction was not constant during the period from the Lower Ordovician to the Earliest Silurian. Instead, subduction was episodic and separated by two major hiatuses (Glen, 1998, 2003). Corbett and Leach, (1998) inferred that the constraints that localised WNW mineralised vein systems of the Cadia deposit and others between N-S arc parallel structures in the LFB were related to the transitory changes from orthogonal to oblique convergence during the Ordovician.

Most LFB Ordovician magmatic suites are either calc-alkaline or high-K calc alkaline (Blevin, 2002; Holliday et al., 2002; Sillitoe, 1997) and therefore are similar to typical Circum-Pacific porphyries. However, the Cadia, Ridgeway and Northparkes have shoshonitic chemical compositions and are therefore chemically distinctive as well as being unusually large deposits within the belt (Glen, 2002; Sillitoe, 1993 and 1997; Holliday et al., 2002; Blevin, 2002; Peccerillo et al., 1976a; Muller et al., 1994). These deposits are unusual in the context of the circum Pacific region as a whole because the Bajo de La Alumbrera porphyry Cu-Au deposit, Catamarca Province, Argentina, is the only other large Cu-Au porphyry deposit associated with a shoshonite suite. Although the larger LFB deposits are somewhat distinctive in terms of magma chemistry they occur in structural settings that are similar to most other Pacific Rim porphyries.

The Lachlan Transverse Zone (LTZ) described in Chapter 1 has been confirmed in the subsurface with evidence from seismic-reflection studies (Glen et al. 2002). The LTZ is WNW-trending and crosses the N-S arc parallel LFB Ordovician volcanic belts (except the Kiandra belt) at high angle (see chapter I) (Glen et al., 1997). The boundaries of the LTZ varied through time between the Middle and Late Ordovician (Glen et al. 1999). The

LFB Cu-Au porphyries are associated with N-S arc parallel faults that are similar to structures found in proximity to other Pacific Rim porphyries Cu-Au (e.g. porphyry Cu-Au of the Chilean Andes, Chuquicamata, Escondida and El Salvador: Corbett and Leach, 1994).

These deposits are often also associated with a second type of structure and occur at or near the intersection of two types of structures. In Papua – New Guinea, the arc-parallel structures are intersected by transfer structures that appear important for mineralisation. The PNG transfer structures are long-lived crustal fractures perpendicular to the strike of the fold belt that were placed in dilation during episodes of oblique collision (Hill et al., 2002). Many porphyry Cu-Au deposits are associated with the intersection of transfer faults and strike-parallel extension faults including the Early-Middle Miocene (14-17 Ma) Frieda River deposit (Britten, 1981; Whalen et al. 1982), the Late Miocene (6.0 Ma) Porgera deposit (Richards and McDougall, 1990), and the Quaternary (1.2 Ma) Ok Tedi deposit (Page and McDougall, 1972).

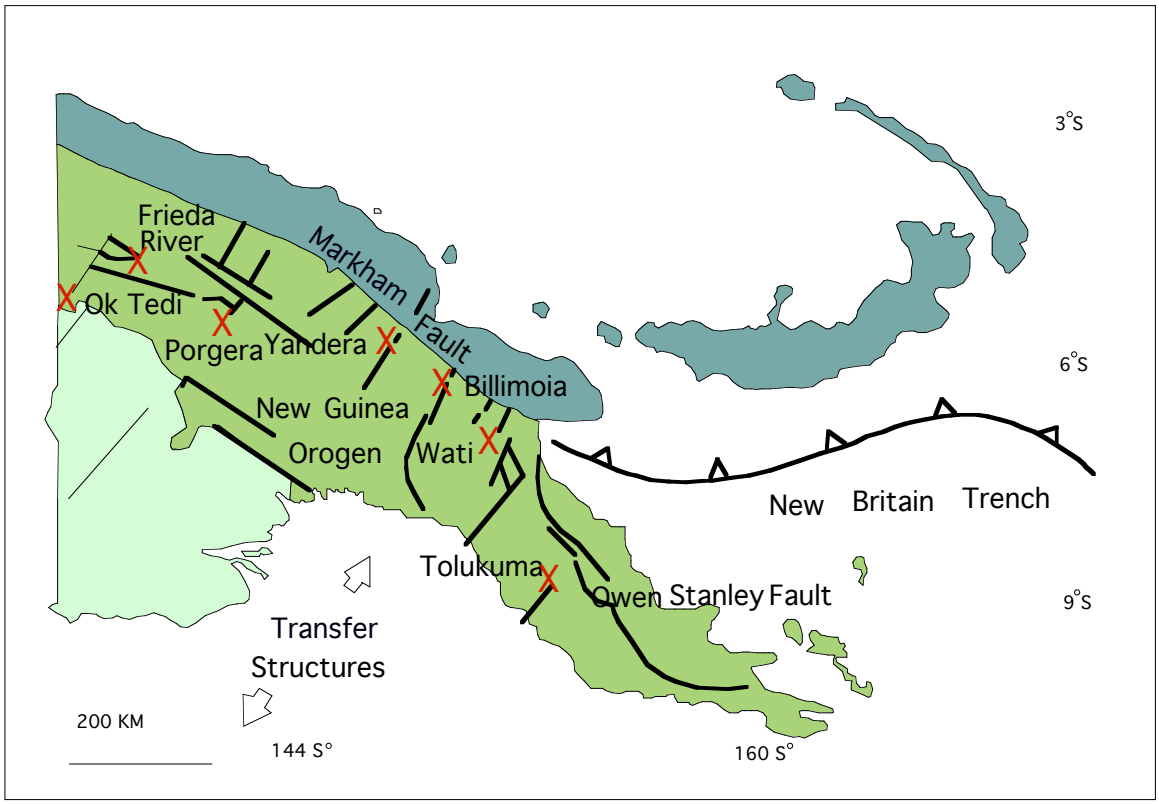

Figure 5.1 PNG transfer structures, major orogen-parallel faults and porphyry related Au-Cu mineralisation. X = Au-Cu deposits. From Corbett and Leach (1994).

There are similarities between the LTZ structure and structures associated with younger porphyry deposits such as transfer structures in Papua - New Guinea (Fig 5.1). Both the LTZ and the PNG transfer structures cross the main subduction-related structures at high angle (Glen et al. 1997; Hill et al. 2002). Seismic reflection profiling results indicate that the LTZ is a major crustal tear oblique to the convergent margin between the Australian and proto-Pacific plates (Glen et al. 1998b and 2002). The LTZ was active in the development of the LFB Ordovician west dipping subduction from at least the Middle Ordovician (Glen et al. 1999, 2003). Although the shoshonitic magmas of Cadia and Ridgeway are somewhat distinct, it is clear that their structural setting is completely consistent with porphyry deposits elsewhere.

5.4 PORPHYRY SUBGROUPS VERSUS TECTONICS OF THE LACHLAN FOLD BELT

Magmatism and the various gold deposits of the LFB can be subdivided in terms of the structural evolution of the fold belt. Glen et al. (1997, 1998b) first showed that Late Ordovician porphyries are richer in potassium (more shoshonitic) along the LTZ than similarly aged magmatism to the north and south. Shoshonites along the LTZ include those at Goonumbla, Forest Reefs and the Blaney Volcanics and the Weemala Formation (Glen et al., 1997). Major LFB Ordovician porphyry Cu-Au deposits (Ridgeway, Cadia and Goonumbla) lie within this zone.

Glen et al. (2003) recognised 4 groups of LFB Ordovician porphyries based on age data (Table 5.1). They are also distinct in terms of petrography and major element chemistry as noted by Glen and demonstrated in chapter 2 and 3 and in terms of trace element chemistry as documented in Chapter 4. They formed during 3 pulses of volcanism over a ~ 50myr time interval punctuated by two major hiatuses (Glen et al. 2003). Mineralisation is not associated with the pre- and syn-LTZ porphyries (Table 5.1; Glen et al. 2003) but did occur with LTZ magmatism during a third pulse of arc volcanism between ~450-~439 Ma (Glen et al., 1998, 2003).

The petrographic data presented in Chapter 2 documents how mineralisation styles and alteration intensities differ inside and outside the LZT. As expected, the larger deposits within the LTZ have stronger alteration signatures and a more diverse assemblage of sulphide and other secondary minerals. The most importance for the following discussion on Nb and Ta are the differing types of magnetite associated with

deposits inside and outside the structure. Porphyries inside the LTZ contain titaniferous and non-titaniferous magnetites that correspond respectively to igneous minerals and alteration related varieties whereas hydrothermal magnetite is less abundant at the smaller deposits outside the LTZ (Fig. 4.9A and B).

Compositional differences between the Cadia-Ridgeway deposits and other LFB localities provide a way to distinguish between the most economically important porphyry subgroups defined by Glen et al. (2003). As described in Chapter 4, these differences include distinctive major element behaviour such as the Fe abundances of some Ridgeway rocks and the Th abundances of Cadia samples. It is desirable to find additional geochemical features that may be clearly and consistently diagnostic of gold-prospective rocks. Accordingly, this study included the acquisition of accurate Nb and Ta data for LFB Ordovician magmas because these elements have recently been the focus of major studies lead by the work of Munker (1998) that indicate previously unrecognised variations in Nb/Ta occur among subduction-related magmas.

Porphyry Group	Age	Geochemical Affinity	Volcanic Belt	Mineralisation
Pre-LTZ Group 1	484 Ma: at the end of phase 1 volcanism	Shoshonite, High-K, Calc-alkaline	Junee-Narromine	No mineralisation found
Pre-LTZ Group 2A	465 Ma; at the initiation of phase 2 volcanism	High-K, Calc-alkaline	Junee-Narromine	No mineralisation found
Syn-LTZ Group 2B	455 Ma; near the end of phase 2 volcanism	High-K, Medium-K, Calc-alkaline	Junee-Narromine	No mineralisation found
Post-LTZ Group 3	450-455 Ma: at the beginning of phase 3 volcanism	Medium-K, Calc-alkaline	All belts	Cu-Au: Copper Hill Cargo, Narromine
Post-LTZ Group 4	439 Ma: at end of phase 3 volcanism	Shoshonite	All belts except Kiandra	Cu-Au: Cadia Ridgeway, Northparkes, Forest Reef

Table 5.1 LFB Ordovician porphyry groups based on age and structural setting. Adapted from Glen et al. (2003).

5.5 A COMPARISON OF Nb/Ta VARIATIONS IN LFB AND OTHER MAGMAS

Oxidised magmas are commonly cited as favourable for the development of porphyry gold deposits. Blevin and Chappell (1992) and others have applied this type of model

specifically to the larger LFB deposits. Therefore, it is possible that geochemical monitors of oxidation state in magmas may provide important exploration criteria. Two elements, Niobium and Tantalum, were a special focus of the present research because of the possibility that they might provide such criteria. The two elements were formerly considered chemical twins that behaved similarly under normal geological conditions because they have the same valency [+5] and similar ionic radii. As a result, the Nb/Ta ratio were considered to be virtually fixed at ~ 17.5. It is now recognised that Nb/Ta of ~ 12 is more typical of the earth's crust and that subduction zone magma systems can have highly variable Nb/Ta (e.g. 8 to 25 in one Cambrian island arc: Munker, 1998). Many studies have now examined Nb/Ta variations in granites, pegmatites and veins (Munker, 1998, Sawka et al., 1990, De et al., 2000, Smith et al., 1997). Nb/Ta ratios are highly variable in late stage units such as pegmatites. Niobium and Ta reside in oxide phases such as columbite {(Fe, Mn) Nb_2O_6} and tantalite {(Fe, Mn) Ta_2O_6} and rutile (TiO_2). Therefore, hydrothermal fluids related to late stage melts could often be associated with distinct Nb/Ta ratios.

As described in Chapter 4, subduction related magmas are characterised by a marked enrichment of large ion lithophile elements (LILE) and a systematic depletion of high field strength elements (HFSE). Fluids and melts derived from the dehydration of the basaltic portion of the subducted slab and of subducted sediments are inferred to enrich the depleted mantle wedge in LILE and light rare earth elements (LREE) (Munker, 1998). All of the Ordovician magmas of the LFB exhibit these features to some degree. The High Field Strength elements Nb and Ta are generally incompatible within evolving magmas but, as the host minerals listed above indicate, they may be concentrated in Fe-bearing minerals. Accordingly, they are plotted against iron oxide in Figure 5.2. Apart from a tendency for high-Fe Cadia-Ridgeway samples to exhibit low Nb and Ta contents, correlations between Nb and Ta versus iron are not obvious. A plot of Nb/Ta versus Fe_2O_3 wt.% does exhibit a correlation between the ratio and increasing iron content that is most obvious for Cadia-Ridgeway samples.

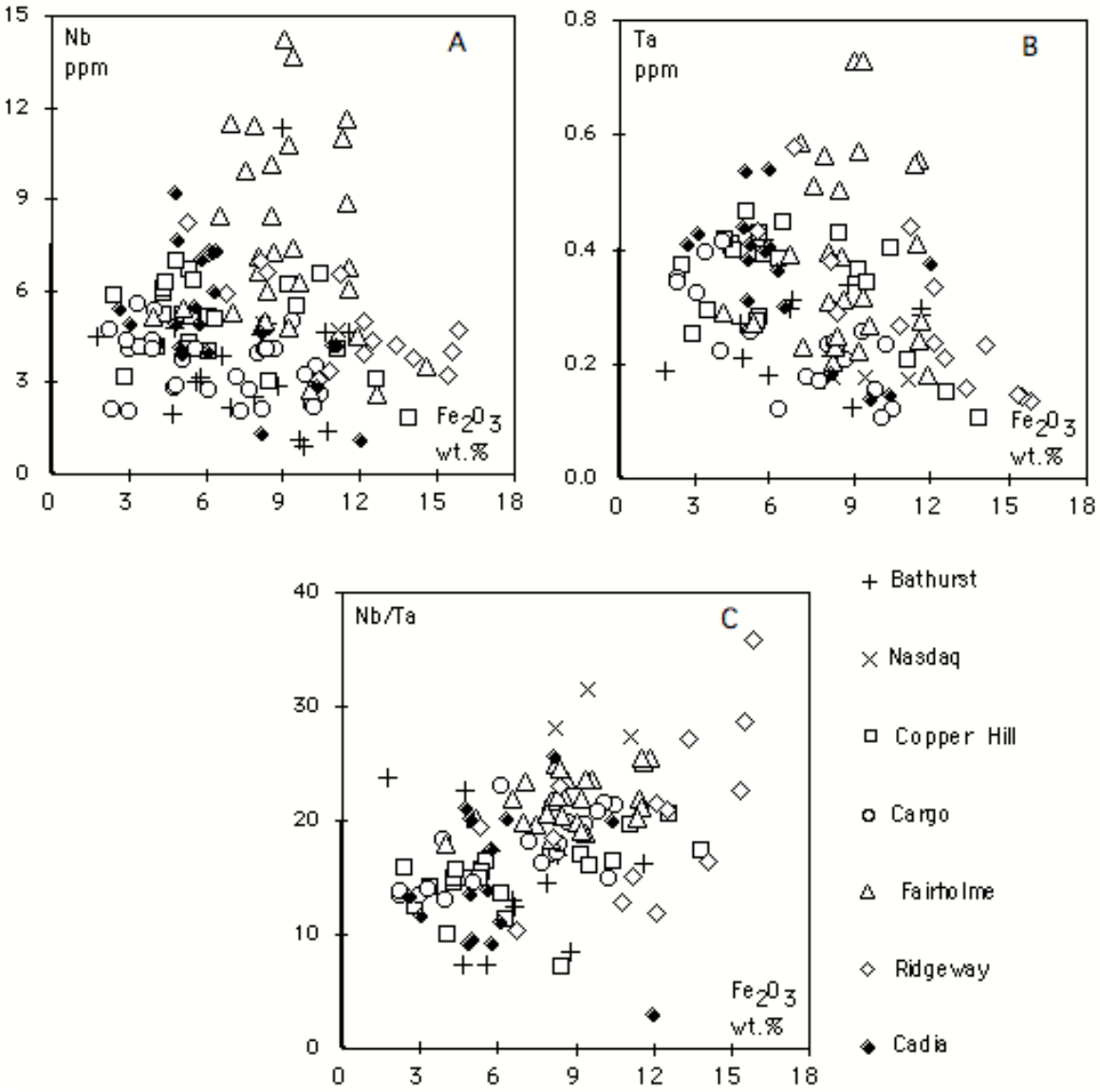

Figure 5.2 Variation of Nb and Ta with iron oxide contents of Lachlan Fold Belt igneous rocks in NSW.

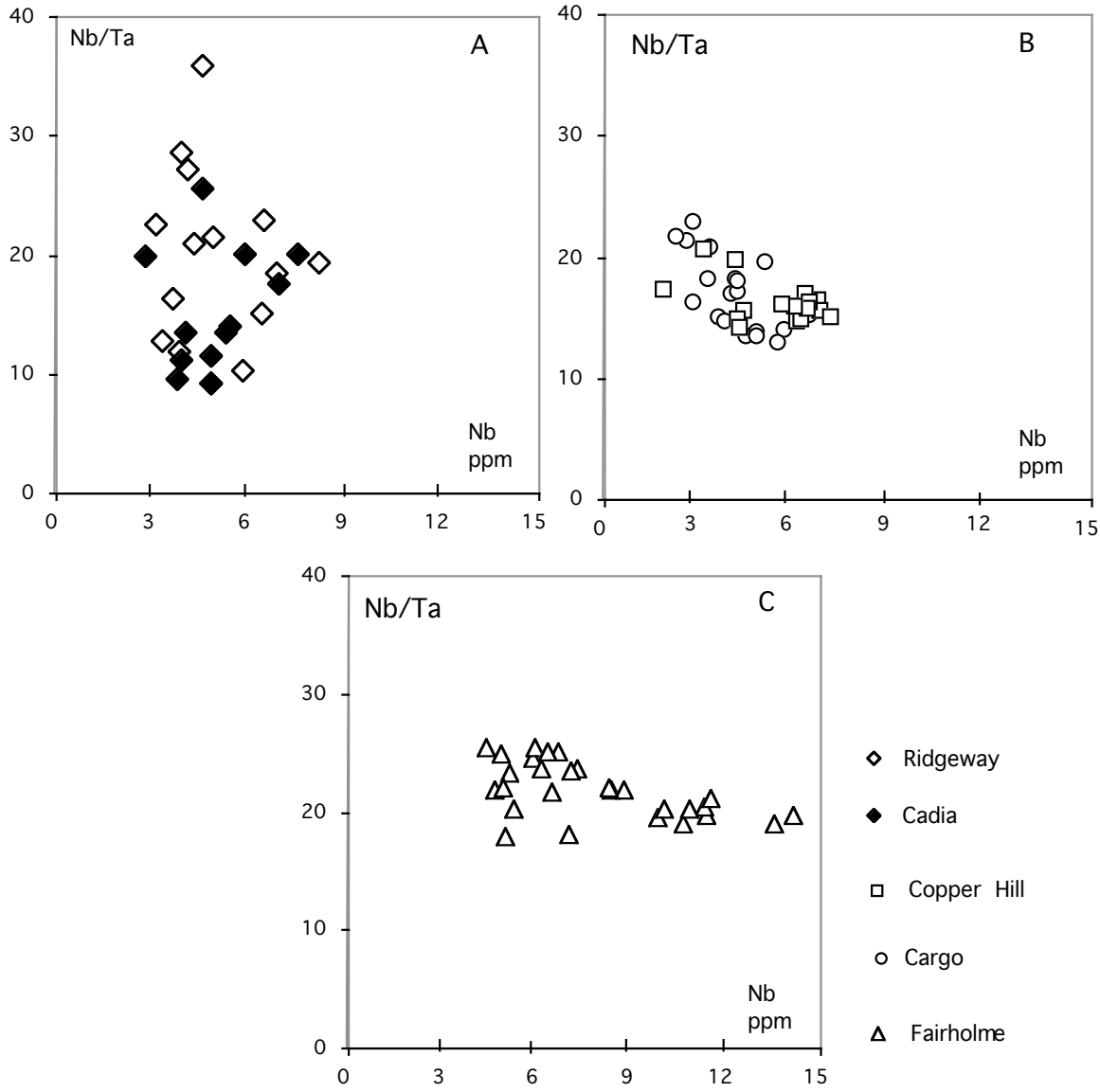

Figure 5.3 Variation in Nb/Ta versus Nb contents (in ppm) for Lachlan Fold Belt igneous suites in NSW associated with gold mineralisation.

Variations in Nb/Ta are commonly plotted against absolute Nb concentrations (eg., Munker, 1998) and the LFB magmas are compared on this type of a plot in Figure 5.3. Important differences in behaviour are obvious between Cadia-Ridgeway and Fairholme, Copper Hill or Cargo. The smaller deposits show nearly constant Nb/Ta or a very gradual decrease in Nb/Ta with increasing Nb. Cargo shows the steepest decline in Nb/Ta whereas Fairholme and Copper Hill exhibit only weak trends to lower Nb/Ta. Overall, data for the smaller deposits indicates a slight preferential incorporation of Nb in a mineral phase, probably a common oxide such as magnetite or perhaps chromite, ilmenite, etc. If the controlling mineral was magnetite then the proportions of Nb and Ta taken up by this oxide may vary with oxidation state of the magma. For example, the

Cadia-Ridgeway data does not display similar declines in Nb/Ta with greater Nb and appears to exhibit a weak positive trend.

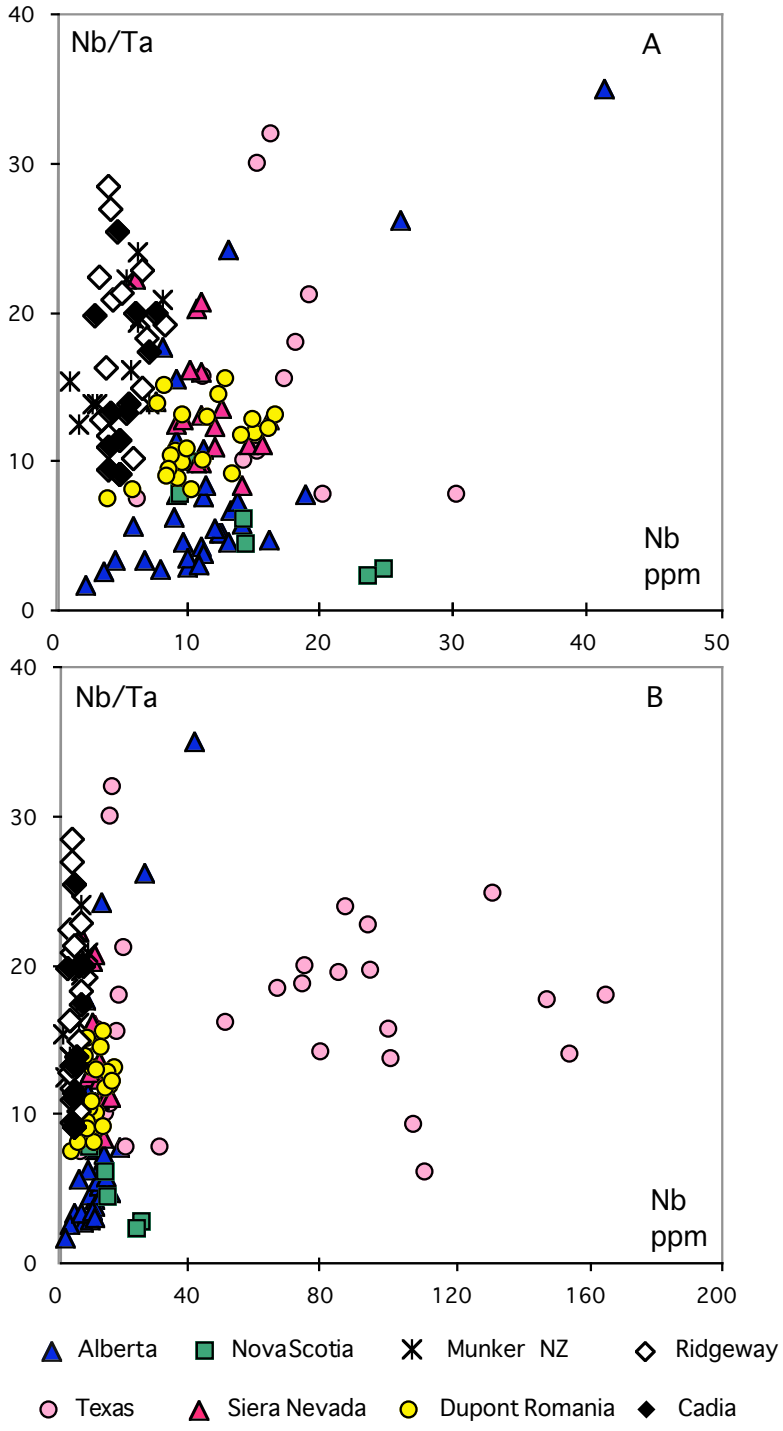

Figure 5.4 A comparison of variations in Nb/Ta versus Nb contents (in ppm) for Cadia – Ridgeway rocks with other igneous suites reported in the literature. See text for a description of the chemical affinities of the various rock suites. Note Fig. 5.4A and 5.4B present the same data but at different horizontal scales.

The Cadia – Ridgeway data is compared to a variety of non-shoshonitic magma suites from around the world, New Zealand, USA and Romania in Figure 5.4. They include aluminous Nova Scotia S-type granites derived from sedimentary precursors (Dostal and Chatterjeb, 2000), calc alkaline magmas from a Cambrian arc – back arc in New Zealand (Munker, 1998) and the Sierra Nevada batholith (Sawka et al., 1990) along with high-K rocks associated with porphyry mineralisation in Romania (Dupont et al., 2002). Two suites of mid-Proterozoic "anorogenic" from Texas granites (Smith et al., 1997) cover a wide range of Nb contents. The New Zealand arc suite most closely resembles the Cadia-Ridgeway suites having low Nb contents and a relatively large range of Nb/Ta. However, the NSW rocks can be distinguished on this basis of higher Nb/Ta ratios for some samples. The Sierra Nevada batholith and Romanian High-K suite are distinguished from the Cadia – Ridgeway suite by their higher Nb contents compared to the NSW samples

The Cadia – Ridgeway data is compared to two other shoshonitic suites in Figure 5.5. The other data sets include the fresh to highly altered rocks associated with porphyry mineralisation at the Bajo de la Alumbrera deposit, Argentina (Ulrich and Heinrich, 2001). The other shoshonite samples are from Northern Capertee area of the Lachlan Fold Belt but are not associated with major porphyry deposits (Carr et al., 2003).

Unaltered Bajo de la Alumbrera samples define a trend that is similar to those defined by non-shoshonite suites of the LFB (e.g. Cargo, Copper Hill in Fig. 5.3) but at higher Nb contents. Altered rocks at Bajo de la Alumbrera have undergone variable degrees of mass loss or mass gain (Ulrich and Heinrich, 2001) which has contributed to a wide range of Nb contents. The Nb/Ta ratios of these rocks are lower than unaltered rocks at low Nb contents (resulting from dilution during mass gain) and higher at high Nb contents that correspond to mass loss and Nb concentration. Neither the fresh rock nor the altered rocks from Bajo de la Alumbrera define trends similar to those of the Cadia-Ridgeway suite. The Capertee samples are similar to the Cadia-Ridgeway samples in terms of their low Nb contents but they do not define as high a Nb/Ta range.

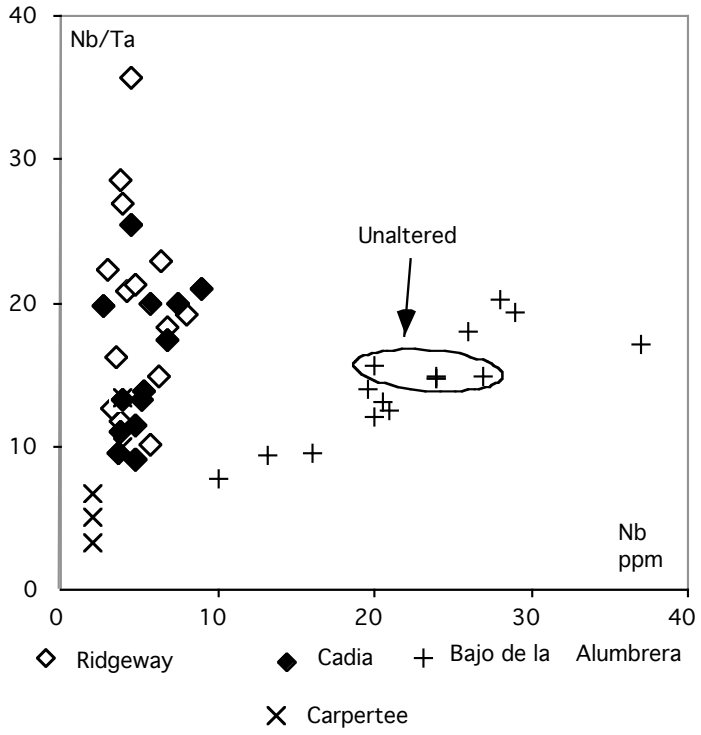

Figure 5.5 A comparison of variations in Nb/Ta versus Nb contents (in ppm) for Cadia – Ridgeway rocks versus mineralised shoshonites (Bajo de la Alumbrera) and unmineralised LFB shoshonites in NSW (Northern Capertee).

In total, these results indicate that the Cadia-Ridgeway magmas have distinctive properties in terms of the behaviour of Nb and Ta that 1) do not appear to be a result of alteration, based on altered shoshonite samples from Bajo de la Alumbrera, and 2) are similar to some subduction related suites but extend to higher Nb/Ta ratios. Similarities between calc alkaline magmas from New Zealand and the Cadia–Ridgeway suite and differences between Cadia-Ridgeway and unaltered Bajo de la Alumbrera or other LFB suites indicates that the behaviour of Nb and Ta is not directly correlated with the shoshonitic classification that is derived from a K_2O versus silica plot (Fig. 3.3).

Although this study did not establish a single distinctive pattern of Nb/Ta behaviour in either shoshonites or ore-related porphyry magmas at the global scale, the results do appear to provide important information for exploration within the LFB itself. Only the Cadia – Ridgeway deposits exhibit a wide range of Nb/Ta values and lack the near-horizontal trend seen for other localities associated with smaller gold deposits. The fact that the weakly prospective Capertee samples exhibit a narrow range of Nb values and lower Nb/Ta suggest that the shoshonite trend for the LFB as whole is a steep one on

these plots of Nb/Ta versus Nb. The higher Nb/Ta values correspond in some way with the less evolved rocks (Fig. 5.2C). Given that Au is derived from the porphyry magmas, this observation indicates that most evolved rocks, in terms of high Na/Ta ratios, correlate with the exsolution and transfer of Au from the magma systems. Evidence from the altered Bajo de la Alumbrera samples suggests that the Cadia-Ridgeway (± Capertee) trend is not the product of hydrothermal transport of either or both of Nb and Ta. This view is supported by the fact that where hydrothermal effects can be distinguished for Ridgeway in the unusual Fe trends, these samples do not have distinctive Nb or Ta contents versus Cadia samples.

5.6 FACTORS CONTRIBUTING TO LARGE PORPHYRY DEPOSITS IN THE LACHLAN FOLD BELT

Sillitoe (1997) outlined mechanisms or factors that may enhance the efficiency of gold concentration and favour the creation of large gold porphyry deposits. These include a range of mechanisms that operate during part of a process, which starts with sub-crustal magma generation and ends with gold accumulation by hydrothermal processes. It may be that a combination of factors are required optimise the gold transport and deposition process that produces large deposits.

The sequence of gold mineralisation events probably includes the following key factors. The mantle processes, post-subduction partial melting of the uppermost seawater –altered parts of stalled (dead) slabs, may generate highly oxidised magma as well as destabilising mantle sulphides to release Cu-Au during arc magmatism (McInnes and Cameron, 1994). The rapid cooling or depressurisation of such magmas promotes the saturation of magmatic fluids and their release from the magmas to shallow crustal levels (Lowenstern, 1993). The favourable hydrothermal processes involve focusing and ponding of these fluids, which is enhanced by marked contrasts in the permeability of rocks and structures at the sites of ore deposition (Sillitoe, 1997).

The tectonic evolution of the Lachlan Fold Belt, and the distribution and size of ore deposits in the belt, appears to correlate with factors outlined by Sillitoe (1997) which favour large Au deposits. For example, the Cadia and Ridgeway igneous suites did not form during steady state of subduction, as was the case for earlier and smaller deposits, but during the final orogenic stages of the Ordovician subduction process (Glen et al. 2003). The Cadia and Ridgeway magmas formed during post subduction partial melting

when magma production was likely associated with slab steepening when oxidised magmas are favoured (Sillitoe, 1997). Major and trace element characteristics of the Ordovician LFB magmas (Chapters 3 and 4) confirm that there are chemically distinctive features in the Cadia-Ridgeway rocks and that, contrary to earlier claims, they are among few examples of shoshonitic magmatism in the belt. The presence of abundant igneous and hydrothermal magnetite in the Cadia and Ridgeway samples confirms the oxidised nature of the sub-crustal melts (Ishihara, 1981; Chapter 2) and is particularly obvious in the chemical trends of the Ridgeway samples.

The Lachlan Transverse Zone represented a major zone of crustal permeability at the time the Cadia-Ridgeway magmas were formed. As a result, the magmas could ascend rapidly to shallow crustal levels with comparatively little evolution during ascent. Rapid cooling and oxidation of magma at shallow crustal levels enhance saturation and the release of magmatic fluid while also increasing Au and Copper incompatibility that leads to their efficient partitions into the magmatic fluid (Sillitoe, 1997). Therefore, the magmas retained a high gold content and had the potential to release large amounts of magmatic fluid. The increase in Au-Cu deposit size from small (Copper Hill-Cargo) to world class (Cadia-Ridgeway) indicates the importance of magma composition during this process. High sulphur and chlorine correlate with increased magma alkalinity and favours gold mineralisation because Au and Cu are transported by sulphur and chlorine in hydrothermal fluids (Muller and Groves, 1997).

A lithological cross section of the Cadia Cu-Au deposit shows marked contrast in permeability (Forster et al. 2003). It consists of Ordovician sediments (limestone, calcareous sandstone and conglomerate), Ordovician lava and tuff, and Ordovician mafic-intermediate igneous rocks. The relatively permeable but potentially receptive calcareous wall rocks are believed to be particularly suitable for the localisation of a large Cu-Au deposit at Cadia. At Cadia, nearly all mineralised vein systems shows WNW orientations and are constrained between N-S arc parallel structures but are specifically associated with dilatant fracture. (Corbett, 1998).

The magmas and fluids associated with these dilatant fractures are linked to larger volumes of magma at depths. Therefore, small igneous bodies, such as at Ridgeway, may narrowly focus volumes of liquid that are similar to those associated with larger low grade deposits such as Cadia. The differing behaviour of Fe in trends of the Cadia and Ridgeway deposits is most likely a result of the diffuse nature of Cadia mineralisation

compared to the focused, high grade, nature of Ridgeway mineralisation. More focused mineralisation produced greater amounts of hydrothermal magnetite in higher grade ore.

The geochemical data reported above indicate that both the Ridgeway and Cadia magmas were similar in terms of Nb and Ta and distinct from most other LFB magmas. The evolution of the magmas to high Nb/Ta ratios over small ranges of Nb indicates the magmas evolved differently from other LFB magmas where Nb/Ta declined slightly with increasing Nb. The different behaviours are probably linked to the state of oxidation of the magmas that may impact on the distribution of Nb and Ta between oxide phases and magma liquids. If Nb-Ta behaviour is linked to oxidation state then the similar results for New Zealand arc magmas indicates other factors must also be important to produce a major porphyry deposit as outlined by Sillitoe (1997). The most obvious differences between the Cadia-Ridgeway and New Zealand rocks described by Munker, (1998) is that the latter are volcanic in origin and associated with an arc – back arc system. Therefore they did not form in a tectonic regime that is suitable for the evolution of porphyry intrusions and the focusing of separated fluids during dilatant episodes despite the fact that they have similar Nb-Ta and Nb/Ta variations that are probably linked to their oxidation state.

5.7 SUMMARY

The LFB Ordovician porphyry deposits in NSW are among the oldest deposits of this type recognised around the Pacific. They resemble younger porphyry deposits, however, in terms of tectonic setting and associated host structures. The larger LFB porphyries are, however, chemically distinct from most other examples in having an association with shoshonite magmas (Cadia, Ridgeway and Northparkes).

The LFB Ordovician porphyries are subdivided into four subgroups on the basis of age, relative emplacement ages in terms of the development of the LTZ (pre-, syn-, post-LTZ), petrography and chemical features (Glen et al., 2003). No mineralisation has been found or reported among pre-LTZ porphyries, but it is common among post-LTZ porphyries. Chemical variations also occur among porphyries of the LFB that are linked to their occurrence inside and outside the LTZ. Compositional differences between larger Cu-Au deposits, Cadia-Ridgeway and smaller deposits, Copper Hill, Cargo and Fairholme are obvious in terms of Nb-Ta abundances and variations in Nb/Ta. The smaller deposits show constant Nb/Ta or negative Nb/Ta trends, but the larger deposits display positive Nb/Ta trends. This distinction is indicative of differences in the host

minerals for Nb and Ta and the presence of oxidised magmas associated with the larger deposits. Distinctions also exist between the trace element behaviours of the Cadia-Ridgeway magmas and other shoshonite magmas at the Bajo de la Alumbrera deposit, Argentina. Conversely, calc alkaline magmas from New Zealand display Nb/Ta trends that are similar to Cadia-Ridgeway. On this basis, it is evident that Nb – Ta behaviour, and perhaps magma oxidation state, are not directly correlated with the shoshonitic classification that is based on K_2O vs. SiO_2.

The distribution and size of ore deposits in the LFB is related to the tectonic evolution of the belt. Important factors that promote large deposits start with the sub-crustal generation of oxidised magma and finish with structural sites that favour Cu-Au accumulation by hydrothermal processes. The increase in Au-Cu deposit size from small (Copper Hill-Cargo) to world class (Cadia-Ridgeway) is partly indicative of the importance of magma composition during this process. The most obvious differences, however, between the Cadia-Ridgeway and New Zealand rocks is that the latter are volcanic in origin and associated with an extensional tectonic setting in an arc-back arc system. Therefore, they did not form significant porphyry intrusions and there was no focussed movement of hydrothermal fluids during short dilatant episodes. As a result, large gold deposits did not form despite the fact that the New Zealand magmas have similar Nb-Ta and Nb/Ta variations that are probably linked to their oxidation state.

CHAPTER 6

CONCLUSIONS

The Cu-Au mineralisation associated with the Ordovician igneous rocks in the Lachlan Fold Belt exhibits many features that are typical of younger porphyry deposits. The petrographic features and microprobe data for the Ordovician igneous suites at Cadia, Ridgeway, Cargo, Copper Hill and Fairholme establish primary and secondary features that distinguish igneous trends and magmatic subgroups. Calc alkaline to shoshonitic rocks are characterised by the variable abundance of primary K-feldspar. Fractionation of primary pyroxenes, amphiboles and igneous magnetite define several igneous trends in the chemical data. The most pervasive alteration is associated with highly mineralised shoshonite Ordovician rocks at Ridgeway and Cadia. Less mineralised calc alkaline Ordovician rocks at Cargo, Copper Hill and Fairholme are less strongly altered.

The hydrothermal mineral assemblages observed in the LFB study areas are characteristic of younger Cu-Au porphyry style mineralisation. The high Ti-Mn-Cr content of iron oxides in the Bathurst, Copper Hill and Fairholme indicate magmatic origin. Whereas the low abundance of these elements in the Ridgeway iron oxides suggests hydrothermal source. The variable contents of Ti-Mn-Cr in Cadia iron oxides reflect a combination of magmatic and hydrothermal origin.

The major element study shows that most of the Ordovician rocks samples are weakly altered. They retain primary igneous trends for most mobile elements. The effect of post magmatic processes, such as veining, can be seen in a few samples that lie far off of certain trends. The K_2O enrichment of Ordovician rock samples is consistent with subduction-modified mantle- wedge source. The high Fe_2O_3 of some Ridgeway samples suggest porphyry-style hydrothermal alteration process. On a K_2O versus Silica plot the Ordovician rocks define two broad trends that correspond to 1) a Low-K to High-K group and 2) shoshonites. These two groups correspond to the alkalic and non-alkalic subdivisions used in TAS diagrams. In these terms, the Cadia and Ridgeway samples are entirely alkalic but the Copper Hill samples are all non-alkalic. Cargo, Fairholme and Bathurst samples are alkalic or tholeiitic. This evidence indicates that alkalic magmas, which are favourable for gold, are widespread in the LFB.

The main trace element characteristics of the LFB Ordovician igneous rocks include LREE and LILE enrichments and HFSE depletions, which are consistent with a subduction-related tectonic setting. The rocks all fall in the volcanic-arc granite and syn-

collisional granite field of the Nb-Y tectonic discrimination diagram of Pearce et al. (1984). Several magma types are identified based on differences in the HFSE and REE trends of the Ordovician samples. The difference in the extent of magma fractionation is evident. The Ridgeway samples define a wider range of trace element concentrations than the Caida samples. Distinct fractionation processes can be observed in trace element plots. Fairholme samples display high Nb trend from the main Nb-Zr trend but its Ta trend lies within the Ta-Zr field. This evidence reflects Nb/Ta variation among the Ordovician rocks.

The LFB Ordovician porphyries are among the oldest porphyries deposits around the Pacific Rim. They share similar tectonic and structural settings with the younger deposits. However, the LFB porphyries are chemically distinct from most other large deposits in being associated with shoshonitic magmas (Cadia, Ridgeway and Northparkes), (Cooke, 1998 and Glen et al., 2003).

The LFB Ordovician porphyries are subdivided into two pre-LTZ subgroups, one syn-LTZ subgroup and one post-LTZ subgroup. No mineralisation has been found or reported among pre-LTZ porphyries, but it is common in post-LTZ porphyries. Chemical distinctions also occur between porphyries inside and outside the LTZ in term of igneous chemistry and the intensity of hydrothermal alteration and gold deposited. Compositional differences exist between larger Cu-Au deposits, Cadia-Ridgeway and smaller deposits such as Copper Hill, Cargo and Fairholme. Differences are obvious in terms of Nb-Ta depletion and variation. The smaller deposits show constant or negative Nb/Ta trends, but the larger deposits display positive Nb/Ta trends. This distinction is indicative of a difference in the type of Nb and Ta-hosting mineral phases and the magmatic evolution processes associated with these deposits. Distinctions were found between the trace element behaviours of the Cadia-Ridgeway magmas and other shoshonite magmas at the Bajo de la Alumbrera deposit, Argentina. Conversely, calc alkaline magmas from New Zealand display Nb/Ta trends that are similar to Cadia-Ridgeway. Therefore, Nb – Ta behaviour and magma oxidation state are not directly correlated with the K_2O vs. SiO_2 shoshonitic classification.

Important factors that promote large deposits start with the generation of oxidised magmas in the subduction-modified mantle and finish with structural sites that favour Cu-Au accumulation by hydrothermal processes. The increase in Au-Cu deposit size from small (Copper Hill-Cargo) to world class (Cadia-Ridgeway) is partly indicative of the importance of magma composition during this process. The most obvious differences,

however, between the Cadia-Ridgeway and New Zealand rocks is the volcanic origin of the latter and their association with an extensional arc-back arc system. Therefore, these magmas did not form in a tectonic regime characterised by suitable minor dilatant episodes. As a result, large gold deposits did not form despite the fact that the New Zealand magmas have similar Nb-Ta and Nb/Ta variations that are probably linked to their oxidation state.

REFERENCES

Blevin, P.L., 2002, The petrograpic and compositional character of variably K-enriched magmatic suites associated with Ordovician porphyry Cu-Au mineralisation in the Lachlan Fold Belt, Australia. Mineralium Deposita 37, 87-99.

Blevin, P.L. and Chappell, B.W., 1992, the role of magma sources, oxidation states and fractionation in determining the granite metallogeny of eastern Australia, Transactions of the Royal Society Edinburgh, Earth Science 83, 305-316.

Bonham, H. F., 1988, bulk mineable gold deposits of the Western United States, Economic Geology Monograph 6, 193-207.

Branagan, D.F., and Packham, G.H., 2000, Field geology of New South Wales (3rd ed.), Department of Mineral Resources of New South Wales, 1-45.

Britten, R., 1981, The Geology of the Frieda River Copper Prospect, PNG, PhD thesis, Australian National University, Canberra.

Bowman, H.N., 1994, Bathurst 1: 250 000 geological sheet excursion guide, Geological Survey of NSW.

Carr, P.F., Fergusson, C.L., Pemberton, J.W., Colquhoun, G.P., Murray, S.I., and Watkins, J., 2003, Late Ordovician island-arc volcanic rocks, northern Capertee Zone, Lachlan Fold Belt, New South Wales, Australian Journal of Earth Sciences 50, 319-330.

Chappell, B.W and White, A.J.R, 1992, I and S type granite in the Lachlan Fold Belt, transactions of the Royal Society of Edinburgh Earth Sciences 83, 1-26.

Collins, A and Jones, M, 1998, Mineral Hill- Exploration beyond drill hole number 776, Australian institute of Geoscientists Bulletin 23, 27-31.

Corbett, G.J, 1998, Lachlan Fold Belt magmatic Au-Cu in a world context, Australian Institute of Geoscientists Bulletin 23, 33-38.

Corbett, G.J and Leach, T.M, 1994, SW Pacific Rim Au/Cu systems: structure, alteration and mineralisation, Exploration Workshop Manual, 51-64. Unpublished Report.

Cooke, D.R., Heithersay, P.S., Wolfe, R., Calderon, A.L., 1998, Australian and western Pacific porphyry deposits, AGSO Journal 17, 97-104.

Creelman, R.A, Lipton, I.T and Stagg, R. N, 1990, Browns Creek gold deposit, Geology of Mineral Deposits of Australia and Papua New Guinea, 1399-1401.

De, S.K., Chacko, T., Creaser, R.A. and Muehlenbachs, K., 2000, geochemical and Nd-Pb-O isotope systematics of granites from the Taltson magmatic zone, NE Alberta:

implication for early Proterozoic tectonics in the western Laurentia, Precambrian Research, 102, 221-249.

Dostal, J., and Chatterjee, A. K., 2000, contrasting behaviour of Nb/Ta and Zr/Hf ratios in a peraluminous granite pluton (Nova Scota, Canada), Chemical Geology, 163, 207-218.

DMR, 2002a, Resource Assessment, Annual Report, 2001-2002, Department of Mineral Resources of New South Wales, 14-27.

DMR, 2002b, Positive outlook for the NSW gold industry, NSW mining and exploration quarterly, Minfo 75, 12-15.

Dawson, K.M., and Kirkham, R.V., 1996, Skarn copper in: Eckstrand, O.R., Sinclair, W.D., and Thorpe, R.I., (eds.) Canadian Mineral Deposit Types, Geological Survey of Canada, Geology of Canada 8., 460-476.

Dupont, A., Auwera, J.V., Pin, C., Marincea, S. and Berza, T., 2002, Trace element and isotope (Sr, Nd) geochemistry of porphyry and skarn mineralising Late Cretaceous intrusions from Banat, western South Carpathians, Romania, Mineralium Deposita, 37, 568-586.

Fergusson, C.L, 2003, Ordovician-Silurian accretion tectonics of the Lachlan Fold Belt, southeastern Australia, Australian Journal of Earth Sciences, 50, 475-490.

Finlayson, D. M, Korsch, R. J., Glen, R.A., Leven, J. H., and Johnstone, D. W., 2002, Seismic imaging and crustal architecture across the Lachlan Transverse Zone, a cross-cutting feature of eastern Australia, Australian Journal of Earth Sciences, 49, 311-321.

Foster, D. A., Gray, D. R., and Bucher, M., 1999, Chronology of deformation within the turbidite-dominated Lachlan Fold Belt: implications of the tectonic evolution of eastern Australia and Gondwana, Tectonics, 18, 452-485.

Foster, D.B and Seccombe, P.K, 2003, Controls on skarn mineralisation and alteration at the Cadia deposit, NSW, Australia, the Ishihara symposium, Geoscience Australia, 59-63.

Glen, R.A, Crawford, A.J and Cooke, D.R, 2003, Tectonic setting of porphyry copper-gold mineralisation in the Macquarie Arc, Geoscience Australia, 65-68.

Glen, R.A et al., 2002, Crustal structure of the Ordovician Macquarie Arc, Eastern Lachlan Orogen, based on seismic-reflection profiling, Australian Journal of Earth Sciences, 49, 323-348.

Glen, R.A., and Beckett, J., 1997, Structure and tectonics along the inner edge of a foreland basin: the Hunter Coalfield in the northern Sydney Basin. Australian Journal of Earth Sciences 44, 853-877.

Glen, R.A., and Walshe, J.L., 1999, Cross-structures in the Lachlan Orogen; the Lachlan transverse zone example. Australian Journal of Earth Science 46, 641-658.

Glen, R.A., 1998b, The Eastern Belts of the Lachlan Orogen, In: Finlayson, D.M. and Jones, L.E.A, eds, Mineral Systems and Crust-Upper Mantle of Southeast Australia, Australian Geological Survey Organisation Record, 1998, 2, 80-82.

Glen, R.A., 1998, Structural Geology, Bathurst, NSW, Geological Survey of NSW 1: 250 000 Geological Series Explanatory Notes, 287-310.

Glen, R.A., Walshe, J.L., Barron, L.M., and Watkins, J.J., 1997, New model for Copper-Gold deposits in Ordovician Volcanics, Minfo 56, 4-6.

Glen, R.A., and Wyborn, J.L., 1997, Inferred thrust imbrication deformation gradients and the Lachlan Transverse Zone in the Eastern Belt of the Lachlan Orogen. Australian Journal of Earth Sciences 44, 49-68.

Glen, R. A and Wyborn, D., 1996, Inferred thrust imbrication, deformation gradients and the Lachlan Transverse Zone in the Eastern Belt of the Lachlan Orogen, Australia Journal of Earth Sciences, 44, 49-68.

Glen, R. A., and Watkins, J.J., 1994, The Orange 1:100 000 sheet, a preliminary account of stratigraphy, structure and tectonics, and implications for mineralisation, Quarterly notes, Geological Survey of NSW, 95, 1-16.

Golden Cross Operations Pty Ltd, 2004, Copper Hill porphyry Cu-Au-Pb project, NSW, Australia, information memorandum report GCO N. 202.

Golden Cross Resources Limited, 2001, Copper Hill and Cargo project, NSW, Annual report, 13-15.

Gray, D. R., and Foster, D. A., 1997, Orogenic concepts-application and definition: Lachlan Fold Belt, eastern Australia. American Journal of Science, 297, 859-891.

Green, E.M, 2001, The geochemistry of Late Ordovician intrusions in the Lachlan Fold Belt, with particular reference to the Cadia Cu-Au porphyry deposit, Honours thesis, the University of Sydney.

Guilbert, J. M. and Park, C. F., 1986, The Geology of Ore Deposits, W. H., Freeman and Company, New York, 985p.

Heithersay, P. S, O'Neill, W.J, Van der Helder, P., Moore, C. R and Harbon, P. G., 1990, Goonumbla porphyry copper district- Endeavour 26 North, Endeavour 22 and

Endeavour 27 copper-gold deposits, geology of mineral deposits of Australia and Papua New Guinea 2, 1385-1398.

Hill, K.C., Kendrick, R.D., Crowhurst, P.V., 2002, Copper–gold mineralisation in New Guinea: tectonics, lineaments, thermochronology and structure, Australian Journal of Earth Sciences 49, 737–752.

Hills, E.S., 1956, A contribution to the morphotectonics of Australia, Journal of the Geological Society of Australia, 3, 1-15.

Hilyard, D., Drummond, M., Clare, A., Sanders, Y., Aung, Z., Glen, R., Ruskowski, P.,Fleming, G., Lewis, P., and Robson, D., 1996, Preliminary Palaeozoic bedrock interpretation of the Narromine and Nyngan 1: 250 000 sheet areas, Geological Survey of NSW quarterly notes, 101, 1-16.

Holliday, J.R, McMillan, C. and Tedder, I.J., 1999, Discovery of the Cadia Ridgeway gold-copper porphyry deposit, New Generation Gold Mines, 101-107.

Holliday, J.R., Wilson, A.J., Blevin, P.L., Tedder, I.J., Dunham, P.D., and Pfitzner, M., 2002, Porphyry gold-copper minerralisation in the Cadia district, eastern Lachlan Fold Belt, New South Wales, and its relationship to shoshonitic magmatism. Mineralium Deposita, 37, 100-116.

Ishihara S., 1981, The granitoid series and mineralisation, Economic Geology, 75th Anniversary Volume, 458-484.

Le Maitre, R. W., Bateman, P., Dudek, A., Keller, J., Lameyre, Le Bas, M. J., Sabine, P. A., Schmid, R., Sorensen, H., Streckeisen, A., Woolley, A. R. and Zanettin, B., 1989, A Classification of Igneous Rocks and Glossary of Terms, Blackwell, Oxford.

Lickfold, V., and Cooke, D. R., 2003, Endeavour copper-gold porphyry deposits, Northparkes, NSW: intrusive history and fluid evolution, Economic Geology, 98, 1607-1636.

Lowenstern, J. B., 1993, Evidence for a copper-bearing fluid in magma erupted at the Valley of Ten Thousand Smokes, Alaska, contribution to mineralogy and petrology, 114, 409-421.

Lowell, D. J., and Gilbert, J. D., 1970, Lateral and vertical alteration-mineralisation zoning in porphyry ore deposits, Economic geology, 65, 373-408.

Keith, J.D, Whitney, J.A., Cannan, T.M., Hook, C and Hattori, K, 1995, The role of magmatic sulphides and mafic alkaline magmatism in the formation of giant porphyry and veins system: example from the Bingham and Tintic mining districts,

Utah, in: Clark A.H. (ed.) Giant Ore deposits-II, 316-339, QMinEx, Department of Geological Sciences, Queen's University, Kingston, Ontario.

McInnes, B.I.A. and Cameron, E. M., Carbonated alkaline hybriding melts from a sub-arc environment mantle wedge samples from the Tabar-Lihir-Tanga-Feni arc, PNG, Earth and Planetary Science letters, 122, 125-141.

Mineral Resources NSW, 2001, 150th anniversary of official discovery of gold, the Ophir rush. , Geological Survey of New South Wales, information brochure, unpaginated.

Muller, D., and Groves, D.I., 1997, Potassic Igneous Rocks and Associated Gold-Copper Mineralization, (2nd Ed.) Springer, Berlin, 238p.

Muller, D., Heithersay, P. S, Groves, D.I., 1994, The shoshonite porphyry Cu-Au association in the Goonumbla district, NSW, Australia, Mineral and Petrology, second edition, 51, 299-324.

Munker, C, 1998, Nb/Ta fractionation in a Cambrian arc/back arc system, New Zealand: source constraints and application of refined ICPMS techniques, Elsevier Science, 24-45.

Newcrest Mining Staff, 1998, Cadia gold-copper deposit, Geology of Australian and Papua New Guinea Mineral Deposits, 641-646.

Newcrest Mining Staff, 1999, Report on exploration of the EL 5328 Cargo for the period November 1998 to November 1999, submitted to the NSW Department of Mineral Resources.

North Limited, 1995, Lake Cowal gold project, Minfo, NSW mining and exploration quarterly 48, 34-38.

Page, R.W. and McDougall, I., 1972, Ages of mineralisation of gold and porphyry copper deposits in the New Guinea highlands, Economic Geology, 67, 1034-1048.

Pearce, J. A., Harris, N. B. W. and Tindle, A. G., 1984, Trace element discrimination diagrams for the tectonic interpretation of granitic rocks, Journal of Petrology 25, 956-983.

Peccerillo, A., Taylor, S.R., 1976, geochemistry of Eocene calcalkaline volcanic rocks from the Kastamonu area, northern Turkey, Mineralogy and Petrology, 58, 63-81.

Perkins, C, Walshe, J.L, and Morrison, G, 1995, Metallogenic episodes of the Tasman Fold Belt system, eastern Australia, Economic Geology, 1443-1450.

Packham, G.H, 1969, The Geology of New South Wales, Journal of the Geological Society of Australia 16, 1-17.

Richards, J.P., and McDougall, I., 1990, geochronology of the Porgera gold deposit, PNG, resolving the effects of excess argon on K-Ar, and $^{40}Ar/^{39}Ar$ age estimates for magmatism and mineralisation, Geochimica et Cosmochimica Acta, 54, 1397-1415.

Rickwood, P. C., 1989, Boundary lines within petrologic diagrams which use oxides of major and minor elements, Lithos, 22, 247-263.

Rollinson, H, 1993, Using Geochemical Data, Longman Scientific & Technical, Harlow, 352p.

Sawka, W. N., Chappell, B. W. and Kistler, R. W., 1990, Granitoid compositional zoning by side-wall boundary layer differentiation: evidence from the Palisade Crest Intrusive Suite, Central Sierra Nevada, California, Journal of Petrology, 31, 519-553.

Scheibner, E., and Basden, H., 1998, Geology of New South Wales-synthesis, Geological Survey of New South Wales, Sydney.

Scheibner, E., and Stevens, B. P. J., 1974, the Lachlan River lineament and its relationship to metallic deposits, Quarterly Notes of the Geological Survey of New South Wales, 14, 8-18.

Sillitoe, R.H., 1979, some thoughts on gold-rich porphyry copper deposits, Mineralium Deposita, 14, 161-174.

Sillitoe, R.H., 1989, Gold deposits in western Pacific island arcs: the magmatic connection. Economic Geology Monograph 6, 274- 291.

Sillitoe, R.H, 1990, Gold rich porphyry deposits of the Circum Pacific, 2, 119-126.

Sillitoe, R.H, 1991, Gold metallogeny of Chile- an introduction, Economic geology 86, 1187-1205.

Sillitoe, R.H, 1992, Gold and copper metallogeny of the central Andes, past, present and future exploration objectives, Economic geology, 87, 2205-2216.

Sillitoe, R.H, 1993, Gold-rich porphyry copper deposits: geological model and exploration implications, Geological Association of Canada, Special Paper 40, 465-478.

Sillitoe, R. H., 1993b, Gold -rich porphyry copper deposits: geological model and exploration implications, In: Kirkham, R. V. Sinclair, W. D., Thorpe, R. I. and Duke, J. M., eds, Mineral Deposits Modelling, 465-478, Geological Association of Canada, Special paper 40.

Sillitoe, R.H, 1997, Characteristics and controls of the largest porphyry copper-gold and epithermal deposits in the circum-Pacific region, Australian journal of Earth Sciences 44, 373-388.

Smith, D. R., Barnes, C., Shannon, W., Roback, R. and James, E., 1997, Petrogenesis of Mid-Proterozoic granitic magmas: example from Central and West Texas, Precambrian research, 53-79.

Stegman, C.I, 2001, Peak Gold Mines- Long-term future in NSW, NSW mineral exploration and investment conference, 58-60.

Stegman, C.L., and Pocock, J. A., 1996, The Cobar Gold Field- A Geological Perspective, in: Cook, W. G., Ford, A. J. H, Dermott, J. J., Standish, P. N., Stegman, C. L. and Stegman, T. M., (eds.), The Cobar Mineral Field- A 1996 Perspective, the Australasian Institute of Mining and Metallurgy 1996 publication, 229-264.

Sun, S. S., and McDonough, W. F., 1989, Chemical and isotopic systematics of oceanic basalts: implications for mantle composition and process, in: Saunders, A. D. and Norry, M. J. (eds.), magmatism in ocean basins, Geo. Soc. London, Spec. Publ., 42, 313-345.

Suppel, D. W., and Scheibner, E., 1990, Lachlan Fold Belt in New South Wales-Regional geology and mineral deposits, in Geology of the mineral deposits of Australia and Papua New Guinea of the Australasian Institute of Mining and Metallurgy, Melbourne, 1321-1327.

Surman, J, 1994, Brown Creek mine, Gold deposits of Central Western NSW excursion, DMR of NSW and AGSO excursion guide: Bathurst 1: 250, 000 geological sheet.

Suppel, D.W, 1984, A study mineral deposits in the Cobar Supergroup, Cobar region, NSW, M. Sc thesis, the University of NSW.

Ulrich, T., and Heinrich, C.A., 2001, Geology and alteration geochemistry of the porphyry Cu-Au deposit at Bajo de la Alumbrera, Argentina, Economic Geology 96, 1719-1742.

Whallen, J.B., Britten, R.M. and McDougall, I., 1982, Geochronology and geochemistry of the Frieda River prospect area, PNG, Economic Geology, 77, 592-616.

Wilson, A. J., Cooke, D. R., and Harper, B. L., 2003, the Ridgeway gold-copper deposits: a high-grade alkalic porphyry deposit in the Lachlan Fold Belt, NSW, Australia, Economic Geology, 98, 1637-1666.

Wyborn, D., and Henderson, G. A. M., 1993, Blayney 1:100 000 scale geological map,

Australian Geological Survey Organisation, Canberra.

Wyborn, D, 1992, The tectonic significant of Ordovician magmatism in the eastern Lachlan Fold Belt: tectonophysics 214, 287-303.

APPENDIX 1: ELECTRON MICROPROBE ANALYSES

1A: pyroxene

Ridgeway

Sample	RW1	RW1	RW1	RW13	RW13	RW13	RW13	RW13	RW13	RW13
	Augite	Augite	Augite	Augite	Augite	Augite	Augite	Augite	Augite	Augite
Na_2O	0.27	0.30	0.30	0.32	0.25	0.29	0.24	0.51	0.35	0.15
MgO	16.00	15.67	16.24	14.50	14.40	14.09	15.47	13.79	14.26	17.85
Al_2O_3	1.97	2.44	1.52	2.66	2.58	2.26	1.37	2.22	1.78	0.94
SiO_2	52.49	52.23	53.14	50.19	50.66	50.71	51.56	50.16	51.40	52.86
K_2O	0.01	0.00	0.01	0.01	0.00	0.02	0.02	0.00	0.04	0.01
CaO	22.53	22.33	22.79	20.38	21.57	21.69	23.55	22.94	22.22	21.91
TiO_2	0.32	0.29	0.18	0.53	0.39	0.41	0.19	0.42	0.23	0.08
Cr_2O_3	0.45	0.24	0.32	0.14	0.14	0.13	0.39	0.22	0.07	0.63
MnO	0.18	0.14	0.13	0.36	0.20	0.20	0.25	0.71	0.40	0.14
FeO	5.52	6.37	5.19	10.00	8.71	9.14	5.33	8.09	8.23	4.21
CuO	0.00	0.09	0.09	0.01	0.14	0.00	0.00	0.00	0.07	0.00
ZnO	0.01	0.00	0.00	0.00	0.03	0.05	0.00	0.01	0.08	0.01
Total	99.75	100.10	99.91	99.10	99.07	98.98	98.35	99.08	99.15	98.78

Pyroxene

	Ridgeway			Fairholme					
Sample	RW13	RW13	RW13	DR37-258	DR42-119	DR42-119	DR42-119	DR42-119	DR42-119
	Augite	Augite	Augite	Augite	Augite	diopside	diopside	diopside	diopside
Na_2O	0.20	0.83	0.18	0.36	0.35	0.35	0.33	0.17	0.16
MgO	15.11	15.53	15.79	13.21	13.84	13.19	12.86	17.71	17.36
Al_2O_3	2.92	3.84	2.31	1.40	2.07	0.71	0.89	1.10	1.09
SiO_2	50.29	49.06	51.03	51.83	50.97	51.33	51.34	52.40	51.38
K_2O	0.00	0.01	0.02	0.02	0.00	0.00	0.00	0.02	0.00
CaO	22.55	19.60	22.01	20.30	24.15	23.85	24.14	23.13	23.24
TiO_2	0.37	0.54	0.32	0.24	0.18	0.04	0.03	0.10	0.13
Cr_2O_3	0.50	0.11	0.32	0.06	0.06	0.01	0.06	0.28	0.31
MnO	0.05	0.10	0.19	0.41	0.26	0.24	0.42	0.07	0.08
FeO	6.58	7.16	6.75	7.05	8.50	7.93	8.33	3.34	2.82
CuO	0.00	0.07	0.14	0.00	0.00	0.00	0.08	0.08	0.01
ZnO	0.00	0.00	0.10	0.31	0.00	0.04	0.06	0.00	0.07
Total	98.58	96.85	99.14	95.18	100.37	97.71	98.53	98.42	96.65

Pyroxene

Fairholme

Sample	**DR42-119**	**DR42-119**	**DR42-119**	**DR42-119**	**DR42-119**	**DR42-119**	**DR42-119**	**DR42-119**	**DR42-119**	**DR42-119**
	Augite	**Diopside**	**Augite**	**Augite**	**Diopside**	**Diopside**	**Augite**	**Augite**	**Diopside**	**Augite**
Na_2O	0.21	0.17	0.13	0.14	0.30	0.37	0.23	0.19	0.43	0.32
MgO	16.77	17.58	16.66	16.93	12.62	13.44	14.66	16.23	13.35	14.88
Al_2O_3	2.32	1.26	1.46	1.35	0.78	0.85	3.16	2.29	0.89	2.92
SiO_2	50.95	52.88	49.10	51.21	50.50	51.11	49.12	49.86	51.63	49.86
K_2O	0.00	0.02	0.00	0.02	0.00	0.00	0.00	0.00	0.00	0.00
CaO	22.88	23.95	22.82	23.00	23.31	24.41	22.45	22.65	24.61	21.68
TiO_2	0.19	0.08	0.19	0.15	0.03	0.02	0.32	0.21	0.05	0.39
Cr_2O_3	0.31	0.21	0.18	0.14	0.00	0.07	0.09	0.62	0.03	0.02
MnO	0.13	0.14	0.14	0.11	0.29	0.19	0.18	0.08	0.23	0.25
FeO	4.13	3.69	4.02	4.22	8.39	7.89	7.29	4.58	8.45	8.11
CuO	0.11	0.00	0.04	0.00	0.03	0.07	0.00	0.00	0.01	0.00
ZnO	0.00	0.08	0.06	0.08	0.00	0.02	0.11	0.00	0.07	0.00
Total	97.99	100.05	94.80	97.34	96.26	98.45	97.60	96.71	99.75	98.43

1B: amphibole

Ridgeway										
Sample	**RW4**	**RW4**	**RW4**	**RW4**	**RW7**	**RW7**	**RW1**	**RW1**	**RW1**	**RW1**
	Tremolite	**Tremolite**	**Tremolite**	**Tremolite**	**Tremolite**	**Tremolite**	**Tremolite**	**Tremolite**	**Tremolite**	**Tremolite**
Na_2O	0.68	0.44	0.62	0.66	0.88	0.87	1.27	1.54	1.54	0.40
MgO	16.41	15.52	14.40	14.84	16.14	17.63	18.77	18.32	18.32	14.54
Al_2O_3	2.45	1.10	3.53	3.21	3.44	2.78	2.83	3.52	3.52	2.92
SiO_2	52.53	54.04	51.15	51.44	51.27	51.70	52.62	51.92	51.92	52.99
K_2O	0.18	0.07	0.17	0.16	0.34	0.23	0.31	0.40	0.40	0.11
CaO	12.51	12.47	12.29	12.22	12.28	12.46	11.77	11.55	11.55	11.76
TiO_2	0.34	0.06	0.21	0.04	0.22	0.31	0.40	0.46	0.46	0.24
Cr_2O_3	0.01	0.01	0.01	0.02	0.03	0.03	0.07	0.00	0.00	0.33
MnO	0.22	0.41	0.32	0.32	0.43	0.28	0.46	0.42	0.42	0.27
FeO	10.74	13.02	13.30	13.19	11.82	9.20	8.83	9.15	9.15	12.69
CuO	0.00	0.06	0.16	0.05	0.00	0.00	0.00	0.02	0.02	0.00
ZnO	0.00	0.00	0.08	0.00	0.02	0.00	0.07	0.00	0.00	0.04
Total	96.06	97.20	96.24	96.15	96.85	95.50	97.40	97.31	97.31	96.29

Amphibole

Ridgeway							**Fairholme**			
Sample	**RW1**	**RW1**	**RW13**	**RW13**	**RW13**	**RW13**	**DR42-180**	**DR42-180**	**DR42-180**	**DR42-180**
	Actinolite	**Tremolite**	**Tremolite**	**Tremolite**	**Tremolite**	**Tremolite**	**Tremolite**	**Tremolite**	**Hornblende**	**Hornblende**
Na_2O	0.29	1.01	1.01	0.88	1.24	0.85	0.25	0.45	2.17	2.10
MgO	13.22	16.26	17.38	17.99	17.08	17.20	12.11	9.91	13.72	13.73
Al_2O_3	2.30	3.15	3.87	3.53	4.61	3.85	1.67	2.07	12.83	12.67
SiO_2	52.11	52.06	50.40	51.40	49.89	49.69	52.66	50.45	41.18	40.97
K_2O	0.13	0.24	0.40	0.37	0.47	0.39	0.07	0.16	0.87	0.86
CaO	12.31	12.23	12.13	12.23	11.92	12.10	12.26	10.40	11.89	11.89
TiO_2	0.20	0.50	0.69	0.70	0.89	0.71	0.12	0.33	1.80	1.70
Cr_2O_3	0.02	0.04	0.03	0.01	0.07	0.03	0.28	0.08	0.00	0.02
MnO	0.46	0.34	0.33	0.34	0.42	0.25	0.45	0.52	0.11	0.08
FeO	15.65	11.01	9.90	9.20	9.94	9.99	6.00	8.37	4.77	5.07
CuO	0.00	0.00	0.01	0.03	0.06	0.04	0.07	0.14	0.00	0.03
ZnO	0.00	0.06	0.03	0.00	0.00	0.00	0.00	0.38	0.00	0.00
Total	96.69	96.91	96.18	96.67	96.59	95.10	85.93	83.27	89.35	89.13

Amphibole

Fairholme					**Cadia**					
Sample	**DR42-180**	**DR42-180**	**DR42-180**	**DR42-180**	**CD14**	**CD14**	**CD14**	**CD14**	**CD14**	**CD14**
	Hornblende	**Hornblende**	**Hornblende**	**Tremolite**	**Tremolite**	**Hornblende**	**Tremolite**	**Tremolite**	**Tremolite**	**Tremolite**
Na_2O	1.98	2.05	2.04	0.19	0.59	0.25	0.17	0.19	0.26	0.41
MgO	13.73	12.96	13.48	10.92	15.71	12.10	14.82	15.14	18.10	16.03
Al_2O_3	12.50	12.26	12.71	1.50	4.08	9.86	3.41	2.36	1.90	2.97
SiO_2	41.45	41.19	41.01	50.75	50.59	50.64	53.30	52.48	55.53	51.75
K_2O	0.79	0.71	0.76	0.08	0.26	3.22	0.37	0.26	0.09	0.11
CaO	12.11	11.84	12.00	12.25	11.77	7.14	11.11	11.43	12.62	12.21
TiO_2	1.74	1.92	1.82	0.03	0.48	0.11	0.14	0.10	0.15	0.16
Cr_2O_3	0.02	0.00	0.04	0.06	0.09	0.13	0.07	0.19	0.05	0.10
MnO	0.09	0.15	0.10	0.49	0.22	0.07	0.35	0.34	0.33	0.29
FeO	5.12	6.15	4.41	6.88	10.66	7.95	11.48	11.35	10.00	10.83
CuO	0.21	0.07	0.00	0.00	0.00	0.00	0.00	0.01	0.00	0.00
ZnO	0.00	0.00	0.00	0.00	0.00	0.00	0.04	0.00	0.00	0.00
Total	89.75	89.31	88.38	83.16	94.44	91.49	95.25	93.87	99.02	94.86

Amphibole Cadia

Sample	CD14	CD14	CD14	CD14	CD14
	Tremolite	Tremolite	Tremolite	Actinolite	Tremolite
Na_2O	0.19	0.13	0.09	0.28	0.33
MgO	17.67	18.90	10.23	15.85	17.21
Al_2O_3	1.34	0.59	10.54	5.91	2.38
SiO_2	53.54	55.80	51.44	49.62	53.17
K_2O	0.02	0.02	3.88	0.35	0.10
CaO	11.89	12.54	7.11	8.02	11.72
TiO_2	0.09	0.01	0.09	0.23	0.18
Cr_2O_3	0.02	0.08	0.02	0.15	0.17
MnO	0.37	0.26	0.17	0.31	0.19
FeO	9.08	8.39	8.94	14.24	9.17
CuO	0.04	0.00	0.03	0.04	0.03
ZnO	0.14	0.00	0.00	0.00	0.05
Total	94.41	96.72	92.51	95.00	94.67

1C: feldspar

Ridgeway

Sample	RW3	RW3	RW3	RW3	RW3	RW3	RW3	RW3	RW9	RW9
	Albite	Albite	Albite	Albite	Albite	Albite	Albite	Albite	Albite	Albite
Na_2O	14.52	14.52	14.52	14.74	14.79	13.44	14.98	14.27	11.35	11.23
MgO	0.00	0.00	0.00	0.00	0.00	0.00	0.01	0.01	0.00	0.02
Al_2O_3	20.55	20.31	19.94	20.08	19.86	19.47	19.81	20.09	20.08	20.30
SiO_2	68.68	69.02	68.61	68.31	68.78	64.56	68.46	68.15	67.91	67.20
K_2O	0.11	0.10	0.11	0.11	0.05	0.04	0.11	0.08	0.07	0.12
CaO	0.10	0.07	0.09	0.09	0.11	0.17	0.10	0.32	0.15	0.27
TiO_2	0.00	0.00	0.00	0.00	0.00	0.01	0.00	0.00	0.00	0.01
Cr_2O_3	0.04	0.02	0.00	0.00	0.00	0.00	0.04	0.00	0.02	0.02
MnO	0.00	0.00	0.00	0.04	0.00	0.04	0.00	0.06	0.00	0.00
FeO	0.34	0.13	0.11	0.33	0.05	0.09	0.08	0.25	0.01	0.30
Total	104.34	104.16	103.38	103.71	103.64	97.82	103.59	103.22	99.59	99.47

Feldspar	Ridgeway								Bathurst	
Sample	**RW9**	**RW9**	**RW9**	**RW9**	**RW9**	**RW9**	**RW9**	**RW9**	**46**	**46**
	Albite	**Albite**	**Albite**	**Albite**	**Albite**	**Albite**	**Albite**	**Albite**	**Albite**	**Albite**
Na_2O	11.58	11.48	10.97	11.54	11.22	11.24	11.28	11.51	11.29	10.07
MgO	0.00	0.01	0.02	0.02	0.00	0.02	0.00	0.00	0.35	0.22
Al_2O_3	19.92	20.04	19.80	19.98	19.62	19.40	19.55	20.20	19.62	20.06
SiO_2	67.71	67.42	66.40	67.34	67.90	67.45	67.97	67.49	67.87	62.85
K_2O	0.07	0.06	0.10	0.04	0.03	0.10	0.08	0.07	0.03	0.75
CaO	0.14	0.08	0.20	0.11	0.16	0.09	0.18	0.13	0.18	0.89
TiO_2	0.00	0.01	0.00	0.05	0.00	0.00	0.04	0.00	0.00	0.41
Cr_2O_3	0.00	0.02	0.00	0.00	0.01	0.00	0.00	0.03	0.08	0.00
MnO	0.03	0.03	0.00	0.00	0.00	0.00	0.02	0.07	0.00	0.07
FeO	0.17	0.78	0.08	0.33	0.03	0.06	0.04	0.03	0.24	3.36
Total	99.63	99.92	97.58	99.42	98.97	98.36	99.14	99.52	99.66	98.68

Feldspar	Bathurst							Cadia		
Sample	**46**	**46**	**46**	**46**	**46**	**46**	**46**	**CD14**	**CD14**	**CD14**
	Albite	**Albite**	**Albite**	**Albite**	**Albite**	**Albite**	**Albite**	**Albite**	**Albite**	**Albite**
Na_2O	11.34	11.40	6.46	9.84	11.29	10.07	11.34	11.12	11.36	10.15
MgO	0.00	0.04	0.01	1.76	0.35	0.22	0.00	0.01	0.00	0.00
Al_2O_3	19.87	19.69	11.52	19.09	19.62	20.06	19.87	19.88	19.18	18.93
SiO_2	67.56	67.89	80.48	63.71	67.87	62.85	67.56	66.55	66.10	62.57
K_2O	0.06	0.06	0.09	0.34	0.03	0.75	0.06	0.12	0.10	0.15
CaO	0.40	0.28	0.29	0.77	0.18	0.89	0.40	1.14	0.82	1.38
TiO_2	0.00	0.05	0.04	0.02	0.00	0.41	0.00	0.03	0.02	0.00
Cr_2O_3	0.00	0.00	0.00	0.08	0.08	0.00	0.00	0.03	0.02	0.05
MnO	0.01	0.01	0.02	0.12	0.00	0.07	0.01	0.00	0.00	0.04
FeO	0.20	0.31	0.28	1.87	0.24	3.36	0.20	0.13	0.42	0.40
Total	99.44	99.74	99.20	97.60	99.66	98.68	99.44	99.01	98.01	93.66

Feldspar	Cadia	Ridgeway					Cadia			
Sample	**CD14**	**RW4**	**RW1**	**RW1**	**RW3**	**RW9**	**CD14**	**CD14**	**CD14**	**CD14**
	Albite	**K feldspar**	**K feldspar**	**K feldspar**	**K feldspar**	**K feldspar**	**K feldspar**	**K feldspar**	**K-Na feldspar**	**Plagioclase**
Na_2O	9.55	0.43	0.81	1.37	1.04	0.21	0.34	0.32	6.36	0.15
MgO	0.02	0.00	0.00	0.02	0.00	0.00	0.00	0.02	0.80	0.01
Al_2O_3	19.63	18.82	19.09	18.10	18.42	18.41	17.36	18.51	20.70	20.76
SiO_2	60.24	63.20	65.53	63.09	65.05	62.88	60.15	66.41	53.71	51.56
K_2O	0.06	16.30	15.99	15.94	15.74	16.62	15.25	16.05	3.77	0.13
CaO	1.51	0.01	0.05	0.11	0.03	0.00	0.11	0.01	0.71	10.98
TiO_2	0.00	0.07	0.00	0.09	0.03	0.00	0.06	0.03	0.01	0.02
Cr_2O_3	0.00	0.00	0.06	0.05	0.06	0.00	0.00	0.00	0.00	0.03
MnO	0.00	0.02	0.06	0.00	0.00	0.00	0.00	0.00	0.00	0.04
FeO	0.10	0.19	0.14	0.25	0.62	0.11	0.13	0.38	1.40	0.09
Total	91.11	99.03	101.72	99.02	100.99	98.24	93.40	101.74	87.47	83.77

Feldspar	Copper Hill					Bathurst				
Sample	**NCH6-142**	**NCH6-142**	**NCH6-142**	**NCH6-142**	**NCH6-142**	**46**	**46**	**46**	**46**	**46**
	K feldspar	**Plagioclase**	**Plagioclase**	**Plagioclase**	**Plagioclase**	**Plagioclase**	**Plagioclase**	**Plagioclase**	**Plagioclase**	**Plagioclase**
Na_2O	0.82	8.53	8.61	7.11	6.66	10.71	9.37	9.46	6.56	7.54
MgO	0.01	0.12	0.03	0.03	0.00	0.02	0.01	0.12	0.00	0.00
Al_2O_3	18.38	22.91	21.83	25.23	26.04	20.60	22.22	21.95	25.82	24.66
SiO_2	64.44	61.45	61.57	59.89	58.82	64.37	63.24	64.10	56.58	59.42
K_2O	15.70	1.32	1.43	0.52	0.41	0.09	0.34	1.55	0.28	0.15
CaO	0.03	2.41	3.30	6.90	7.65	1.85	3.59	1.05	8.16	6.16
TiO_2	0.01	0.00	0.02	0.00	0.01	0.00	0.01	0.00	0.01	0.00
Cr_2O_3	0.00	0.00	0.02	0.00	0.00	0.00	0.03	0.00	0.01	0.01
MnO	0.02	0.00	0.00	0.00	0.03	0.02	0.03	0.02	0.00	0.02
FeO	0.02	0.12	0.01	0.16	0.15	0.00	0.13	0.34	0.12	0.05
Total	99.43	96.87	96.83	99.84	99.76	97.66	98.99	98.58	97.55	98.00

Feldspar **Fairholme** **1D: chlorite** **Ridgeway**

Sample	**DR37-258**	**DR37-258**	**DR37-258**	**DR37-258**	**RW7**	**RW7**	**RW7**	**RW7**	**RW3**	**RW3**
	Plagioclase	**Plagioclase**	**Plagioclase**	**Plagioclase**	**Chlorite**	**Chlorite**	**Chlorite**	**Chlorite**	**Chlorite**	**Chlorite**
Na_2O	5.68	5.24	2.27	5.37	0.04	0.03	0.04	0.06	0.25	0.56
MgO	0.01	0.01	0.11	0.00	20.81	18.40	22.76	20.55	14.15	14.92
Al_2O_3	28.05	28.57	28.69	28.64	17.54	17.81	18.69	18.60	15.94	16.43
SiO_2	55.29	54.99	44.39	54.98	28.51	27.22	27.95	27.70	24.66	25.94
K_2O	0.27	0.21	0.20	0.28	0.02	0.00	0.01	0.03	0.06	0.07
CaO	9.88	10.98	14.11	10.62	0.08	0.09	0.05	0.03	0.29	0.17
TiO_2	0.04	0.03	0.07	0.04	0.10	0.09	0.00	0.05	0.02	0.08
Cr_2O_3	0.04	0.00	0.03	0.00	0.00	0.01	0.00	0.04	0.04	0.02
MnO	0.00	0.00	0.05	0.04	0.43	0.26	0.41	0.43	0.20	0.15
FeO	0.10	0.08	0.61	0.28	19.29	21.48	16.02	18.67	22.77	20.06
Total	99.35	100.10	90.54	100.25	86.82	85.37	85.93	86.17	78.39	78.40

	Ridgeway									
Sample	**RW3**	**RW3**	**RW3**	**RW3**	**RW3**	**RW3**	**RW3**	**RW3**	**RW3**	**RW3**
	Chlorite	**Chlorite**	**Chlorite**	**Chlorite**	**Chlorite**	**Chlorite**	**Chlorite**	**Chlorite**	**Chlorite**	**Chlorite**
Na_2O	0.31	0.18	0.12	0.08	0.06	0.07	0.02	0.04	0.10	0.14
MgO	17.06	17.41	22.07	21.65	20.79	21.41	20.10	21.38	20.27	20.88
Al_2O_3	16.25	16.37	15.48	15.43	15.18	15.06	15.17	15.52	16.41	15.54
SiO_2	27.27	28.52	30.00	30.03	28.69	30.83	28.61	29.97	29.21	30.17
K_2O	0.06	0.06	0.03	0.02	0.02	0.04	0.03	0.01	0.02	0.02
CaO	0.56	0.19	0.40	0.31	0.37	0.24	0.27	0.27	0.43	0.05
TiO_2	0.08	0.05	1.69	1.49	1.14	1.30	1.47	1.68	2.24	0.01
Cr_2O_3	0.00	0.00	0.00	0.06	0.03	0.01	0.00	0.00	0.08	0.00
MnO	0.17	0.22	0.24	0.21	0.21	0.16	0.17	0.21	0.22	0.15
FeO	21.88	22.17	16.83	15.51	16.18	16.29	16.69	15.91	17.61	19.32
Total	83.65	85.16	86.86	84.80	82.67	85.42	82.52	84.99	86.58	86.31

Chlorite	Ridgeway									
Sample	**RW3**	**RW3**	**RW9**	**RW9**	**RW9**	**RW9**	**RW9**	**RW9**	**RW9**	**RW9**
	Chlorite	**Chlorite**	**Chlorite**	**Chlorite**	**Chlorite**	**Chlorite**	**Chlorite**	**Chlorite**	**Chlorite**	**Chlorite**
Na_2O	0.11	0.62	0.09	0.06	0.00	0.07	0.02	0.27	0.04	0.06
MgO	21.38	12.07	18.17	16.03	13.71	20.24	23.22	15.91	22.77	20.03
Al_2O_3	15.87	16.30	17.54	16.87	19.82	19.10	16.91	18.68	18.70	18.13
SiO_2	29.87	25.69	29.95	29.74	27.93	28.35	29.78	30.38	27.60	27.26
K_2O	0.04	0.13	0.17	0.06	0.02	0.04	0.02	0.07	0.02	0.01
CaO	0.57	3.33	0.15	0.30	0.09	0.12	0.54	0.21	0.05	0.07
TiO_2	1.52	0.20	0.30	0.01	0.00	0.03	1.56	0.23	0.07	0.02
Cr_2O_3	0.00	0.05	0.03	0.00	0.00	0.00	0.00	0.00	0.02	0.01
MnO	0.28	0.18	0.23	0.18	0.28	0.19	0.34	0.24	0.24	0.16
FeO	16.20	24.03	19.81	23.11	26.66	18.26	14.42	21.72	17.15	19.96
Total	85.84	82.60	86.44	86.36	88.51	86.40	86.83	87.71	86.67	85.71

Chlorite	Ridgeway			Copper Hill					Bathurst	
Sample	**RW9**	**RW9**	**RW9**	**NCH6-413**	**NCH6-413**	**NCH6-142**	**NCH6-424**	**NCH6-424**	**45.2**	**45.2**
	Chlorite	**Chlorite**	**Chlorite**	**Chlorite**	**Chlorite**	**Chlorite**	**Chlorite**	**Chlorite**	**Chlorite**	**Chlorite**
Na_2O	0.03	0.06	0.03	0.00	0.04	0.16	0.01	0.16	0.03	0.00
MgO	20.19	20.03	20.19	18.73	19.51	17.27	18.39	18.84	13.72	14.12
Al_2O_3	18.03	18.13	18.03	18.59	18.91	18.72	18.76	18.44	17.21	17.01
SiO_2	28.18	27.26	28.18	26.75	27.19	27.66	27.20	27.40	27.25	25.95
K_2O	0.01	0.01	0.01	0.03	0.01	0.00	0.00	0.01	0.02	0.03
CaO	0.04	0.07	0.04	0.14	0.10	0.09	0.09	0.19	0.20	0.42
TiO_2	0.04	0.02	0.04	0.10	0.00	0.07	0.00	0.09	0.02	0.01
Cr_2O_3	0.00	0.01	0.00	0.00	0.00	0.28	0.32	0.38	0.00	0.00
MnO	0.24	0.16	0.24	1.24	1.50	0.75	0.64	0.63	0.42	0.40
FeO	19.70	19.96	19.70	16.49	16.52	9.17	11.87	10.57	25.28	25.17
Total	86.47	85.71	86.47	82.07	83.77	74.17	77.28	76.70	84.14	83.12

Chlorite	Bathurst	Cargo								Fairholme
Sample	45.2	CN1-195-6	CN1-195-6	CN1-195-6	CN1-195-6	CN1-195-6	CN1-195-6	CN1-195-6	CN1-195-6	DR42-119
	Chlorite	Chlorite	Chlorite	Chlorite	Chlorite	Chlorite	Chlorite	Chlorite	Chlorite	Chlorite
Na_2O	0.01	0.02	0.02	0.02	0.06	0.06	0.01	0.16	0.02	0.17
MgO	14.14	18.02	17.98	17.71	18.42	17.50	16.96	18.20	17.54	15.97
Al_2O_3	16.44	18.40	19.09	17.73	15.90	15.48	17.42	15.95	18.13	18.91
SiO_2	25.67	26.81	26.88	28.04	28.94	28.83	27.36	29.12	27.94	25.83
K_2O	0.05	0.01	0.01	0.01	0.20	0.23	0.02	0.01	0.03	0.02
CaO	0.28	0.10	0.07	0.04	0.17	0.15	0.08	0.03	0.07	0.27
TiO_2	0.02	0.08	0.07	0.06	0.97	1.64	0.11	0.06	0.10	0.01
Cr_2O_3	0.03	0.01	0.05	0.05	0.00	0.00	0.00	0.00	0.00	0.13
MnO	0.36	0.07	0.15	0.10	0.16	0.12	0.13	0.09	0.13	0.27
FeO	26.22	11.35	11.84	12.18	10.80	11.20	13.02	10.83	11.09	23.27
Total	83.21	74.86	76.14	75.94	75.62	75.21	75.12	74.45	75.04	84.85

Chlorite	Fairholme	
Sample	DR42-119	DR42-180
	Chlorite	Chlorite
Na_2O	0.17	0.06
MgO	16.67	14.70
Al_2O_3	17.70	18.73
SiO_2	27.44	26.25
K_2O	0.56	0.01
CaO	0.66	0.04
TiO_2	0.07	0.00
Cr_2O_3	0.69	0.24
MnO	0.26	0.20
FeO	22.52	14.31
Total	86.74	74.55

1E: mica	Fairholme			Cargo	Ridgeway
Sample	DR37-258	DR37-295	DR37-295	CN1-195-6	RW7
	Biotite	Biotite	Biotite	Biotite	Mica
Na_2O	0.12	0.07	0.14	0.03	0.07
MgO	13.55	11.82	12.70	16.93	7.74
Al_2O_3	16.33	14.94	15.70	15.70	11.58
SiO_2	26.73	37.24	32.95	30.27	28.65
K_2O	0.01	7.04	6.86	1.51	0.00
CaO	2.60	0.01	0.02	0.05	18.75
TiO_2	2.54	2.46	4.29	1.42	15.95
Cr_2O_3	0.00	0.00	0.03	0.00	0.00
MnO	0.32	0.26	0.24	0.11	0.02
FeO	15.73	19.56	19.26	10.22	7.88
CuO	0.00	0.01	0.09	0.00	0.00
ZnO	0.00	0.00	0.05	0.00	0.15
Total	77.94	93.41	92.32	76.24	90.80

1F: epidote

	Ridgeway			Copper Hill						Ridgeway
Sample	**RW7**	**RW7**	**RW7**	**NCH6-424**	**NCH6-424**	**NCH6-424**	**NCH6-424**	**NCH6-424**	**NCH6-142**	**RW1**
	Epidote	**Epidote**	**Epidote**	**Epidote**	**Epidote**	**Epidote**	**Epidote**	**Epidote**	**Epidote**	**Bornite**
Na_2O	0.00	0.03	0.02	0.01	0.01	0.01	0.02	0.01	0.05	0.02
MgO	0.04	0.00	0.03	0.08	0.01	0.06	0.05	0.11	0.18	0.01
Al_2O_3	21.18	24.00	22.35	23.80	24.24	22.69	22.52	24.12	21.55	0.00
SiO_2	36.35	36.96	36.43	37.33	37.38	37.52	37.09	37.11	34.32	0.05
K_2O	0.01	0.02	0.00	0.00	0.02	0.03	0.00	0.00	0.01	0.00
CaO	22.60	23.35	23.17	23.62	23.47	23.05	23.43	23.16	24.26	0.01
TiO_2	0.11	0.06	0.05	0.00	0.01	0.00	0.02	0.02	0.04	0.02
Cr_2O_3	0.00	0.04	0.04	0.00	0.03	0.02	0.03	0.00	0.02	0.06
MnO	0.23	0.11	0.03	0.14	0.27	0.26	0.24	0.18	0.33	0.00
FeO	13.94	10.66	13.03	5.43	4.87	5.60	5.77	5.23	4.31	0.85
CuO	0.05	0.00	0.00	0.00	0.03	0.10	0.00	0.00	0.10	85.27
ZnO	0.00	0.09	0.00	0.46	0.00	0.00	0.00	0.00	0.08	0.00
Total	94.52	95.33	95.15	90.88	90.34	89.34	89.18	89.95	85.25	86.30

1G: sulphides

	Ridgeway					Fairholme			
Sample	**RW1**	**RW1**	**RW7**	**RW4**	**RW9**	**RW1**	**DR42-119**	**DR42-119**	**DR42-119**
	Bornite	**Bornite**	**Chalcopyrite**	**Chalcopyrite**	**Chalcopyrite**	**Chalcopyrite**	**Chalcopyrite**	**Chalcopyrite**	**Chalcopyrite**
Na_2O	0.20	0.00	0.00	0.06	0.07	0.01	0.14	0.16	0.13
MgO	0.05	0.00	0.03	0.03	0.01	0.00	0.03	0.01	0.03
Al_2O_3	0.02	0.01	0.00	0.02	0.00	0.00	0.01	0.00	0.00
SiO_2	0.15	0.01	0.01	0.03	0.00	0.00	0.00	0.00	0.02
K_2O	0.00	0.04	0.00	0.03	0.02	0.03	0.02	0.02	0.02
CaO	0.08	0.00	0.03	0.06	0.00	0.02	0.06	0.02	0.04
TiO_2	0.04	0.02	0.05	0.06	0.00	0.03	0.00	0.04	0.01
Cr_2O_3	0.00	0.02	0.05	0.00	0.00	0.00	0.00	0.02	0.04
MnO	0.00	0.02	0.00	0.06	0.06	0.00	0.00	0.01	0.00
FeO	1.02	6.59	37.19	37.55	37.87	35.74	37.33	37.42	38.58
CuO	81.49	77.13	42.55	42.27	42.55	44.26	42.83	42.51	44.38
ZnO	0.05	0.00	0.12	0.10	0.05	0.17	0.00	0.17	0.16
Total	83.11	83.83	80.03	80.27	80.63	80.26	80.42	80.37	83.40

Sulphides	Copper Hill			Cargo	
Sample	**NCH6-413**	**NCH6-413**	**NCH6-413**	**CN1-195-6**	**CN1-195-6**
	Pyrite	**Pyrite**	**Pyrite**	**Pyrite**	**Pyrite**
Na_2O	0.81	0.39	0.63	0.00	0.00
MgO	0.01	0.13	0.01	0.00	0.01
Al_2O_3	0.00	0.04	0.02	0.04	0.03
SiO_2	0.01	0.09	0.02	0.02	0.01
K_2O	0.00	0.00	0.00	0.00	0.05
CaO	0.03	0.02	0.01	0.00	0.00
TiO_2	0.02	0.03	0.02	0.05	0.07
Cr_2O_3	0.00	0.01	0.00	0.00	0.02
MnO	0.03	0.05	0.00	0.09	0.02
FeO	60.09	62.12	59.50	71.54	69.65
CuO	0.00	0.00	0.00	0.00	0.16
ZnO	0.00	0.03	0.12	0.27	0.00
Total	61.00	62.91	60.34	72.02	70.02

1H: carbonate

	Ridgeway		
Sample	**RW3**	**RW3**	**RW3**
	Carbonate	**Carbonate**	**Carbonate**
Na_2O	0.05	0.00	0.13
MgO	0.00	0.00	0.03
Al_2O_3	0.00	0.02	0.00
SiO_2	0.01	0.00	0.00
K_2O	0.00	0.00	0.00
CaO	47.35	54.05	54.04
TiO_2	0.00	0.00	0.00
Cr_2O_3	0.00	0.03	0.02
MnO	0.08	0.09	0.06
FeO	0.03	0.11	0.13
Total	47.52	54.31	54.41

1H: carbonate

	Ridgeway					Cadia				
Sample	**RW3**	**RW3**	**RW3**	**RW3**	**RW3**	**RW1**	**RW1**	**RW1**	**CD8**	**CD8**
	Carbonate	**Carbonate**	**Carbonate**	**Carbonate**	**Carbonate**	**Carbonate**	**Carbonate**	**Carbonate**	**Carbonate**	**Carbonate**
Na_2O	0.03	0.02	0.06	0.05	0.0004	0.17	0.18	0.14	0.00	0.00
MgO	0.05	0.00	0.00	0.00	0.0003	7.45	1.21	4.57	0.03	0.08
Al_2O_3	0.00	0.00	0.00	0.00	0.0082	0.14	0.06	0.19	0.01	0.00
SiO_2	0.02	0.00	0.00	0.00	0.0003	0.02	0.03	0.00	0.01	0.13
K_2O	0.00	0.01	0.01	0.02	0.0152	0.03	0.00	0.02	0.00	0.01
CaO	53.44	59.76	56.05	55.86	61.1312	7.88	2.07	6.67	60.70	58.22
TiO_2	0.00	0.03	0.01	0.00	0.0002	0.00	0.06	0.05	0.00	0.01
Cr_2O_3	0.00	0.05	0.03	0.00	0.0002	0.01	0.09	0.05	0.00	0.01
MnO	0.28	0.00	0.08	0.10	0.1747	0.06	0.12	0.23	0.81	0.45
FeO	0.08	0.04	0.02	0.05	0.0668	41.20	55.94	46.74	0.06	0.18
Total	53.90	59.91	56.26	56.09	61.40	56.96	59.76	58.68	61.63	59.10

Carbonate	Cadia									
Sample	**CD8**	**CD8**	**CD8**	**CD10**	**CD10**	**CD10**	**CD10**	**CD8**	**CD10**	**CD10**
	Carbonate	**Carbonate**	**Carbonate**	**Carbonate**	**Carbonate**	**Carbonate**	**Carbonate**	**Carbonate**	**Carbonate**	**Carbonate**
Na_2O	0.00	0.02	0.00	0.02	0.00	0.00	0.05	0.00	0.04	0.02
MgO	0.05	0.10	0.04	0.00	0.00	0.00	0.00	0.04	0.02	0.00
Al_2O_3	0.00	0.00	0.01	0.00	0.00	0.00	0.00	0.01	0.01	0.00
SiO_2	0.07	0.00	0.07	0.01	0.01	0.01	0.02	0.07	0.03	0.04
K_2O	0.00	0.01	0.05	0.00	0.00	0.00	0.04	0.05	0.00	0.02
CaO	59.69	59.67	57.76	55.30	58.69	60.61	57.49	57.76	60.93	62.03
TiO_2	0.02	0.01	0.00	0.01	0.00	0.02	0.00	0.00	0.00	0.00
Cr_2O_3	0.03	0.00	0.01	0.00	0.00	0.00	0.00	0.01	0.00	0.00
MnO	0.54	0.59	0.48	0.08	0.07	0.10	0.00	0.48	0.02	0.01
FeO	0.10	0.04	0.12	0.04	0.00	0.00	0.04	0.12	0.02	0.00
Total	60.50	60.45	58.55	55.46	58.77	60.74	57.64	58.55	61.07	62.12

Carbonate	Cadia	Fairholme						Copper Hill		
Sample	**CD10**	**DR42-119**	**DR42-119**	**DR42-119**	**DR37**	**DR37**	**DR37**	**DR37**	**NCH6-413**	**NCH6-413**
	Carbonate	**Carbonate**	**Carbonate**	**Carbonate**	**Carbonate**	**Carbonate**	**Carbonate**	**Carbonate**	**Carbonate**	**Carbonate**
Na_2O	0.00	0.01	0.03	0.00	0.02	0.04	0.05	0.02	0.00	0.00
MgO	0.00	0.18	0.17	0.15	0.31	0.30	0.26	0.30	0.00	0.01
Al_2O_3	0.01	0.04	0.01	0.01	0.01	0.00	0.02	0.00	0.01	0.02
SiO_2	0.06	0.09	0.02	0.01	0.00	0.01	0.10	0.02	0.04	0.12
K_2O	0.01	0.00	0.00	0.00	0.01	0.00	0.01	0.00	0.00	0.00
CaO	62.01	66.25	65.08	65.99	60.59	64.61	56.93	60.53	63.43	56.26
TiO_2	0.00	0.03	0.00	0.00	0.00	0.00	0.00	0.04	0.00	0.00
Cr_2O_3	0.00	0.08	0.00	0.00	0.00	0.03	0.00	0.00	0.00	0.00
MnO	0.02	0.71	0.67	0.59	1.04	1.02	0.90	1.00	0.99	0.74
FeO	0.00	0.35	0.30	0.25	0.54	0.45	0.53	0.50	0.02	0.06
Total	62.11	67.74	66.28	66.99	62.52	66.46	58.79	62.41	64.49	57.21

Carbonate Copper Hill

Sample	NCH6-413	NCH6-413	NCH6-413	NCH6-413	NCH6-413	NCH6-413	NCH6-413	NCH8-47	NCH8-47	NCH8-47
	Carbonate	Carbonate	Carbonate	Carbonate	Carbonate	Carbonate	Carbonate	Carbonate	Carbonate	Carbonate
Na_2O	0.00	0.00	0.03	0.01	0.01	0.00	0.03	0.06	0.01	0.00
MgO	0.00	0.01	0.03	0.00	0.03	0.03	0.04	0.02	0.09	0.53
Al_2O_3	0.00	0.00	0.01	0.00	0.00	0.00	0.02	0.89	0.12	0.00
SiO_2	0.02	0.00	0.01	0.00	0.00	0.03	0.03	98.04	0.14	0.02
K_2O	0.00	0.02	0.00	0.00	0.00	0.00	0.00	0.04	0.06	0.00
CaO	61.82	60.97	56.30	58.48	66.55	55.85	53.93	0.06	58.32	57.05
TiO_2	0.01	0.01	0.04	0.00	0.00	0.03	0.00	0.01	0.00	0.00
Cr_2O_3	0.00	0.00	0.00	0.00	0.02	0.01	0.00	0.02	0.00	0.00
MnO	1.20	0.60	0.42	0.61	1.75	2.08	0.62	0.00	0.72	2.18
FeO	0.03	0.03	0.05	0.07	0.04	0.08	0.01	0.01	0.02	0.49
Total	63.09	61.64	56.88	59.16	68.39	58.11	54.68	99.15	59.50	60.28

Carbonate Copper Hill Bathurst

Sample	NCH8-47	NCH8-47	45.2	45.2	45.2	46	46
	Carbonate	Carbonate	Carbonate	Carbonate	Carbonate	Carbonate	Carbonate
Na_2O	0.00	0.01	0.00	0.02	0.01	0.00	0.00
MgO	0.24	0.03	0.29	0.23	0.22	0.01	0.00
Al_2O_3	0.00	0.00	0.00	0.01	0.00	0.01	0.00
SiO_2	0.03	0.00	0.00	0.01	0.00	0.02	0.03
K_2O	0.02	0.01	0.00	0.00	0.00	0.00	0.01
CaO	53.51	61.71	58.91	57.06	57.19	59.96	61.11
TiO_2	0.00	0.01	0.00	0.01	0.00	0.01	0.00
Cr_2O_3	0.00	0.00	0.00	0.00	0.05	0.02	0.00
MnO	0.80	0.50	0.84	1.68	1.86	2.09	1.51
FeO	0.20	0.18	1.64	1.01	1.22	0.04	0.06
Total	54.80	62.46	61.68	60.03	60.56	62.16	62.74

1I: magnetite

	Ridgeway									
Sample	**RW3**	**RW9**	**RW9**	**RW9**	**RW4**	**RW4**	**RW4**	**RW4**	**RW3**	**RW1**
	Magnetite	**Magnetite**	**Magnetite**	**Magnetite**	**Magnetite**	**Magnetite**	**Magnetite**	**Magnetite**	**Magnetite**	**Magnetite**
Na_2O	0.07	0.03	0.06	0.02	0.02	0.0006	0.0006	0.0076	0.07	0.08
MgO	0.05	0.00	0.01	0.00	0.02	0.0205	0.0058	0.0126	0.05	0.00
Al_2O_3	0.04	0.05	0.10	0.04	0.02	0.0249	0.0786	0.0742	0.04	0.05
SiO_2	0.02	0.02	0.02	0.01	0.00	0.0003	0.0563	0.0248	0.02	0.06
K_2O	0.01	0.03	0.00	0.02	0.00	0.001	0.0077	0.0135	0.01	0.01
CaO	0.09	0.00	0.00	0.00	0.04	0.0309	0.0161	0.011	0.09	0.06
TiO_2	0.16	0.03	0.04	0.02	0.02	0.0227	0.0642	0.0194	0.16	0.03
Cr_2O_3	0.12	0.00	0.04	0.04	0.00	0.0001	0.0064	0.0001	0.12	0.09
MnO	0.00	0.01	0.03	0.00	0.05	0.0001	0.0456	0.0001	0.00	0.04
FeO	89.09	92.60	91.74	88.39	90.54	91.724	90.8861	90.9948	89.09	87.98
CuO	0.16	0.01	0.00	0.01	0.00	0.0193	0.034	0.0001	0.16	0.02
ZnO	0.02	0.00	0.10	0.07	0.10	0.0001	0.1275	0.0001	0.02	0.00
Total	89.83	92.77	92.14	88.63	90.82	91.84	91.33	91.16	89.83	88.44

magnetite	**Cadia**								**Fairholme**	
Sample	**CD12**	**CD12**	**CD12**	**CD12**	**CD8**	**CD8**	**CD8**	**CD8**	**DR42-119**	**DR42-119**
	Magnetite	**Magnetite**	**Magnetite**	**Magnetite**	**Magnetite**	**Magnetite**	**Magnetite**	**Magnetite**	**Magnetite**	**Magnetite**
Na_2O	0.00	0.06	0.04	0.04	0.04	0.00	0.03	0.01	0.05	0.00
MgO	0.00	0.01	0.00	0.00	0.00	0.02	0.00	0.00	0.00	0.05
Al_2O_3	0.34	0.52	0.27	0.72	3.23	3.01	0.98	2.32	0.09	2.03
SiO_2	0.05	0.12	0.06	0.06	0.14	0.27	1.46	0.12	0.13	0.26
K_2O	0.00	0.00	0.00	0.01	0.00	0.00	0.05	0.01	0.02	0.02
CaO	0.05	0.00	0.01	0.05	0.10	0.14	1.32	0.08	0.02	0.08
TiO_2	0.50	0.62	0.66	0.56	10.06	9.61	10.17	10.53	3.56	5.10
Cr_2O_3	0.05	0.00	0.03	0.00	0.32	0.29	0.34	0.27	0.30	0.17
MnO	0.07	0.10	0.07	0.02	0.12	0.12	0.09	0.15	0.44	0.59
FeO	89.22	86.86	87.28	87.94	74.01	72.96	73.84	73.49	87.95	85.04
CuO	0.00	0.00	0.04	0.07	0.00	0.00	0.10	0.00	0.00	0.00
ZnO	0.05	0.19	0.00	0.03	0.09	0.20	0.14	0.24	0.00	0.17
Total	90.33	88.47	88.45	89.49	88.11	86.62	88.50	87.21	92.57	93.50

magnetite	Cadia		Fairholme		Bathurst			1J: hematite Ridgeway		Fairholme
Sample	CD8	CD8	DR42-119	DR42-119	45.2	45.2	45.2	RW1	RW1	DR42-180
	Magnetite	Magnetite	Magnetite	Magnetite	Magnetite	Magnetite	Magnetite	Hematite	Hematite	Hematite
Na_2O	0.03	0.01	0.05	0.00	0.00	0.01	0.00	0.11	0.09	0.06
MgO	0.00	0.00	0.00	0.05	0.44	0.01	0.01	0.00	0.05	0.00
Al_2O_3	0.98	2.32	0.09	2.03	4.40	4.67	3.03	0.04	0.06	0.05
SiO_2	1.46	0.12	0.13	0.26	1.03	0.10	0.10	0.03	0.05	0.31
K_2O	0.05	0.01	0.02	0.02	0.00	0.00	0.01	0.02	0.02	0.03
CaO	1.32	0.08	0.02	0.08	0.35	0.07	0.01	0.15	0.09	0.12
TiO_2	10.17	10.53	3.56	5.10	6.92	4.35	5.90	0.03	0.07	0.02
Cr_2O_3	0.34	0.27	0.30	0.17	0.01	0.08	0.08	0.10	0.04	1.74
MnO	0.09	0.15	0.44	0.59	0.03	0.00	0.03	0.00	0.03	0.04
FeO	73.84	73.49	87.95	85.04	71.68	77.74	75.88	60.19	67.53	52.39
CuO	0.10	0.00	0.00	0.00	0.00	0.00	0.00	0.00	0.09	0.00
ZnO	0.14	0.24	0.00	0.17	0.00	0.00	0.08	0.04	0.00	0.00
Total	88.50	87.21	92.57	93.50	84.88	87.04	85.14	60.71	68.12	54.77

1J: hematite

	Fairholme				Copper Hill				
Sample	DR42-180	DR42-180	DR42-180	DR42-180	NCH8-47	NCH8-47	NCH6-142	NCH6-142	NCH6-142
	Hematite	Hematite	Hematite	Hematite	Hematite	Hematite	Hematite	Hematite	Hematite
Na_2O	0.06	0.04	0.01	0.05	0.15	0.19	0.02	0.03	0.26
MgO	0.00	0.00	0.03	0.36	0.01	0.00	0.00	0.01	0.01
Al_2O_3	0.05	1.75	0.51	1.35	0.00	0.03	0.47	0.57	0.00
SiO_2	0.22	0.04	4.96	1.50	0.00	0.05	0.05	0.03	0.00
K_2O	0.01	0.00	0.03	0.00	0.05	0.02	0.00	0.02	0.02
CaO	0.11	0.01	5.63	0.70	0.02	0.01	0.04	0.06	0.00
TiO_2	0.00	5.36	6.95	5.47	0.01	0.03	4.18	3.79	0.00
Cr_2O_3	4.25	0.03	0.09	0.06	0.01	0.02	0.07	0.15	0.00
MnO	0.00	0.24	0.00	0.18	0.02	0.04	1.32	0.78	0.00
FeO	52.60	61.20	52.62	61.55	40.54	42.72	58.79	58.70	36.11
CuO	0.00	0.06	0.00	0.00	0.00	0.00	0.00	0.00	0.00
ZnO	0.34	0.00	0.00	0.00	0.27	0.14	0.00	0.00	0.00
Total	57.66	68.74	70.83	71.21	41.07	43.25	64.94	64.14	36.41

1K: sphene and garnet

	Ridgeway	Cadia		Copper Hill		
Sample	RW7	CD10	CD10	NCH6-142	NCH6-142	NCH6-142
	Sphene	Garnet	Garnet	Sphene	Sphene	Garnet
Na_2O	0.03	0.11	0.19	0.00	0.03	0.03
MgO	0.00	0.07	0.01	0.01	0.01	0.03
Al_2O_3	0.84	21.99	21.28	0.42	4.06	17.16
SiO_2	29.70	41.02	42.24	6.06	29.96	34.85
K_2O	0.00	0.02	0.01	0.00	0.02	0.03
CaO	28.19	25.74	25.77	6.28	27.64	24.67
TiO_2	37.43	0.02	0.03	44.83	31.35	9.64
Cr_2O_3	0.01	0.00	0.00	0.07	0.00	0.28
MnO	0.10	0.02	0.00	3.41	0.08	0.20
FeO	1.05	1.71	2.89	13.30	0.13	3.43
CuO	0.00	0.00	0.04	0.06	0.00	0.00
ZnO	0.01	0.07	0.03	0.07	0.22	0.00
Total	97.37	90.76	92.49	74.52	93.5	90.31

Appendix 2. Major (wt.%) and Trace Element (ppm) Data for Igneous Rocks of the LFB

Locality	Ridgeway	Ridgeway	Ridgeway	Ridgeway	Ridgeway	Ridgeway	Ridgeway
Rock Type	Diorite	Diorite	Monzodiorite	Diorite	Monzodiorite	Diorite	Diorite
Sample Name	RW6	RW7	RW2	RW1	RW4	RW8	RW13
SiO_2	49.51	49.61	50.72	53.11	53.90	54.82	53.22
TiO_2	0.53	0.87	0.50	0.53	0.57	0.58	0.64
Al_2O_3	12.80	12.67	10.52	12.70	15.10	14.90	13.92
Fe_2O_3	15.94	15.62	13.47	15.45	12.58	12.21	10.44
FeO	14.35	14.06	12.12	13.90	11.32	10.99	9.39
MnO	0.17	0.14	0.17	0.11	0.08	0.08	0.17
MgO	8.23	6.12	10.73	4.60	4.11	3.78	7.21
CaO	6.40	7.86	8.73	5.92	4.11	4.48	7.68
K_2O	3.54	3.17	2.92	4.73	5.56	4.25	3.01
Na_2O	2.39	3.03	1.89	2.63	3.46	4.45	3.42
P_2O_5	0.48	0.91	0.34	0.21	0.52	0.46	0.30
Ti	3186	5176	2956	3156	3404	3457	3816
Cr	335	38	486	119			216
Co	32	28	31	18	15	18	27
Ni	53	29	69	25		16	39
Rb	52	44	41	57	65	49	52
Sr	406	501	352	433	679	585	554
Ba	496	679	285	773	972	662	754
Sc	26.0	31.4	29.1	25.0	21.9	20.4	39.7
V	229	356	200	203	197	187	251
Ta	0.1	0.1	0.2	0.1	0.2	0.2	
Nb	4.6	3.9	4.1	3.2	4.3	5.0	3.0
Zr	39	57	38	46	68	64	51
Hf	1.19	1.76	1.19	1.44	1.99	1.87	1.54
Th	2.50	2.50	2.65	1.38	3.52	3.22	1.51
U	0.54	0.53	0.44	0.73	1.06	0.80	0.70
Y	14.58	17.07	13.17	13.58	16.52	16.17	16.27
La	11.33	15.34	8.99	7.75	15.14	10.36	10.38
Ce	22.28	31.89	19.17	15.59	30.13	23.05	20.55
Pr	2.89	4.24	2.56	2.07	3.88	3.23	2.73
Nd	12.37	18.48	11.04	9.00	16.54	14.27	11.63
Sm	3.04	4.33	2.69	2.32	3.79	3.57	2.80
Eu	0.77	1.13	0.74	0.71	1.06	0.93	0.90
Gd	2.83	3.95	2.71	2.31	3.52	3.28	2.79
Tb	0.41	0.54	0.39	0.36	0.48	0.46	0.43
Dy	2.78	3.13	2.77	2.43	3.19	3.09	2.72
Ho	0.48	0.59	0.48	0.48	0.54	0.53	0.56
Er	1.34	1.88	1.36	1.60	1.73	1.61	1.68
Tm	0.20	0.22	0.19	0.21	0.23	0.22	0.24
Yb	1.39	1.45	1.33	1.44	1.54	1.48	1.68
Cu	3970	3359	1910	6244	3730	3726	988
Zn	78	94	104	73	57	46	97
Mo					2.1		3.3
Ag	1.2			0.9		0.8	
Tl	0.29	0.17	0.23	0.30	0.33	0.20	0.13
Pb				6.2			5.1
Sn	2.75	3.44	3.45	3.62	2.66	4.33	2.96
Sb		0.23	0.57	0.40			
Ga	17.2	17.6	12.9	15.7	17.1	16.9	14.5
Ge	1.94	2.36	2.79	2.24	1.58	2.23	1.82

Appendix 2. Continued

Locality	Ridgeway	Ridgeway	Ridgeway	Ridgeway	Ridgeway	Ridgeway	Ridgeway
Rock Type	Diorite	Monzonite	Monzonite	Monzonite	Monzodiorite	Monzodiorite	Monzodiorite
Sample Name	RW12	RW3	RW5	RW9	RW10	RW11	RW14
SiO_2	56.10	61.17	62.64	62.22	61.12	62.72	58.52
TiO_2	0.53	0.34	0.41	0.32	0.41	0.42	0.53
Al_2O_3	18.63	13.64	15.66	13.83	14.82	16.35	16.57
Fe_2O_3	8.45	12.19	6.84	10.89	11.32	5.38	8.24
FeO	7.60	10.97	6.15	9.80	10.19	4.84	7.41
MnO	0.05	0.05	0.04	0.04	0.04	0.04	0.08
MgO	2.35	2.91	2.13	1.84	1.83	2.14	3.14
CaO	3.92	1.46	3.09	2.42	2.18	3.01	3.93
K_2O	5.32	5.53	5.32	5.29	4.28	5.59	3.51
Na_2O	4.17	2.57	3.63	3.07	3.83	4.12	5.27
P_2O_5	0.48	0.14	0.23	0.08	0.17	0.22	0.21
Ti	3175	1989	2411	1886	2412	2493	3168
Cr		35	24	39		29	32
Co	8	10	7	12	9	10	12
Ni							
Rb	84	57	64	61	62	69	54
Sr	963	282	476	314	514	370	618
Ba	1050	569	1067	557	764	1118	639
Sc	12.2	9.2	10.3	9.3	10.2	10.3	16.3
V	125	102	93	78	136	103	133
Ta	0.3	0.3	0.6	0.3	0.4	0.4	0.4
Nb	6.5	3.9	5.8	3.3	6.4	8.2	6.9
Zr	72	106	111	104	107	118	68
Hf	1.96	2.76	3.04	2.80	2.96	3.17	1.86
Th	5.32	4.47	5.54	4.63	5.47	5.32	1.70
U	1.49	1.02	1.21	0.51	2.11	1.70	0.66
Y	17.10	9.45	9.85	8.86	13.49	20.23	13.66
La	21.18	6.95	10.82	6.21	15.08	15.19	10.37
Ce	39.17	13.44	20.84	11.97	27.00	33.68	19.91
Pr	4.72	1.72	2.54	1.52	3.22	4.57	2.40
Nd	18.18	7.04	10.17	6.35	12.46	18.88	9.46
Sm	3.93	1.67	2.14	1.56	2.70	4.28	2.20
Eu	1.25	0.46	0.77	0.54	0.87	1.13	0.79
Gd	3.54	1.61	1.93	1.46	2.46	3.80	2.23
Tb	0.48	0.23	0.28	0.22	0.36	0.56	0.35
Dy	3.05	1.65	1.75	1.35	2.43	3.85	2.37
Ho	0.55	0.31	0.36	0.28	0.45	0.67	0.47
Er	1.65	1.05	1.06	0.91	1.51	2.02	1.23
Tm	0.23	0.15	0.17	0.13	0.21	0.32	0.21
Yb	1.61	1.11	1.29	0.99	1.47	2.23	1.42
Cu	3096	7390	130	6034	2434	606	2277
Zn	56	41	36	26	36	31	66
Mo			2.2			6.9	2.3
Ag	0.6	0.9			1.2		0.7
Tl	0.28	0.33	0.46	0.32	0.32	0.34	0.19
Pb	5.5	9.1	5.3	5.9	6.0		6.0
Sn	2.40	1.66	2.98	1.43	3.15	3.20	2.94
Sb		0.37					
Ga	18.1	16.7	14.0	15.3	17.2	15.2	16.4
Ge	1.07	1.43	1.36	1.64	1.17	0.84	1.63

Appendix 2. Continued

Locality	Ridgeway	Cargo	Cargo	Cargo	Cargo	Cargo	Cargo
Rock Type	Monzodiorite	Quartz diorite	Diorite	Diorite	Quartz diorite	Intrusive	Diorite
Sample Name	RW15	DDH011 *	DDH003 *	DDH004 *	DDH009 *	DDH013 *	DDH005 *
SiO_2	57.47	58.02	64.93	65.16	65.42	66.58	66.06
TiO_2	0.43	0.49	0.30	0.31	0.37	0.33	0.29
Al_2O_3	12.73	16.56	16.43	16.70	17.12	15.84	16.73
Fe_2O_3	14.16	7.35	4.80	4.84	3.04	4.06	5.60
FeO	12.75	6.61	4.32	4.35	2.73	3.65	5.04
MnO	0.07	0.07	0.03	0.03	0.02	0.04	0.02
MgO	2.73	4.93	2.80	2.36	3.04	2.74	1.85
CaO	3.90	5.21	3.83	3.49	2.80	3.05	2.80
K_2O	5.39	2.66	1.61	1.60	2.87	2.70	2.04
Na_2O	2.95	4.51	5.11	5.37	5.15	4.53	4.48
P_2O_5	0.17	0.20	0.14	0.15	0.16	0.13	0.13
Ti	2549	2929	1799	1864	2248	1957	1728
Cr		111	31	37	53	36	22
Co	16						
Ni		37	17	15	16	13	38
Rb	55	51	38	42	56	33	30
Sr	313	495	358	336	439	377	557
Ba	566	559	239	291	550	677	647
Sc	15.4	26.7	14.5	16.6	18.5	14.7	11.9
V	118	166	130	128	107	118	76
Ta	0.2	0.0	0.0	0.0	0.0	0.0	0.0
Nb	3.7	2.1	2.8	2.9	4.1	4.2	4.1
Zr	55	88	103	103	92	88	101
Hf	1.41						
Th	1.04	3.08	3.73	3.63	3.08	3.15	3.58
U	0.20	1.03	2.59	1.04	1.03	2.10	1.29
Y	11.77	13.34	12.11	11.09	11.30	9.45	12.22
La	4.41	14.37	8.59	5.80	14.38	14.70	6.66
Ce	9.36	41.06	27.12	24.45	30.81	31.49	32.20
Pr	1.20						
Nd	5.29		19.04	17.82			12.32
Sm	1.48						
Eu	0.47						
Gd	1.61						
Tb	0.27						
Dy	1.92						
Ho	0.37						
Er	1.17						
Tm	0.17						
Yb	1.20						
Cu	2930	12	25	148	14	73	3160
Zn	46	27	20	24	16	19	24
Mo			6.3	25.8			0.4
Ag							
Tl	0.22						
Pb	5.2		3.2	3.5		2.1	3.3
Sn	2.35		0.31	0.52			0.99
Sb			0.41	0.41			0.30
Ga	16.2	15.4	17.2	17.0	13.4	13.6	15.9
Ge	2.30		1.55	1.14			1.69

Appendix 2. Continued

Locality	Cargo	Cargo	Cargo	Cargo	Cargo	Cargo	Cargo
Rock Type	Intrusive	Monzonite	Intrusive	ded porphyry	Diorite	Granodiorite	Granodiorite
Sample Name	DDH012 *	DDH001 *	DDH015 *	DDH016 *	DDH017 *	CN11-43.8	C4-603
SiO_2	72.39	66.18	69.05	67.49	72.30	72.46	66.02
TiO_2	0.22	0.29	0.25	0.25	0.58	0.17	0.30
Al_2O_3	12.82	16.03	15.14	16.12	11.63	14.29	16.04
Fe_2O_3	2.32	3.91	3.02	3.45	5.26	2.95	5.08
FeO	2.09	3.52	2.71	3.10	4.74	2.65	4.57
MnO	0.03	0.05	0.04	0.04	0.02	0.01	0.02
MgO	1.84	2.34	2.24	2.33	1.49	1.04	3.08
CaO	3.71	3.44	2.22	2.24	2.82	1.90	2.59
K_2O	2.46	2.71	3.35	2.68	0.69	1.59	2.49
Na_2O	4.11	4.94	4.59	5.29	4.86	5.46	4.25
P_2O_5	0.09	0.11	0.09	0.11	0.35	0.13	0.12
Ti	1292	1714	1521	1518	3454	1041	1764
Cr	25	25	29	31	0	64	92
Co						5	13
Ni	8	8	10	8	0		
Rb	26	30	35	36	10	42	58
Sr	268	576	270	376	141	245	466
Ba	1088	653	570	475	73	172	510
Sc	8.5	12.3	10.4	10.3	18.7	5.1	10.3
V	74	80	81	74	93	50	97
Ta	0.0	0.0	0.0	0.0	0.0	0.3	0.3
Nb	2.1	4.4	2.1	4.1	0.0	4.3	3.7
Zr	80	100	87	93	93	86	86
Hf						2.22	2.12
Th	3.17	4.19	4.14	4.13	2.07	7.33	3.12
U	0.00	1.02	2.07	2.07	1.04	3.73	2.46
Y	6.34	10.52	8.28	7.24	19.69	7.71	9.52
La	8.45	6.74	14.50	14.47	16.58	40.39	15.95
Ce	21.13	28.89	25.89	31.01	41.45	70.05	28.67
Pr						6.93	3.05
Nd		15.93				22.65	11.29
Sm						3.14	2.06
Eu						0.94	0.68
Gd						2.33	1.79
Tb						0.24	0.24
Dy						1.30	1.69
Ho						0.23	0.31
Er						0.78	0.81
Tm						0.11	0.15
Yb						0.81	1.05
Cu	8	6	21	21	99	55	323
Zn	11	19	12	19	17		
Mo		0.9					3.4
Ag							
Tl						0.16	0.13
Pb		3.0					
Sn		0.31					1.29
Sb		0.41					
Ga	11.6	14.5	12.4	13.4	11.4	13.6	14.7
Ge	0.00	1.33	0.00	0.00	0.00	0.88	1.32

Appendix 2. Continued

Locality	Cargo	Cargo	Cargo	Cargo	Cargo	Cargo	Cargo
Rock Type	Rhyodacite	Rhyodacite	Rhyodacite	Rhyodacite	Rhyodacite	Rhyodacite	Diorite
Sample Name	C4-531	CN11-44.4	C4-321	C4-319	CN1-125.8	JG97-1-197	CN1-12.11
SiO_2	71.95	72.50	71.98	71.16	67.47	71.27	58.41
TiO_2	0.16	0.18	0.16	0.16	0.40	0.61	0.86
Al_2O_3	14.35	14.22	14.40	13.56	14.95	12.70	16.93
Fe_2O_3	4.02	3.32	2.25	2.26	3.91	6.14	9.34
FeO	3.62	2.99	2.03	2.04	3.52	5.53	8.41
MnO	0.02	0.01	0.02	0.01	0.02	0.03	0.02
MgO	0.92	0.92	0.95	0.79	1.63	0.65	2.95
CaO	1.84	1.29	1.53	2.93	2.62	1.20	2.57
K_2O	1.78	1.42	5.45	6.21	4.43	1.21	3.96
Na_2O	4.86	6.04	3.18	2.77	4.41	5.73	4.38
P_2O_5	0.09	0.10	0.08	0.15	0.17	0.46	0.58
Ti	941	1065	974	925	2381	3653	5164
Cr				125			
Co	18	5	6	14	6	3	13
Ni							28
Rb	38	31	73	73	58	16	84
Sr	439	233	253	222	159	117	302
Ba	400	150	1478	1848	790	203	922
Sc	2.0	4.1	3.0	3.1	11.3	21.5	22.7
V	37	46	32	26	133	124	258
Ta	0.4	0.4	0.3	0.3	0.2	0.1	0.3
Nb	5.3	5.6	4.7	4.7	4.1	2.8	5.0
Zr	78	86	83	81	69	97	129
Hf	2.10	2.33	2.14	2.11	1.81	2.89	3.54
Th	5.16	5.22	4.89	4.88	3.30	1.81	3.80
U	1.75	3.24	2.11	2.30	4.01	1.97	3.39
Y	7.62	7.98	6.46	8.23	21.56	21.87	25.61
La	27.38	22.73	10.42	9.02	38.69	24.24	25.87
Ce	48.62	39.67	17.28	16.54	66.02	55.51	53.75
Pr	4.99	3.89	1.88	1.94	7.08	7.63	6.72
Nd	17.02	12.50	7.09	7.91	26.08	34.03	28.17
Sm	2.56	1.71	1.25	1.65	5.31	7.48	6.10
Eu	0.74	0.65	0.58	0.83	1.21	2.15	1.45
Gd	1.99	1.53	1.13	1.45	4.68	6.22	5.28
Tb	0.23	0.18	0.14	0.20	0.65	0.79	0.73
Dy	1.39	1.18	0.94	1.43	4.05	4.39	4.47
Ho	0.24	0.26	0.18	0.23	0.76	0.81	0.88
Er	0.84	0.76	0.71	0.76	2.36	2.44	2.79
Tm	0.12	0.14	0.10	0.12	0.34	0.31	0.40
Yb	0.91	1.05	0.77	0.85	2.28	2.16	2.71
Cu	355	83	334	841	1851	13	1047
Zn	36				31		30
Mo	8.3		44.0	41.1	108.8	2.4	9.6
Ag							
Tl	0.08	0.15	0.18	0.18	0.12	0.06	0.15
Pb							
Sn							1.34
Sb					0.46	1.01	0.51
Ga	11.4	12.3	12.3	10.7	14.9	12.2	18.3
Ge	0.74	1.07	1.34	1.20	1.44		1.17

Appendix 2. Continued

Locality	Cargo	Cargo	Cargo	Cargo	Cargo	Cargo	Cargo
Rock Type	Monzonite	Monzonite	Monzonite	Monzonite	Andesite	Dacite	Latite
Sample Name	C2-110	C2-130	C2-141	C2-198	CN1-170.3	CN1-195.6	CN11-17.7
SiO_2	54.39	53.90	54.56	52.83	53.42	64.27	64.11
TiO_2	0.58	0.61	0.60	0.60	0.79	0.56	0.57
Al_2O_3	17.58	17.27	17.56	17.96	21.62	15.29	14.32
Fe_2O_3	8.01	8.74	8.26	8.40	10.49	8.21	10.11
FeO	7.21	7.87	7.43	7.56	9.44	7.39	9.10
MnO	0.14	0.16	0.11	0.14	0.03	0.02	0.02
MgO	4.33	5.10	5.85	4.95	2.23	1.28	2.32
CaO	5.43	4.08	3.55	5.71	2.83	2.22	1.85
K_2O	5.17	5.93	5.70	4.93	5.72	0.86	1.10
Na_2O	3.80	3.59	3.23	3.88	2.55	6.97	5.29
P_2O_5	0.56	0.62	0.57	0.60	0.30	0.31	0.31
Ti	3476	3652	3547	3603	4766	3337	3356
Cr	63	53	56	43			33
Co	22	21	20	20	13	14	5
Ni	117	23	21	19			
Rb	60	73	74	61	168	23	31
Sr	1308	1074	881	900	174	213	408
Ba	870	1317	1075	867	376	112	135
Sc	12.3	12.5	12.5	12.7	29.7	19.4	24.7
V	204	207	204	206	390	132	77
Ta	0.2	0.2	0.2	0.2	0.1		0.1
Nb	3.9	4.1	4.1	4.1	2.6	2.1	2.2
Zr	58	56	59	59	58	81	89
Hf	1.56	1.60	1.68	1.68	1.72	2.35	2.67
Th	3.22	3.16	3.39	3.46	1.17	1.18	1.12
U	1.60	1.56	1.68	2.11	1.25	2.15	3.17
Y	14.27	14.51	14.55	15.15	13.04	20.19	26.05
La	23.16	25.82	24.92	25.19	19.61	14.29	12.99
Ce	41.18	45.11	43.66	44.18	38.69	37.50	32.28
Pr	4.67	5.06	4.88	4.95	4.66	5.33	4.79
Nd	18.27	19.44	19.15	19.16	18.80	23.48	22.21
Sm	3.70	3.92	3.82	3.95	3.99	5.45	5.85
Eu	1.24	1.34	1.27	1.34	1.12	1.58	1.28
Gd	3.41	3.60	3.46	3.63	3.33	4.68	5.31
Tb	0.44	0.46	0.45	0.47	0.43	0.64	0.75
Dy	2.39	2.83	2.56	2.86	2.23	3.84	4.60
Ho	0.49	0.51	0.50	0.53	0.47	0.73	0.93
Er	1.40	1.47	1.36	1.40	1.50	2.27	2.77
Tm	0.20	0.20	0.21	0.22	0.21	0.31	0.40
Yb	1.34	1.39	1.40	1.44	1.43	2.09	2.67
Cu	212	223	213	208	825	616	506
Zn	85	109	83	84	48		
Mo					7.6	9.8	3.4
Ag							
Tl	0.06	0.08	0.07		0.41		0.12
Pb	13.2	12.5	13.4	14.1			
Sn					1.58		
Sb	0.88	0.48		0.34	16.69	0.29	
Ga	17.1	17.4	16.9	17.2	22.7	16.8	15.2
Ge	1.08	1.27	0.87	1.01	1.36	0.75	1.46

Appendix 2. Continued

Locality	Cargo	Cargo	Cargo	Cargo	Cargo	Copper Hill	Copper Hill
Rock Type	Dacite	Dacite	Latite	Andesite	Latite	Diorite	Diorite
Sample Name	CN11-35.8	CN11-38.4	C4-526	JG97-1-176	JG97-1-200	NCH6-119-00	NCH6-119-70
SiO_2	64.10	60.87	62.92	57.80	62.90	57.58	57.07
TiO_2	0.56	0.55	0.56	0.43	0.79	0.61	0.60
Al_2O_3	14.27	14.86	15.94	15.58	14.36	16.33	16.03
Fe_2O_3	10.18	10.32	7.18	7.69	9.91	10.47	9.19
FeO	9.17	9.29	6.46	6.92	8.92	9.42	8.27
MnO	0.02	0.05	0.08	0.11	0.03	0.32	0.41
MgO	2.32	3.40	3.52	5.53	1.28	3.57	4.25
CaO	1.86	4.39	2.56	5.53	2.42	5.39	6.68
K_2O	1.08	1.91	0.51	3.47	1.91	0.59	0.51
Na_2O	5.32	3.48	6.45	3.67	5.92	4.88	5.07
P_2O_5	0.29	0.18	0.27	0.17	0.49	0.26	0.19
Ti	3355	3285	3313	2584	4736	3601	3545
Cr	30	123	79	163		99	193
Co	5	15	13	18	7	23	12
Ni		30		23			24
Rb	31	47	9	57	39	8	7
Sr	408	314	172	502	190	696	640
Ba	136	387	55	640	277	124	105
Sc	24.6	27.9	13.4	26.7	25.3	18.6	19.0
V	77	200	135	167	155	211	163
Ta		0.2	0.2	0.2	0.2	0.4	0.4
Nb	2.2	3.5	3.2	2.7	3.2	6.6	6.2
Zr	88	70	121	75	130	85	84
Hf	2.61	1.84	3.44	1.97	3.74	2.40	2.43
Th	1.10	2.02	2.77	1.95	2.55	1.05	0.70
U	3.19	2.19	2.48	1.56	1.93	0.66	0.74
Y	26.02	15.82	21.13	12.96	25.59	15.69	17.55
La	13.14	11.55	26.94	14.62	17.43	10.94	12.97
Ce	32.75	23.94	63.73	29.50	42.92	23.81	28.94
Pr	4.81	2.90	8.57	3.52	6.08	2.99	3.69
Nd	22.79	11.87	35.75	13.94	27.61	12.23	15.36
Sm	6.02	2.74	7.50	2.89	6.76	2.57	3.24
Eu	1.29	0.83	1.60	0.88	1.58	0.73	0.93
Gd	5.29	2.69	5.71	2.51	5.69	2.58	3.20
Tb	0.77	0.43	0.70	0.36	0.79	0.38	0.49
Dy	4.57	2.43	4.21	2.39	4.74	2.48	2.89
Ho	0.93	0.56	0.72	0.45	0.87	0.54	0.63
Er	3.01	1.67	2.14	1.55	2.86	1.68	1.83
Tm	0.40	0.26	0.30	0.20	0.40	0.26	0.28
Yb	2.62	1.76	1.99	1.36	2.75	1.86	1.97
Cu	444	310		10		1150	218
Zn		32	48	43	33	604	444
Mo	3.2					3.4	3.7
Ag			0.5				
Tl	0.12	0.23		0.23	0.17		
Pb						5.3	
Sn		1.10	2.66		2.42		
Sb		2.48		1.67	0.35		
Ga	15.4	17.0	14.8	14.4	17.3	19.2	16.8
Ge	1.39	1.52		1.37	0.53	1.06	0.85

Appendix 2. Continued

Locality	Copper Hill	Copper Hill	Copper Hill	Copper Hill	Copper Hill	Copper Hill	Copper Hill
Rock Type	Granodiorite	Monzonite	Rhyodacite	Dacite	Rhyodacite	Dacite	Rhyodacite
Sample Name	NCH6-135	NCH6-142	NCH6-378	NCH6-397	NCH6-404	NCH6-413	NCH6-417
SiO_2	63.14	63.41	65.87	65.80	66.94	64.89	69.74
TiO_2	0.47	0.47	0.36	0.40	0.37	0.37	0.35
Al_2O_3	17.26	17.73	16.68	16.71	16.52	17.08	16.59
Fe_2O_3	5.37	4.86	4.32	4.35	5.54	4.42	2.42
FeO	4.83	4.37	3.88	3.91	4.99	3.98	2.17
MnO	0.26	0.27	0.26	0.32	0.15	0.23	0.07
MgO	2.08	1.96	1.64	1.77	2.84	1.80	2.05
CaO	5.31	4.04	5.15	6.14	2.95	6.30	2.88
K_2O	1.34	2.34	1.31	1.40	2.06	1.08	1.91
Na_2O	4.60	4.74	4.27	3.00	2.47	3.69	3.92
P_2O_5	0.17	0.19	0.14	0.13	0.16	0.14	0.07
Ti	2771	2770	2170	2352	2177	2211	2089
Cr			51		74		76
Co	5	5	9	10	26	7	7
Ni		16	19				
Rb	21	22	21	26	39	20	32
Sr	845	1033	713	621	760	672	1438
Ba	320	1282	351	378	868	294	567
Sc	9.3	9.2	7.2	7.3	8.5	6.3	7.3
V	107	102	74	84	126	77	101
Ta	0.4	0.5	0.4	0.4	0.4	0.4	0.4
Nb	6.7	7.0	5.9	6.1	6.3	6.2	5.9
Zr	96	92	84	90	90	91	90
Hf	2.66	2.52	2.35	2.47	2.50	2.50	2.40
Th	1.23	1.36	0.82	0.85	1.01	0.83	0.93
U	0.74	0.70	0.96	1.02	38.66	1.00	0.77
Y	14.11	12.97	13.19	13.78	21.16	13.16	11.31
La	11.82	11.76	11.58	11.27	48.22	16.01	13.32
Ce	24.72	24.20	23.32	22.97	83.95	30.19	25.25
Pr	3.11	2.93	2.82	2.74	9.07	3.47	2.98
Nd	12.74	11.87	11.23	11.06	33.29	13.11	11.62
Sm	2.67	2.44	2.40	2.35	6.14	2.55	2.33
Eu	0.88	0.78	0.81	0.83	1.59	0.91	0.69
Gd	2.49	2.22	2.25	2.32	5.11	2.40	2.11
Tb	0.37	0.32	0.34	0.35	0.70	0.34	0.29
Dy	2.45	1.86	2.27	2.31	4.16	2.27	2.06
Ho	0.48	0.42	0.43	0.45	0.78	0.43	0.36
Er	1.45	1.25	1.32	1.54	2.26	1.28	1.13
Tm	0.22	0.20	0.20	0.21	0.32	0.19	0.16
Yb	1.56	1.41	1.41	1.42	2.19	1.36	1.10
Cu	151	367	11	23	988		265
Zn	135	140	152	623	382	109	79
Mo	2.3				62.0		15.8
Ag							
Tl	0.08	0.10	0.09	0.13	0.24	0.09	0.13
Pb	6.1	6.1	21.5	12.8	10.1	12.5	7.2
Sn					1.27		
Sb					0.96		
Ga	17.5	17.2	17.3	17.2	14.4	17.8	15.5
Ge	0.81	0.83	0.98	0.78		0.91	0.95

Appendix 2. Continued

Locality	Copper Hill	Copper Hill	Copper Hill	Copper Hill	Copper Hill	Copper Hill	Copper Hill
Rock Type	Dacite	Basalt	Dacite	Andesite	Rhyodacite	Dacite	Basalt
Sample Name	NCH6-424	NCH8-31	NCH8-41	NCH8-47	NCH8-48	NCH8-51	NCH8-75
SiO_2	59.45	53.11	65.69	56.44	66.39	69.66	51.45
TiO_2	0.78	0.96	0.42	0.76	0.40	0.24	0.70
Al_2O_3	16.25	18.53	16.59	15.71	16.38	16.62	16.44
Fe_2O_3	9.57	11.13	5.36	12.62	5.27	3.41	13.88
FeO	8.61	10.02	4.83	11.35	4.75	3.07	12.49
MnO	0.29	0.23	0.23	0.32	0.22	0.16	0.25
MgO	5.08	5.06	2.89	6.09	2.89	1.35	5.39
CaO	5.67	7.51	5.28	4.99	4.76	3.81	8.38
K_2O	0.47	2.17	2.12	2.73	2.18	3.10	0.28
Na_2O	2.21	0.90	1.28	0.06	1.36	1.56	3.03
P_2O_5	0.24	0.38	0.13	0.29	0.13	0.10	0.21
Ti	4618	5598	2464	4479	2391	1416	4173
Cr	197	52	153	44	141	56	41
Co	20	23	12	11	10	6	19
Ni	16	21	20		20		
Rb	10	45	48	55	46	63	7
Sr	571	143	130	35	129	99	305
Ba	152	184	173	228	182	453	292
Sc	24.3	38.4	11.9	28.4	15.1	6.3	43.2
V	222	433	109	261	103	49	343
Ta	0.3	0.2	0.3	0.2	0.3	0.3	0.1
Nb	5.5	4.1	4.3	3.1	4.1	4.2	1.8
Zr	80	75	73	63	73	77	45
Hf	2.23	2.23	2.18	1.79	2.15	2.21	1.36
Th	0.72	1.90	0.16	1.45	0.16	0.20	0.54
U	1.11	1.57	0.78	1.47	0.77	0.68	1.26
Y	22.10	25.05	9.09	11.87	7.83	6.94	20.67
La	16.66	15.48	6.74	12.30	6.98	7.65	12.41
Ce	29.51	36.25	14.86	27.60	14.72	16.34	25.71
Pr	3.64	5.34	1.89	3.57	1.81	1.97	3.38
Nd	15.83	24.98	7.92	15.10	7.22	7.77	14.84
Sm	3.98	6.25	1.75	3.23	1.53	1.48	3.77
Eu	1.56	1.88	0.59	0.89	0.53	0.46	1.35
Gd	3.99	5.54	1.64	2.73	1.45	1.35	3.70
Tb	0.59	0.82	0.25	0.37	0.22	0.18	0.57
Dy	3.05	4.70	1.56	1.79	1.42	1.19	3.71
Ho	0.76	0.96	0.31	0.41	0.27	0.23	0.75
Er	2.16	2.69	1.02	1.09	0.82	0.69	2.18
Tm	0.32	0.39	0.14	0.18	0.13	0.11	0.32
Yb	2.17	2.47	1.00	1.25	0.93	0.76	2.11
Cu	521	1511	124	268	38	25	223
Zn	519	249	562	1004	3644	214	215
Mo	10.6	71.6		5.0			
Ag				1.4			
Tl	0.03	0.19	0.28	0.34	0.35	0.50	
Pb	9.1	15.4		289.0	10.6	11.8	7.6
Sn	1.07	2.56	1.63	2.40	1.44		1.72
Sb	0.22	3.98					0.65
Ga	18.1	18.7	17.6	17.9	17.0	15.8	15.9
Ge	1.67	0.77	0.98	0.87	0.98	0.74	1.18

Appendix 2. Continued

Locality	Copper Hill	Copper Hill	Copper Hill	Copper Hill	Copper Hill	Copper Hill	Copper Hill
Rock Type	Dacite	rtz monzonite	artz monzonite	Dacite	Dacite	rogranodiorite	rogranodiorite
Sample Name	COH4*	COH12*	COH13*	COH5*	COH6*	COH7*	COH8*
SiO_2	67.24	68.98	66.11	65.14	61.90	56.15	61.76
TiO_2	0.34	0.24	0.39	0.43	0.55	0.69	0.54
Al_2O_3	15.87	16.00	16.40	16.83	16.80	17.00	15.80
Fe_2O_3	4.08	2.82	4.32	5.14	6.13	8.50	6.34
FeO	3.68	2.54	3.89	4.63	5.52	7.65	5.71
MnO	0.10	0.19	0.35	0.32	0.29	0.17	0.12
MgO	2.37	1.17	1.56	1.99	2.60	4.05	3.54
CaO	3.54	4.53	5.53	4.84	5.21	8.12	5.86
K_2O	0.69	2.58	1.28	0.94	1.33	1.28	1.70
Na_2O	5.65	3.41	3.94	4.22	5.00	3.81	4.20
P_2O_5	0.10	0.08	0.13	0.16	0.19	0.23	0.14
Ti	2067	1455	2320	2552	3285	4138	3225
Cr	49	27	26	20	34	88	99
Co							
Ni	14	7	7	11	11	35	26
Rb	10	49	21	17	13	17	22
Sr	622	452	680	794	889	726	645
Ba	157	517	330	1329	403	284	462
Sc	12.5	7.4	9.4	8.3	16.5	25.4	23.3
V	73	53	76	87	131	180	138
Ta	0.4	0.3	0.0	0.0	0.4	0.4	0.4
Nb	4.2	3.2	5.2	5.2	5.2	3.0	5.1
Zr	83	77	97	96	99	69	88
Hf	2.48	2.35			2.70	2.04	2.53
Th	1.57	1.06	2.09	2.08	2.58	1.02	2.54
U	0.00	0.53	1.05	1.56	1.03	0.00	1.02
Y	9.40	7.39	12.55	14.53	14.47	15.23	14.21
La	8.36	7.39	10.46	12.46	11.37	12.18	9.14
Ce	18.80	19.00	20.92	24.92	26.88	24.36	22.33
Pr							
Nd							
Sm	2.04	1.72			3.31	3.59	2.96
Eu	0.68	0.58			1.12	1.21	1.02
Gd							
Tb							
Dy							
Ho							
Er							
Tm							
Yb	1.15	0.94			1.79	1.79	1.62
Cu	17	3	4	277	30	82	30
Zn	46	242	222	1827	204	69	63
Mo	0.9	0.6	1.8	1.5	1.0	1.9	1.1
Ag	0.3		0.4	0.4	0.3	0.5	0.3
Tl							
Pb	3.1	4.2	19.9	15.6	9.3	1.0	4.1
Sn	0.21	0.42	0.94	0.52	0.52	0.71	0.51
Sb	0.10	0.63	1.05	1.14	1.45		
Ga	16.2	16.9	17.8	17.1	17.6	17.3	16.2
Ge							

Appendix 2. Continued

Locality	Copper Hill	Copper Hill	Fairholme	Fairholme	Fairholme	Fairholme
Rock Type	Monzonite	Monzonite	Basalt	Basalt	Basalt	Basalt
Sample Name	COH9*	COH11*	DR42.119	DR37.158	DR42.377	DR37.303
SiO_2	61.47	64.41	49.97	50.54	50.56	50.88
TiO_2	0.54	0.42	0.81	0.89	0.76	1.18
Al_2O_3	17.39	16.96	13.95	18.52	15.48	17.52
Fe_2O_3	6.12	5.42	12.70	11.98	14.65	11.68
FeO	5.51	4.88	11.43	10.78	13.19	10.51
MnO	0.11	0.12	0.21	0.13	0.12	0.21
MgO	2.12	1.96	8.38	4.47	4.97	4.42
CaO	6.16	3.56	9.68	7.03	7.22	8.03
K_2O	1.61	2.05	1.24	2.53	0.65	2.62
Na_2O	4.30	4.92	2.90	3.76	5.42	3.08
P_2O_5	0.18	0.17	0.16	0.15	0.17	0.40
Ti	3216	2536	4871	5312	4543	6972
Cr	9	20	209		157	26
Co			45	20	18	28
Ni	4	5	36	19	37	27
Rb	18	25	36	55	9	27
Sr	673	779	675	511	462	1161
Ba	445	562	166	370	44	569
Sc	15.2	12.4	44.8	29.2	25.8	27.8
V	109	91	363	265	322	312
Ta	0.0	0.0		0.2		0.3
Nb	4.0	5.2	2.5	4.5	3.5	6.7
Zr	88	102	57	73	61	56
			1.68	2.02	1.70	1.50
Th	2.02	2.06	1.74	1.33	2.20	1.35
U	1.01	1.03	2.07	0.86	1.56	0.69
Y	15.18	13.41	16.32	21.08	17.03	22.52
La	10.12	11.35	13.13	8.14	20.28	15.78
Ce	24.29	24.76	28.17	17.13	35.38	31.23
Pr			3.97	2.34	4.27	4.10
Nd			17.76	10.15	17.73	17.41
Sm			4.20	2.83	4.04	4.21
Eu			1.19	1.40	1.30	1.48
Gd			3.47	2.90	3.58	4.16
Tb			0.47	0.49	0.48	0.61
Dy			3.08	3.39	3.30	3.82
Ho			0.54	0.69	0.55	0.73
Er			1.60	2.07	1.54	2.17
Tm			0.22	0.31	0.22	0.28
Yb			1.48	2.17	1.52	1.91
Cu	45	66		31	63	92
Zn	43	73	104	65	62	113
Mo	0.7	2.9	2.1		2.3	
Ag	0.2					
Tl			0.13	0.28		
Pb	4.0	4.1				15.1
Sn	0.61	1.65	2.30	1.70	1.66	1.36
Sb	0.40	0.52	1.14	0.75	0.33	1.76
Ga	17.2	19.1	14.9	18.6	15.5	18.8
Ge			1.44	1.30	2.33	1.61

Appendix 2. Continued

Locality	Fairholme	Fairholme	Fairholme	Fairholme	Fairholme	Fairholme	Fairholme
Rock Type	Diorite	Diorite	Basalt	Basalt	Andesite	Latite	Latite
Sample Name	DR42.139	DR37.258	DR42.114	DR37.299	DR37.301	DR42.409A	DR37.295
SiO_2	51.01	51.42	52.61	52.66	51.39	52.08	52.81
TiO_2	2.50	1.06	0.78	1.14	1.12	1.04	1.10
Al_2O_3	14.84	17.14	14.50	17.04	17.79	17.21	17.89
Fe_2O_3	13.80	11.56	10.15	11.58	11.64	9.11	11.42
FeO	12.42	10.41	9.13	10.42	10.48	8.20	10.28
MnO	0.24	0.21	0.19	0.16	0.20	0.09	0.15
MgO	4.22	4.32	6.16	4.69	4.38	3.17	4.61
CaO	7.68	7.95	10.15	6.17	6.86	10.06	5.28
K_2O	0.80	2.57	0.71	2.67	2.54	1.79	2.07
Na_2O	4.36	3.37	4.50	3.47	3.65	5.14	4.29
P_2O_5	0.54	0.40	0.25	0.42	0.43	0.31	0.37
Ti	14777	6290	4629	6712	6639	6194	6497
Cr			199			51	
Co	31	29	26	32	31	62	28
Ni	54	25	35	27	25	34	25
Rb	9	30	12	43	44	30	34
Sr	528	1016	538	706	585	459	740
Ba	268	401	73	318	341	141	315
Sc	34.0	25.5	40.9	28.0	28.2	23.2	26.6
V	373	277	339	314	315	232	294
Ta	0.3	0.4		0.6	0.2	0.7	0.5
Nb	6.4	8.8	2.7	11.6	6.0	14.2	10.9
Zr	153	73	55	90	58	115	82
Hf	3.95	1.91	1.59	2.32	1.56	2.90	2.18
Th	0.97	1.69	1.81	1.97	1.43	2.69	1.89
U	0.39	0.86	2.20	0.99	0.76	1.52	0.94
Y	46.01	22.01	18.74	23.51	23.55	22.92	23.28
La	16.39	15.61	16.20	17.15	15.53	22.58	16.75
Ce	40.01	30.89	33.66	33.78	30.55	45.99	32.83
Pr	5.93	4.00	4.60	4.24	3.99	5.50	4.15
Nd	28.34	17.21	20.36	17.54	17.37	21.45	17.38
Sm	7.69	4.19	4.74	4.24	4.24	4.72	4.19
Eu	2.53	1.38	1.56	1.31	1.68	1.30	1.34
Gd	7.83	4.02	3.95	4.16	4.26	4.59	4.11
Tb	1.23	0.59	0.54	0.63	0.64	0.64	0.62
Dy	8.00	3.72	3.07	4.03	4.20	4.00	4.15
Ho	1.54	0.71	0.62	0.77	0.75	0.76	0.75
Er	4.77	1.86	1.87	2.45	2.24	2.43	2.36
Tm	0.62	0.29	0.24	0.31	0.29	0.33	0.32
Yb	3.96	1.90	1.59	2.14	1.97	2.27	2.13
Cu	48	127	244	203	183	1602	82
Zn	139	117	66	113	103	77	112
Mo	2.3		2.7			5.8	
Ag	0.9					0.7	
Tl				0.12	0.10		0.06
Pb		5.7	5.6	7.4			7.9
Sn	2.79		1.15			3.19	1.08
Sb	0.52		0.60	1.02	1.85	231.26	0.62
Ga	20.8	18.0	14.3	18.7	19.0	19.5	18.8
Ge	0.91	1.30	1.94	1.55	0.98	1.69	1.41

Appendix 2. Continued

Locality	Fairholme	Fairholme	Fairholme	Fairholme	Fairholme	Fairholme	Fairholme
Rock Type	Basalt	Andesite	Andesite	Andesite	Andesite	Andesite	Andesite
Sample Name	16 DR9 180-18	DR42.317	DR35.198	17 DR9 183-18	DR37.166	DR42.165	DR42.180
SiO_2	57.08	54.19	57.29	63.71	54.90	59.37	54.31
TiO_2	0.61	0.93	0.56	0.48	0.93	0.34	0.87
Al_2O_3	17.89	16.88	18.54	18.06	18.58	17.87	17.36
Fe_2O_3	8.15	9.49	9.69	4.06	9.29	5.19	8.63
FeO	7.33	8.55	8.72	3.65	8.36	4.67	7.76
MnO	0.09	0.11	0.18	0.04	0.12	0.08	0.10
MgO	3.36	3.38	4.88	1.56	3.73	1.96	3.59
CaO	5.28	6.77	3.90	2.70	4.43	3.62	6.18
K_2O	2.36	3.78	0.31	1.90	3.08	6.27	4.75
Na_2O	4.82	4.19	4.36	7.16	4.67	5.11	3.96
P_2O_5	0.36	0.28	0.29	0.34	0.27	0.20	0.26
Ti	3650	5617	3386	2872	5487	2045	5179
Cr	45	41		31	41	26	65
Co	28	20	11	4	21	11	16
Ni	17	29			24		25
Rb	38	56	3	33	39	78	80
Sr	348	475	711	338	575	557	883
Ba	232	408	137	255	688	742	540
Sc	19.2	21.2	20.9	11.5	20.8	7.1	19.3
V	166	213	183	133	205	111	182
Ta	0.4	0.7	0.3	0.3	0.6	0.3	0.4
Nb	7.0	13.6	6.2	5.1	10.7	5.3	8.4
Zr	65	114	60	46	100	68	80
Hf	1.93	2.89	1.69	1.38	2.70	1.92	2.03
Th	1.68	2.71	2.40	1.38	2.53	2.45	1.92
U	0.99	1.19	1.01	0.59	1.10	1.22	0.80
Y	15.48	26.08	19.74	6.02	22.46	11.19	19.54
La	12.30	20.98	18.33	8.01	15.58	9.90	13.46
Ce	24.45	40.26	36.07	15.24	31.65	20.28	28.99
Pr	3.16	4.95	4.53	1.93	4.11	2.54	3.81
Nd	13.19	20.07	18.95	7.75	22.14	10.38	16.06
Sm	3.10	4.72	4.08	1.62	4.03	2.24	3.75
Eu	0.83	1.48	1.20	0.45	1.31	0.80	1.20
Gd	2.87	4.49	3.50	1.39	4.00	2.11	3.52
Tb	0.44	0.68	0.51	0.19	0.61	0.29	0.52
Dy	2.77	4.46	3.28	1.12	4.74	1.75	3.61
Ho	0.54	0.84	0.67	0.21	0.74	0.36	0.62
Er	1.51	2.75	2.15	0.64	2.23	1.13	1.96
Tm	0.23	0.36	0.30	0.10	0.32	0.16	0.25
Yb	1.62	2.41	2.04	0.74	2.18	1.21	1.71
Cu	235	762	389	18	46		11
Zn	48	56	131	21	73	36	51
Mo	2.7	9.0		3.7		5.5	3.7
Ag							
Tl	0.06	0.17			0.18	0.26	0.28
Pb							
Sn	1.45	2.47	2.10	1.75	1.14		
Sb	2.25	7.03	0.74	1.55	0.77		
Ga	17.6	18.0	17.7	15.9	18.2	15.9	17.0
Ge	1.71	1.53	1.29	1.67	0.71	1.35	1.09

Appendix 2. Continued

Locality	Fairholme	Fairholme	Fairholme	Fairholme	Fairholme	Fairholme	Fairholme
Rock Type	Volcanic	Andesite	Andesite	Volcanic	Volcanic	Andesite	Volcanic
Sample Name	DR37.115	DR35.211	DR35.220	DR35.108	DR35.229	DR35.117	24 DR32 199-1
SiO_2	58.66	58.21	61.92	61.66	58.82	62.12	58.80
TiO_2	0.73	0.63	0.52	0.46	0.56	0.43	0.64
Al_2O_3	19.13	20.27	18.79	19.71	19.02	19.10	16.80
Fe_2O_3	8.41	8.73	7.58	7.03	8.58	7.92	9.48
FeO	7.57	7.86	6.82	6.32	7.72	7.13	8.53
MnO	0.06	0.12	0.07	0.27	0.07	0.18	0.09
MgO	1.94	4.27	3.52	2.78	2.25	2.92	3.81
CaO	3.10	3.43	2.93	2.39	6.51	1.44	4.58
K_2O	1.38	1.81	1.70	1.59	1.51	2.34	1.52
Na_2O	6.36	2.19	2.73	3.88	2.46	3.35	4.03
P_2O_5	0.23	0.34	0.25	0.22	0.22	0.21	0.27
Ti	4319	3762	3112	2782	3305	2582	3827
Cr	84		23			29	112
Co	15	21	15	10	20	14	23
Ni	23						20
Rb	17	28	27	23	22	34	25
Sr	556	371	302	498	399	330	441
Ba	247	235	208	389	172	501	132
Sc	19.8	22.7	19.3	15.8	17.3	14.7	29.2
V	225	200	160	128	148	136	221
Ta	0.2	0.3	0.5	0.6	0.5	0.6	0.3
Nb	5.0	7.2	9.9	11.4	10.1	11.4	7.3
Zr	88	68	73	66	67	63	61
Hf	2.36	1.92	2.05	1.86	1.90	1.87	1.70
Th	2.31	2.71	2.72	3.22	2.31	3.19	2.51
U	0.99	1.06	1.33	0.87	0.92	0.96	1.09
Y	16.16	21.07	20.13	19.35	12.04	13.81	17.22
La	14.18	15.65	19.14	15.89	10.26	12.24	16.92
Ce	26.87	31.81	35.96	28.01	18.67	21.16	31.73
Pr	3.78	4.05	4.32	3.64	2.26	2.76	4.00
Nd	15.73	16.83	16.98	14.88	8.92	11.07	16.49
Sm	3.52	3.77	3.63	3.26	2.00	2.41	3.52
Eu	1.01	1.05	1.04	0.90	0.68	0.84	1.12
Gd	2.94	3.30	3.37	2.96	1.85	2.15	3.05
Tb	0.43	0.50	0.50	0.44	0.28	0.32	0.44
Dy	2.90	3.70	3.46	3.27	1.99	2.25	3.02
Ho	0.53	0.67	0.65	0.62	0.40	0.46	0.58
Er	1.56	2.16	2.10	2.07	1.30	1.56	1.86
Tm	0.24	0.32	0.29	0.30	0.21	0.22	0.26
Yb	1.64	2.28	2.07	2.15	1.50	1.69	1.90
Cu	79	197	426	142	84	25	285
Zn	125	168	59	332	70	215	114
Mo	2.3	3.3	3.9	4.1			15.4
Ag							0.6
Tl	0.13	0.14	0.16	0.14	0.12	0.22	
Pb		10.7	8.7	6.0	7.9	6.0	9.8
Sn			1.22	2.49	1.31	2.21	3.70
Sb	0.40			0.66	0.40	0.44	3.48
Ga	17.9	19.2	17.7	17.4	15.9	17.7	14.5
Ge	1.03	1.46	1.24	1.23	1.31	1.03	1.75

Appendix 2. Continued

Locality	Fairholme	Fairholme	Fairholme	Fairholme	Fairholme	Fairholme
Rock Type	Volcanic	Volcanic	Granodiorite	Granodiorite	Granodiorite	Granodiorite
Sample Name	23 DR32 198-	22 DR32 195-	18 DR27 198-	19 DR27 200-2	20 DR27 202-2	21 DR27 203-204
SiO_2	62.31	59.59	56.76	58.01	55.44	56.94
TiO_2	0.48	0.57	0.64	0.68	0.74	0.69
Al_2O_3	16.49	15.82	15.87	17.95	16.84	18.13
Fe_2O_3	6.64	8.45	9.26	7.11	8.31	8.10
FeO	5.97	7.61	8.33	6.40	7.47	7.29
MnO	0.05	0.09	0.23	0.12	0.15	0.12
MgO	4.35	3.91	2.21	2.33	3.08	3.00
CaO	4.34	6.55	9.71	6.73	8.75	6.29
K_2O	0.73	1.05	1.26	2.64	3.22	1.94
Na_2O	4.43	3.81	3.81	4.00	3.21	4.49
P_2O_5	0.18	0.16	0.25	0.43	0.27	0.31
Ti	2883	3420	3823	4075	4445	4179
Cr	40	149	102	49	92	41
Co	17	22	21	20	16	17
Ni		20	20	22	20	20
Rb	11	16	18	50	60	41
Sr	568	415	674	298	433	456
Ba	90	90	476	302	341	506
Sc	24.6	26.1	18.4	19.7	21.3	20.4
V	172	192	180	191	215	200
Ta	0.4	0.2	0.2	0.2	0.2	0.3
Nb	8.4	5.9	4.7	5.2	4.9	6.6
Zr	51	57	85	99	90	96
Hf	1.40	1.63	2.32	2.65	2.38	2.60
Th	2.14	1.93	2.16	2.39	2.27	2.60
U	0.94	1.04	1.39	1.79	1.53	1.83
Y	15.81	17.23	16.17	17.83	18.09	18.01
La	14.68	16.66	14.86	14.66	14.29	16.92
Ce	26.58	31.83	31.12	31.43	29.83	34.58
Pr	3.21	3.97	4.16	4.09	3.92	4.40
Nd	13.14	16.51	17.33	17.34	16.66	18.35
Sm	2.75	3.67	3.87	3.91	3.80	4.05
Eu	0.86	0.97	1.14	1.09	1.07	1.23
Gd	2.44	3.19	3.24	3.36	3.40	3.49
Tb	0.37	0.46	0.46	0.49	0.48	0.49
Dy	2.38	3.25	2.90	2.59	2.89	3.40
Ho	0.51	0.58	0.56	0.60	0.60	0.60
Er	1.62	1.99	1.60	1.98	1.86	1.94
Tm	0.25	0.26	0.24	0.27	0.26	0.26
Yb	1.78	1.81	1.69	1.88	1.81	1.80
Cu	697	526	119	72	54	48
Zn	43	43	71	66	51	54
Mo	19.7	11.0		2.5		
Ag	0.6			0.7		
Tl		0.07	0.05	0.20	0.15	0.14
Pb	6.1	6.8				
Sn	1.90	1.57	1.32	3.62	2.12	2.25
Sb	0.85	0.48	1.33	3.80	3.62	3.51
Ga	13.6	13.6	16.1	16.8	17.1	17.9
Ge	1.75	1.17	1.14	0.93	1.17	0.92

Appendix 2. Continued

Locality	Nasdaq	Nasdaq	Nasdaq
Rock Type	Microdiorite	Microdiorite	Latite
Sample Name	NAS-1	NAS-1B	NAS-3
SiO_2	51.82	54.62	53.62
TiO_2	0.82	0.71	0.83
Al_2O_3	18.92	18.89	20.08
Fe_2O_3	11.10	8.21	9.42
FeO	9.99	7.39	8.48
MnO	0.12	0.08	0.25
MgO	5.19	5.04	2.68
CaO	3.91	2.51	5.38
K_2O	4.72	4.88	5.43
Na_2O	3.05	4.76	1.81
P_2O_5	0.34	0.30	0.49
Ti	4923	4264	4966
Cr			
Co	30	18	39
Ni	31		42
Rb	46	72	32
Sr	458	368	1011
Ba	760	1010	1010
Sc	25.8	19.6	24.7
V	216	178	247
Ta	0.2	0.2	0.2
Nb	4.7	4.9	5.5
Zr	64	64	130
Hf	1.78	1.71	3.68
Th	1.12	1.08	3.95
U	0.53	0.55	3.07
Y	19.42	17.10	28.68
La	9.07	9.90	32.51
Ce	19.70	20.26	72.75
Pr	2.65	2.61	9.80
Nd	11.86	11.36	42.41
Sm	2.96	2.68	8.28
Eu	1.10	1.10	1.98
Gd	3.27	2.81	7.26
Tb	0.53	0.44	0.92
Dy	3.43	2.81	5.09
Ho	0.70	0.59	1.03
Er	2.29	1.69	2.88
Tm	0.30	0.25	0.43
Yb	1.94	1.59	2.76
Cu	41	35	804
Zn	46		240
Mo			
Ag			
Tl	0.51	0.95	0.18
Pb			
Sn		2.94	1.32
Sb			2.04
Ga	16.0	16.1	17.5
Ge	1.22	0.84	